Title

Energetics of Vanilloid Activation of TRPV1 Ion Channel

Author

Li, Shisheng

Publication Date

2024

Peer reviewed|Thesis/dissertation

Energetics of Vanilloid Activation of TRPV1 Ion Channel

By

SHISHENG LI

DISSERTATION

Submitted in partial satisfaction of the requirements for the degree of

DOCTOR OF PHILOSOPHY

in

Molecular, Cellular and Integrated Physiology

in the

OFFICE OF GRADUATE STUDIES

of the

UNIVERSITY OF CALIFORNIA

DAVIS

Approved:

Jie Zheng, Chair

Vladimir Yarov-Yarovoy

Qizhi Gong

Rose Dixon
Committee in Charge
2024

Abstract

Ligand activation of the nociceptive TRPV1 ion channel by vanilloids is a proven and powerful pathway for pain management and serves as one of the best model systems for analyzing allosteric coupling in ion channels. However, vanilloid binding and activation have been mostly described only qualitatively in the past. We developed a novel method to isolate channel gating states with a specific number of bound ligands and bound configuration, which allowed direct measurement of binding affinity and gating energetics on a per subunit basis. We determined that capsaicin binds to a rat TRPV1 subunit with an association constant of $2.4X10^{6}$ M^{-1}, and found ligand binding to each subunit is nearly independent. Each ligand binding contributes 1.70 to 1.86 kcal/mol activation energy. Subunit contributions are nearly equal as postulated in the MWC model, with a minor deviation that two capsaicin molecules bound to diagonal subunits yield stronger cooperativity (by 0.3 to 0.4 kcal/mol) than those bound to neighboring subunits.

Table of Contents

Chapter I: Capsaicin Receptor TRPV1: Biophysics, Physiology, and Pharmacology

Shisheng Li and Jie Zheng

Abstract

The animal receptor for capsaicin, an important metabolite found in chili peppers that bestows the signature spiciness, is TRPV1 (Transient Receptor Potential Vanilloid 1). It is a cation channel that allows cations to permeate through cell membranes to initiate action potentials in nociceptive neurons. In addition to sensing pungent chemicals in plants, TRPV1 responds to extracellular protons, animal peptide toxins and membrane depolarization. It also serves as a thermosensor involved in controlling body core high-temperature protection from noxious high temperature hazards by initialing pain signals. Rapid developments of pharmacology, electrophysiology and structural biology yield high-resolution TRPV1 structures bound with different ligands and evolving mechanistic understanding of the activation mechanisms of TRPV1. In this chapter, we review the biophysics, physiology and pharmacology of TRPV1.

Keywords: TRPV1, Capsaicin, Ion channel, Nociceptor, Biophysics, Physiology, Pharmacology.

Introduction

Spicy food is appreciated all over the world and is popular in many regions of south-western part of China, India, and Mexico. The history of humans cultivating and consuming chili pepper can be traced back to 6000 years ago in east-central Mexico (Kraft, Brown et al. 2014). Mirroring the enthusiasm for spicy food, scientists have put in great efforts to reveal the mechanism underlying spiciness sensory physiology. Early research focused on identification of the principle ingredients in chili peppers that are responsible for spiciness, and later work identified the receptor in animals that detect spiciness and elucidated its activation mechanism (Szallasi and Blumberg 1999).

When chili pepper plants were first transported from the Americas in the Columbian exchange, the Europeans were attracted to both their exotic appearance and pungent taste. John Clough Thresh, who is best known for his efforts advocating hygiene of public water supply, was among the first to try isolating the material in chili peppers that yielded the signature spiciness. In 1876, he succeeded in obtaining an almost pure sample of the spicy compound, apparently from tens of pounds of chili peppers; the pure compound would form beautiful crystals in the form of pearly white leaflets (Thresh 1846). It was Thresh who gave the compound its name, capsaicin. Once pure capsaicin was obtained, the logical next step was to find out its chemical nature. Achieving this goal took nearly another 50 years. E.K. Nelson, who worked at the US Department of Agriculture, pointed out in 1910 that the proposed molecular formula for capsaicin ($C_{18}H_{28}NO_3$), by a German Karl Micho, was chemically impossible. In 1923, Nelson finally solved the molecular structure of capsaicin (Figure 1A) (Nelson and Dawson 1923). The final step of the decade-long project was determining the location of a C=C double-bond. Nelson proved that this double-bond locates between the 6^{th} and 7^{th} carbon in capsaicin's tail and, by doing so, putting down the last piece of the puzzle. In the process of this work, he also showed that this double-bond does not contribute to the spiciness of capsaicin. This corrected another misconception at the time. Capsaicin is a small lipophilic molecule with a vanillyl head group, an amide neck, and a fatty acid tail (Figure 1A).

Since the discovery of capsaicin, it has been used widely in biomedical research. It is particularly useful for the research of pain, as intraplantar injection of capsaicin has served as a robust animal pain model. By 1990s, capsaicin was shown to activate primary sensory neurons, and the existence of a membrane ion channel as the capsaicin receptor was predicted(Bevan and Szolcsányi 1990). In 1997, this capsaicin receptor was cloned in David Julius' laboratory, from a cDNA library from

the rat dorsal root ganglia sensory neurons (Caterina, Schumacher et al. 1997). Originally named VR1 (vanilloid receptor member 1), it was later changed to TRPV1 (Transient Receptor Potential Vanilloid 1) (Caterina, Schumacher et al. 1997, Montell, Birnbaumer et al. 2002). This landmark study started a flourishing field of research that has already yielded important findings concerning many aspects of human physiology (Yang and Zheng 2017, Cheng 2022). This chapter focuses on the biophysics, physiology, and pharmacology of TRPV1.

TRPV1 biophysics

Overall structural features of TRPV1

TRPV1 is a non-selective cation channel belonging to the voltage-gated potassium channel superfamily (Yu and Catterall 2004). It is a homotetramer with each subunit containing six transmembrane helixes and intracellularly located N- and C- termini (Cao, Liao et al. 2013, Gao, Cao et al. 2016, Kwon, Zhang et al. 2021, Zhang, Julius et al. 2021) (Figure 1B). The S1-S4 helixes form a voltage sensor-like domain surrounding the channel pore formed by the S5-S6 helixes and the P-loop. The channel pore has two constricted regions: the upper constriction is formed by the selectivity filter which determines the ion types that can pass through the pore when it opens; the lower constriction, also called the lower gate, is formed by the S6 helixes which move during channel activation (Zheng and Ma 2014). Within the transmembrane domain of TRPV1—as well as other ion channels of the same TRPV subfamily—there is a ligand binding pocket formed by the S3 and S4 helixes and the S4-S5 linker from one subunit and the S6 helix from a neighbor subunit (Figure 1C). This is the vanilloid binding pocket for pungent capsaicinoids such as capsaicin. Binding of ligands causes a global conformational rearrangement in TRPV1 that opens the channel pore to initiate ion conduction.

Capsaicin activation

Capsaicin is the most abundant capsaicinoids in chili peppers (Scoville 1912). Being a lipophilic compound, capsaicin has a vanilloid head and flexible hydrophobic tail, linked by a covalent amide bond neck (Figure 1A). It is membrane permeable, an assessment supported by observations that capsaicin can activate TRPV1 from both intracellular and extracellular sides. Combining observations from CryoEM structures, computational modeling and mutagenesis tests, it was proposed that capsaicin takes a "head-down tail-up" configuration in the vanilloid binding pocket, which was confirmed in the latest TRPV1 structure containing capsaicin (Yang and Zheng 2017, Kwon, Zhang et al. 2021) (Figure 1C). The head of capsaicin forms a hydrogen bond with E570 (rat and human TRPV1, equals to E571 in mouse TRPV1); the neck of capsaicin forms another hydrogen bond with T550 (rat and human TRPV1, equals to T551 in mouse TRPV1); the hydrophobic tail of capsaicin is flexible and makes non-specific interactions with residues in the upper part of the vanilloid binding pocket. In addition, Y511 (rat and human TRPV1, equals to Y512 in mouse TRPV1) is found to interact with a bound capsaicin to stabilize its binding; mutating this residue to an alanine substantially right-shifts the concentration dependent curve of capsaicin (Hazan, Kumar et al. 2015). Fluorescence resonance energy transfer (FRET) experiments combined with computational modeling methods showed that binding of capsaicin inside the vanilloid binding pocket triggers a conformational wave that propagates through the S4-S5 linker to the S6 bundle and further induces a conformational change in the selectivity filter (Yang, Xiao et al. 2015, Yang, Xiao et al. 2018).

TRPV1 as a polymodal receptor

While it was first identified as the capsaicin receptor, TRPV1 also functions as a sensor for other noxious stimuli, such as high temperature, low pH, toxins from venomous animals and poisonous

plants (Caterina, Schumacher et al. 1997, Julius 2013). It also exhibits weak voltage sensitivity (Figure 2A), which makes TRPV1's response to a stimulus variable according to the state of the host sensory neuron (Matta and Ahern 2007, Yang, Xu et al. 2020). Voltage activation of TRPV1 does not occur within the physiologically relevant range (the half-activation voltage, V_{half}, being above +60 mV) (Figure 2B). Nonetheless, it is anticipated that under physiological conditions, transmembrane voltage changes may modulate TRPV1 activity induced by other stimuli.

The activation threshold temperature of TRPV1 is around 40°C, with a Q_{10} (a parameter for temperature dependence defined as folds change in activity upon a 10 ℃ rise in temperature) value over 20 (Cao, Cordero-Morales et al. 2013). This high Q_{10} value and the threshold temperature suggest that TRPV1 can serve as a body temperature sensor involved in both sensing noxious high temperatures and regulating the body core temperature. The structural mechanism for temperature sensing in TRPV1 is still not resolved. Lowering extracellular pH (a.k.a., increasing extracellular proton concentration) below pH6.5 activates TRPV1, indicating protons can be an endogenous activator for TRPV1. Protonation of two key residues, E600 and E648 (of rat TRPV1), have been suggested as proton-sensing residues (Jordt, Tominaga et al. 2000, Zhang, Julius et al. 2021).

Ion selectivity

When TRPV1 is activated, it allows both mono- and di-valent cations to pass through the open pore. As a non-selective cation channel, TRPV1 causes membrane depolarization when it is activated, which in turn activates voltage-gated sodium channels to initiate action potential firing (Goldstein, Katz et al. 2017). The permeabilities of TRPV1 to Li^+, Na^+, K^+, Rb^+, Cs^+ are nearly equal (Bevan, Quallo et al. 2014), whereas the permeabilities to divalent cations such as Ca^{2+} and Mg^{2+} are higher compared with that for Na^+ (with a P_{Ca}/P_{Na} value of about 5 and a P_{Mg}/P_{Na} value of about 10). TRPV1 also exhibits permeability to larger cations including N-Methyl-D-glucamine

（NMDG), Tetraethylammonium (TEA), and polyamines. It is reported that different stimuli or extended activation may cause changes in the ion selectivity property of TRPV1 (Chung, Güler et al. 2008). It is found that the outer pore domain contributes to the dynamic process of ion selectivity (Munns, Chung et al. 2015).

Desensitization

TRPV1 utilizes multiple desensitization mechanisms to prevent overloading cells with influx cations when a lasting stimulus is present. One desensitization mechanism is Ca^{2+} dependent. Repeated or extended activation of TRPV1 by capsaicin or other stimuli without chelating the intracellular calcium leads to gradually reduced responses (Lishko, Procko et al. 2007). Desensitized TRPV1 in the presence of intracellular Ca^{2+} exhibits a reduced apparent binding affinity for capsaicin (Vyklický, Nováková-Tousová et al. 2008). It is also reported that extended ligand activation and calcium influx can induce channel internalization, leaving less TRPV1 channels in the plasma membrane (Sanz-Salvador, Andrés-Borderia et al. 2012). Substantial calcium influx may produce cytotoxicity and degeneration of nerve termini (Chung and Campbell 2016). Desensitization and internalization of TRPV1 as well as degeneration of TRPV1-expressing nerve termini may help explain that capsaicin patch can relieve pain in muscles and joints. Interestingly, TRPV1 also shows heat dependent desensitization following heat activation even in the absence of calcium, suggesting a distinct mechanism (Cao, Ma et al. 2014, Yang, Ma et al. 2014). This type of desensitization can also be channel species dependent; for example, platypus TRPV1 channel lacks this heat dependent desensitization (Luo, Wang et al. 2019).

TRPV1 Physiology

Expression and splice variants

TRPV1 is mainly expressed in primary sensory neurons, located in both the cell body and the nerve endings, for sensing noxious stimuli. However, expression of TRPV1 is not limited to sensory neurons. Its expression has been reported in central nervous system (both neurons and glia in the brain), muscles, skin, endothelium cells, epithelium cells, immune cells and adipose tissues(Shuba 2020). Expression of TRPV1 in the brain appears to be rather restricted to hypothalamus (Cavanaugh, Chesler et al. 2011).

As a eukaryotic membrane protein, TRPV1 is controlled by alternative splicing. There are multiple human *Trpv1* gene splice variants, four of which generate identical proteins with 839 amino acids. This is the canonical TRPV1 channel (Dorfman, Tsui et al. 2010, Schumacher and Eilers 2010). A TRPV1b variant (lack exon 7) has been reported which can also form a functional channel. The TRPV1b channel is resistant to capsaicin and protons but is responsive to heat, with a higher temperature threshold (>47°C) compared to the canonical form. When co-expressed with the canonical TRPV1, TRPV1b exhibits a dominant negative effect, suggesting co-assembly of the canonical and variant subunits into heteromeric channels (Lu, Henderson et al. 2005). It is known that TRPV1 subunits are capable of co-assembling with subunits of other TRPV types (Cheng , Yang et al. 2007, Cheng, Yang et al. 2012), further expanding TRPV1 functional diversity (Cheng, Sun et al. 2010).

At least three murine TRPV1 variants have been reported. One of them is TRPV1beta, equivalent to human TRPV1b, with exon 7 being recognized as an intron (Wang, Hu et al. 2004). A second variant is VR.5'sv, which lacks most of the N terminal. A third variant, named TRPV1var, contains only a portion of N terminal intracellular part. The last two variants do not form functional channels by themselves, but are reported to show a dominant negative effect over the canonical form when co-expressed (Tian, Fu et al. 2006, Eilers, Lee et al. 2007).

Temperature sensation and regulation

One major physiological role of TRPV1 is sensing noxious high temperatures (threshold 40-42°C). Strong heat activation of TRPV1 generates pain sensation by depolarizing the membrane potential in primary sensory neurons in the dorsal root ganglia and trigeminal ganglia. It should be noted that, TRPV1 probably is not the only high temperature sensor. Indeed, TRPV1 knock out mice still exhibit robust heat responses (Caterina, Leffler et al. 2000). Transient receptor potential cation channel, subfamily A member 1 (TRPA1), Transient receptor potential cation channel subfamily M member 2 (TRPM2) and Transient receptor potential cation channel subfamily M member 3 (TRPM3) are also reported to be involved in heat sensing (Vandewauw, De Clercq et al. 2018, Vilar, Tan et al. 2020).

Besides sensing noxious high temperatures, TRPV1 is also involved in body temperature regulation. TRPV1 knock out mice experience prolonged hyperthermia when exposed to ambient temperatures above 35°C; in comparison, wildtype mice only exhibit transient hyperthermia (Yonghak, Miyata et al. 2020). Subcutaneous injection of capsaicin induces acute hypothermia in rat; the effect exhibits a clear dose-dependent manner (Hori 1984); similar effects have been reported for other TRPV1 agonists such as resiniferatoxin. On the other hand, systemic administration of TRPV1 antagonists can induce hyperthermia in laboratory mammals (Garami, Shimansky et al. 2020).

Target for plant and animal toxins

Since activation of TRPV1 can induce strong pain sensation, TRPV1 has been the target for many plant and animal toxins. Capsaicin and resiniferatoxin (produced by resin spurge *Euphorbia resinifera*) are good examples of the protective role in plants against fungal infection (Tewksbury,

Reagan et al. 2008) and animal herbivory (Han, Li et al. 2018). Humans appear to be the only animal enjoying the spiciness sensation elicited by consuming spicy food, which is clearly an acquired behavior through learning. For most animals the spicy sensory from consuming chili peppers is clearly repulsive. For these animals, a spicy diet appears to elicit a hot and painful sensation. Certain animals, such as tree shrew and birds, eat plants containing capsaicinoids. It is found that in these animals, the TRPV1 channels are much less sensitive to capsaicin, due to point mutations to the key hydrogen bond forming residues mentioned earlier (Jordt and Julius 2002, Han, Li et al. 2018). It is hypothesized that the genetic changes may be driven by the beneficial outcome: birds get food whereas the chili pepper seeds get spread around in the process (together with fertilizer!).

Like plants, certain venomous animals generate peptide toxins in their venoms that target TRPV1, for either hunting or protecting themselves from predators. Double-knot toxin (DkTx) from Chinese bird spider *Ornithoctonus huwena* and red head toxin (RhTx) from Chinese red-headed centipede *Scolopendra subspinipes mutilans* are good examples of peptide toxins targeting TRPV1 as potent agonists (Cao, Liao et al. 2013, Yang, Yang et al. 2015). These toxins bind to the outer pore region of TRPV1 to induce strong activation. It is anticipated that the pain produced by strong TRPV1 activation would send a deterrent signal.

Regulation of blood vessel tone

TRPV1 is expressed in smooth muscle cells, endothelial cells and peri-vascular nerves where the channel participates in the regulation of vascular tone and blood pressure (Baylie and Brayden 2011, Storozhuk, Moroz et al. 2019). In endothelia cells, TRPV1 can be activated by endocannabinoids and contribute to vasodilation. Capsaicin has been reported to evoke constriction in skeleton muscle arteries and carotid artery (Tóth, Czikora et al. 2013). Long-term

use of capsaicin has been shown to have the effect of reducing hypertension induced by long-term high-salt diet (Hao, Chen et al. 2011). The mechanism for regulating vasoconstriction and blood pressure may be linked to downstream effects of TRPV1 activation, such as activating substance P (SP) and calcitonin gene related peptide (CGRP) release, nitrogen oxide (NO) generation (Du, Liao et al. 2019) .

TRPV1 Pharmacology

Ligand regulation of TRPV1

As a nociceptor, TRPV1 has attracted substantial attention as a potential target of new drugs for pain relief and anesthesia. In support of these efforts, vanilloids have been thoroughly tested for their effects on TRPV1 (Table 1). Capsaicin activates TRPV1 with an EC50 value of about 700 nM at room temperature (Figure 2C&D). Resiniferatoxin (RTX) activates TRPV1 with a reported EC50 value of about 40 nM (Raisinghani, Pabbidi et al. 2005), though the slow and irreversible binding kinetics of RTX makes estimation of the EC50 value challenging. Dermal patches containing 8% capsaicin have been approved by FDA for topical pain relief. RTX is undergoing clinical trials to treat severe pain associated with advanced cancer and osteoarthritic knee. The mechanism for capsaicin and RTX acting as pain relief agents is likely related to defunctionalization of afferent neurons and loss of unmyelinated as well as myelinated nerve fibers through cytotoxicity associated with strong activation of TRPV1.

Vanilloids produced by other plants are found to also activate TRPV1 (Figure 2D). Gingers, for example, produce a group of vanilloids that vary in molecular structures and potencies in activating TRPV1 (Yin, Dong et al. 2019). Even non-vanilloid molecules are found to activate TRPV1 by binding to the same ligand binding pocket when used at high enough concentrations; an example

is piperine, the pungent compound found in black peppers (Dong, Yin et al. 2019). Activation of TRPV1 by non-vanilloids may help explain certain flushing reactions (cutaneous vasodilation and symptoms of hot flashes and burning) in humans, for example, when patients with dyslipidemias are treated with niacin (Ma, Lee et al. 2014, Clifton, Inceoglu et al. 2015).

Vanilloids can also be strong antagonists for TRPV1 (Table 1). Capsazepine is a strong inhibitor with an IC50 value of about 400 nM (Phillips, Reeve et al. 2004). 5'-iodoresiniferatoxin is also a strong inhibitor with an IC50 of about 4 nM (Wahl, Foged et al. 2001); it has been used in animal models to inhibit TRPV1 activity. Many non-vanilloid chemicals have been explored to regulate TRPV1. Allicin can covalently modify a cystine in the N terminus of TRPV1 to activate the channel with an EC50 value of about 50 μM (Macpherson, Geierstanger et al. 2005). Allyl isothiocyanate (AITC), the pungent component in wasabi, can also activate TRPV1 as a partial agonist.

Table 1: Commonly used TRPV1 agonists, antagonists and pore blockers

category	**Name**	**EC50 OR IC50 range**
Agonist	Capsaicin	500-700 nM
	Resiniferatoxin (RTX)	10 pM-40 nM
	2-Aminoethoxydiphenyl Borate (2-APB)	110 μM
	Proton	>0.3 μM (<pH6.5)
	Allicin	50 μM
	Capsazepine	400 nM

	5'-Iodoresiniferatoxin	4 nM
Pore blocker	Ruthenium Red	—
	Barrium	0.89 mM

Challenges for targeting TRPV1 for analgesic purposes

TRPV1 plays an important role in heat sensing and body temperature regulation. While there are plenty of chemicals which can either potently activate TRPV1 or strongly inhibit its function, attempts for using TRPV1 agonists or antagonists has been hindered by the hypothermia or hyperthermia caused by these chemicals. Global administration of TRPV1 agonists such as capsaicin and RTX induces hypothermia in animal models; on the other hand, global application of TRPV1 inhibitors would induce hyperthermia. A selective TRPV1 blockade AMG517 induced hyperthermia in rats, dogs, monkeys and human trials which prevented it from systemic usage to treat pain and other diseases (Gavva, Treanor et al. 2008). New strategies need to be developed to reduce the sensitivity of TRPV1 to a specific stimulus without affecting the temperature sensing. This is indeed the goal of many ongoing promising research projects.

Conclusions and future perspectives

Being a temperature sensor and nociceptor, TRPV1 has been the subject of intense biophysical and pharmacological investigation as an attractive potential target for novel analgesics. With rapidly developing techniques and newly designed ligands, we are expecting to see more detailed research works to elucidate the mechanism of TRPV1 activation and regulation, which will guide the pharmaceutical efforts. For structural investigation, TRPV1 structures representing different

functional states are eagerly anticipated. While in the last two decades much has been learned about how capsaicin binds and activates TRPV1, how the receptor distinguishes partial and full agonists as well as antagonists is still not well understood. Much less is known about how TRPV1 responds to heat and various other stimuli. Future studies will also help to elucidate TRPV1's contributions to a wide range of physiological processes.

References

Baylie, R. L. and J. E. Brayden (2011). "TRPV channels and vascular function." Acta Physiol (Oxf) **203**(1): 99-116.

Bevan, S., T. Quallo and D. A. Andersson (2014). TRPV1. Mammalian Transient Receptor Potential (TRP) Cation Channels: Volume I. B. Nilius and V. Flockerzi. Berlin, Heidelberg, Springer Berlin Heidelberg**:** 207-245.

Bevan, S. and J. Szolcsányi (1990). "Sensory neuron-specific actions of capsaicin: mechanisms and applications." Trends Pharmacol Sci **11**(8): 330-333.

Cao, E., J. F. Cordero-Morales, B. Liu, F. Qin and D. Julius (2013). "TRPV1 channels are intrinsically heat sensitive and negatively regulated by phosphoinositide lipids." Neuron **77**(4): 667-679.

Cao, E., M. Liao, Y. Cheng and D. Julius (2013). "TRPV1 structures in distinct conformations reveal activation mechanisms." Nature **504**(7478): 113-118.

Cao, X., L. Ma, F. Yang, K. Wang and J. Zheng (2014). "Divalent cations potentiate TRPV1 channel by lowering the heat activation threshold." Journal of General Physiology **143**(1): 75-90.

Caterina, M. J., A. Leffler, A. B. Malmberg, W. J. Martin, J. Trafton, K. R. Petersen-Zeitz, M. Koltzenburg, A. I. Basbaum and D. Julius (2000). "Impaired Nociception and Pain Sensation in Mice Lacking the Capsaicin Receptor." Science **288**(5464): 306-313.

Caterina, M. J., M. A. Schumacher, M. Tominaga, T. A. Rosen, J. D. Levine and D. Julius (1997). "The capsaicin receptor: a heat-activated ion channel in the pain pathway." Nature **389**(6653): 816-824.

Cavanaugh, D. J., A. T. Chesler, A. C. Jackson, Y. M. Sigal, H. Yamanaka, R. Grant, D. O'Donnell, R. A. Nicoll, N. M. Shah and D. Julius (2011). "Trpv1 reporter mice reveal highly restricted brain distribution and functional expression in arteriolar smooth muscle cells." Journal of Neuroscience **31**(13): 5067-5077.

Cheng, W., C. Sun and J. Zheng (2010). "Heteromerization of TRP channel subunits: extending functional diversity." Protein & Cell **1**(9): 802-810.

Cheng, W., F. Yang, S. Liu, C. K. Colton, C. Wang, Y. Cui, X. Cao, M. X. Zhu, C. Sun and K. Wang (2012). "Heteromeric heat-sensitive transient receptor potential channels exhibit distinct temperature and chemical response." Journal of Biological Chemistry **287**(10): 7279-7288.

Cheng , W., F. Yang , C. L. Takanishi and J. Zheng (2007). "Thermosensitive TRPV Channel Subunits Coassemble into Heteromeric Channels with Intermediate Conductance and Gating Properties." Journal of General Physiology **129**(3): 191-207.

Cheng, Y. (2022). "TRPV1 and Piezo: the 2021 Nobel Prize in Physiology or Medicine." IUCrJ **9**(Pt 1): 4-5.

Chung, M.-K. and J. N. Campbell (2016). "Use of Capsaicin to Treat Pain: Mechanistic and Therapeutic Considerations." Pharmaceuticals **9**(4): 66.

Chung, M.-K., A. D. Güler and M. J. Caterina (2008). "TRPV1 shows dynamic ionic selectivity during agonist stimulation." Nature Neuroscience **11**(5): 555-564.

Clifton, H. L., B. Inceoglu, M. Linlin, J. Zheng and S. Schaefer (2015). "TRPV1 channels are involved in niacin-induced cutaneous vasodilation in mice." Journal of cardiovascular pharmacology **65**(2): 184.
Dong, Y., Y. Yin, S. Vu, F. Yang, V. Yarov-Yarovoy, Y. Tian and J. Zheng (2019). "A distinct structural mechanism underlies TRPV1 activation by piperine." Biochemical and Biophysical Research Communications **516**(2): 365-372.
Dorfman, R., H. Tsui, M. W. Salter and H.-M. Dosch (2010). TRPV1 genetics, J Wiley & Sons, Hoboken, NJ.
Du, Q., Q. Liao, C. Chen, X. Yang, R. Xie and J. Xu (2019). "The Role of Transient Receptor Potential Vanilloid 1 in Common Diseases of the Digestive Tract and the Cardiovascular and Respiratory System." Frontiers in Physiology **10**.
Eilers, H., S. Y. Lee, C. W. Hau, A. Logvinova and M. A. Schumacher (2007). "The rat vanilloid receptor splice variant VR.5'sv blocks TRPV1 activation." Neuroreport **18**(10): 969-973.
Gao, Y., E. Cao, D. Julius and Y. Cheng (2016). "TRPV1 structures in nanodiscs reveal mechanisms of ligand and lipid action." Nature **534**(7607): 347-351.
Garami, A., Y. P. Shimansky, Z. Rumbus, R. C. L. Vizin, N. Farkas, J. Hegyi, Z. Szakacs, M. Solymar, A. Csenkey, D. A. Chiche, R. Kapil, D. J. Kyle, W. D. Van Horn, P. Hegyi and A. A. Romanovsky (2020). "Hyperthermia induced by transient receptor potential vanilloid-1 (TRPV1) antagonists in human clinical trials: Insights from mathematical modeling and meta-analysis." Pharmacology & Therapeutics **208**: 107474.
Gavva, N. R., J. J. Treanor, A. Garami, L. Fang, S. Surapaneni, A. Akrami, F. Alvarez, A. Bak, M. Darling and A. Gore (2008). "Pharmacological blockade of the vanilloid receptor TRPV1 elicits marked hyperthermia in humans." Pain **136**(1-2): 202-210.
Goldstein, R. H., B. Katz, S. Lev and A. M. Binshtok (2017). "Ultrafast optical recording reveals distinct capsaicin-induced ion dynamics along single nociceptive neurite terminals in vitro." J Biomed Opt **22**(7): 76010.
Han, Y., B. Li, T. T. Yin, C. Xu, R. Ombati, L. Luo, Y. Xia, L. Xu, J. Zheng, Y. Zhang, F. Yang, G. D. Wang, S. Yang and R. Lai (2018). "Molecular mechanism of the tree shrew's insensitivity to spiciness." PLoS Biol **16**(7): e2004921.
Hao, X., J. Chen, Z. Luo, H. He, H. Yu, L. Ma, S. Ma, T. Zhu, D. Liu and Z. Zhu (2011). "TRPV1 activation prevents high-salt diet-induced nocturnal hypertension in mice." Pflügers Archiv - European Journal of Physiology **461**(3): 345-353.
Hazan, A., R. Kumar, H. Matzner and A. Priel (2015). "The pain receptor TRPV1 displays agonist-dependent activation stoichiometry." Scientific reports **5**(1): 1-13.
Hori, T. (1984). "Capsaicin and central control of thermoregulation." Pharmacol Ther **26**(3): 389-416.
Jordt, S.-E., M. Tominaga and D. Julius (2000). "Acid potentiation of the capsaicin receptor determined by a key extracellular site." Proceedings of the National Academy of Sciences **97**(14): 8134-8139.
Jordt, S. E. and D. Julius (2002). "Molecular basis for species-specific sensitivity to "hot" chili peppers." Cell **108**(3): 421-430.
Julius, D. (2013). "TRP channels and pain." Annual review of cell and developmental biology **29**: 355-384.
Kraft, K. H., C. H. Brown, G. P. Nabhan, E. Luedeling, J. d. J. Luna Ruiz, G. Coppens d'Eeckenbrugge, R. J. Hijmans and P. Gepts (2014). "Multiple lines of evidence for the origin of domesticated chili pepper, Capsicum annuum, in Mexico." Proceedings of the National Academy of Sciences **111**(17): 6165-6170.
Kwon, D. H., F. Zhang, Y. Suo, J. Bouvette, M. J. Borgnia and S.-Y. Lee (2021). "Heat-dependent opening of TRPV1 in the presence of capsaicin." Nature Structural & Molecular Biology **28**(7): 554-563.
Lishko, P. V., E. Procko, X. Jin, C. B. Phelps and R. Gaudet (2007). "The ankyrin repeats of TRPV1 bind multiple ligands and modulate channel sensitivity." Neuron **54**(6): 905-918.
Lu, G., D. Henderson, L. Liu, P. H. Reinhart and S. A. Simon (2005). "TRPV1b, a functional human vanilloid receptor splice variant." Mol Pharmacol **67**(4): 1119-1127.

Luo, L., Y. Wang, B. Li, L. Xu, P. M. Kamau, J. Zheng, F. Yang, S. Yang and R. Lai (2019). "Molecular basis for heat desensitization of TRPV1 ion channels." Nature Communications **10**(1): 2134.
Ma, L., B. H. Lee, R. Mao, A. Cai, Y. Jia, H. Clifton, S. Schaefer, L. Xu and J. Zheng (2014). "Nicotinic acid activates the capsaicin receptor TRPV1: Potential mechanism for cutaneous flushing." Arteriosclerosis, thrombosis, and vascular biology **34**(6): 1272-1280.
Macpherson, L. J., B. H. Geierstanger, V. Viswanath, M. Bandell, S. R. Eid, S. Hwang and A. Patapoutian (2005). "The pungency of garlic: activation of TRPA1 and TRPV1 in response to allicin." Curr Biol **15**(10): 929-934.
Matta, J. A. and G. P. Ahern (2007). "Voltage is a partial activator of rat thermosensitive TRP channels." The Journal of physiology **585**(2): 469-482.
Montell, C., L. Birnbaumer, V. Flockerzi, R. J. Bindels, E. A. Bruford, M. J. Caterina, D. E. Clapham, C. Harteneck, S. Heller, D. Julius, I. Kojima, Y. Mori, R. Penner, D. Prawitt, A. M. Scharenberg, G. Schultz, N. Shimizu and M. X. Zhu (2002). "A unified nomenclature for the superfamily of TRP cation channels." Mol Cell **9**(2): 229-231.
Munns, C. H., M.-K. Chung, Y. E. Sanchez, L. M. Amzel and M. J. Caterina (2015). "Role of the outer pore domain in transient receptor potential vanilloid 1 dynamic permeability to large cations." Journal of Biological Chemistry **290**(9): 5707-5724.
Nelson, E. K. and L. E. Dawson (1923). "THE CONSTITUTION OF CAPSAICIN, THE PUNGENT PRINCIPLE OF CAPSICUM. III." Journal of the American Chemical Society **45**(9): 2179-2181.
Phillips, E., A. Reeve, S. Bevan and P. McIntyre (2004). "Identification of species-specific determinants of the action of the antagonist capsazepine and the agonist PPAHV on TRPV1." Journal of Biological Chemistry **279**(17): 17165-17172.
Raisinghani, M., R. M. Pabbidi and L. S. Premkumar (2005). "Activation of transient receptor potential vanilloid 1 (TRPV1) by resiniferatoxin." J Physiol **567**(Pt 3): 771-786.
Sanz-Salvador, L., A. Andrés-Borderia, A. Ferrer-Montiel and R. Planells-Cases (2012). "Agonist- and Ca2+-dependent desensitization of TRPV1 channel targets the receptor to lysosomes for degradation." J Biol Chem **287**(23): 19462-19471.
Schumacher, M. A. and H. Eilers (2010). "TRPV1 splice variants: structure and function." Front Biosci (Landmark Ed) **15**(3): 872-882.
Scoville, W. L. (1912). "Note on Capsicums." The Journal of the American Pharmaceutical Association (1912) **1**(5): 453-454.
Shuba, Y. M. (2020). "Beyond Neuronal Heat Sensing: Diversity of TRPV1 Heat-Capsaicin Receptor-Channel Functions." Front Cell Neurosci **14**: 612480.
Storozhuk, M. V., O. F. Moroz and A. V. Zholos (2019). "Multifunctional TRPV1 Ion Channels in Physiology and Pathology with Focus on the Brain, Vasculature, and Some Visceral Systems." BioMed Research International **2019**: 5806321.
Szallasi, A. and P. M. Blumberg (1999). "Vanilloid (Capsaicin) receptors and mechanisms." Pharmacol Rev **51**(2): 159-212.
Tewksbury, J. J., K. M. Reagan, N. J. Machnicki, T. A. Carlo, D. C. Haak, A. L. C. Peñaloza and D. J. Levey (2008). "Evolutionary ecology of pungency in wild chilies." Proceedings of the National Academy of Sciences **105**(33): 11808-11811.
Thresh, L. (1846). "Isolation of capsaicin." Pharm J **6**: 941.
Tian, W., Y. Fu, D. H. Wang and D. M. Cohen (2006). "Regulation of TRPV1 by a novel renally expressed rat TRPV1 splice variant." Am J Physiol Renal Physiol **290**(1): F117-126.
Tóth, A., Á. Czikora, E. T. Pásztor, B. Dienes, P. Bai, L. Csernoch, I. Rutkai, V. Csató, I. S. Mányiné, R. Pórszász, I. Édes, Z. Papp and J. Boczán (2013). "Vanilloid Receptor-1 (TRPV1) Expression and Function in the Vasculature of the Rat." Journal of Histochemistry & Cytochemistry **62**(2): 129-144.

Vandewauw, I., K. De Clercq, M. Mulier, K. Held, S. Pinto, N. Van Ranst, A. Segal, T. Voet, R. Vennekens, K. Zimmermann, J. Vriens and T. Voets (2018). "A TRP channel trio mediates acute noxious heat sensing." Nature **555**(7698): 662-666.
Vilar, B., C.-H. Tan and P. A. McNaughton (2020). "Heat detection by the TRPM2 ion channel." Nature **584**(7820): E5-E12.
Vyklický, L., K. Nováková-Tousová, J. Benedikt, A. Samad, F. Touska and V. Vlachová (2008). "Calcium-dependent desensitization of vanilloid receptor TRPV1: a mechanism possibly involved in analgesia induced by topical application of capsaicin." Physiol Res **57 Suppl 3**: S59-s68.
Wahl, P., C. Foged, S. Tullin and C. Thomsen (2001). "Iodo-resiniferatoxin, a new potent vanilloid receptor antagonist." Molecular pharmacology **59**(1): 9-15.
Wang, C., H. Z. Hu, C. K. Colton, J. D. Wood and M. X. Zhu (2004). "An alternative splicing product of the murine trpv1 gene dominant negatively modulates the activity of TRPV1 channels." J Biol Chem **279**(36): 37423-37430.
Yang, F., L. Ma, X. Cao, K. Wang and J. Zheng (2014). "Divalent cations activate TRPV1 through promoting conformational change of the extracellular region." Journal of General Physiology **143**(1): 91-103.
Yang, F., X. Xiao, W. Cheng, W. Yang, P. Yu, Z. Song, V. Yarov-Yarovoy and J. Zheng (2015). "Structural mechanism underlying capsaicin binding and activation of the TRPV1 ion channel." Nat Chem Biol **11**(7): 518-524.
Yang, F., X. Xiao, B. H. Lee, S. Vu, W. Yang, V. Yarov-Yarovoy and J. Zheng (2018). "The conformational wave in capsaicin activation of transient receptor potential vanilloid 1 ion channel." Nature communications **9**(1): 1-9.
Yang, F., L. Xu, B. H. Lee, X. Xiao, V. Yarov‐Yarovoy and J. Zheng (2020). "An unorthodox mechanism underlying voltage sensitivity of TRPV1 ion channel." Advanced Science **7**(20): 2000575.
Yang, F. and J. Zheng (2017). "Understand spiciness: mechanism of TRPV1 channel activation by capsaicin." Protein & cell **8**(3): 169-177.
Yang, S., F. Yang, N. Wei, J. Hong, B. Li, L. Luo, M. Rong, V. Yarov-Yarovoy, J. Zheng, K. Wang and R. Lai (2015). "A pain-inducing centipede toxin targets the heat activation machinery of nociceptor TRPV1." Nat Commun **6**: 8297.
Yin, Y., Y. Dong, S. Vu, F. Yang, V. Yarov-Yarovoy, Y. Tian and J. Zheng (2019). "Structural mechanisms underlying activation of TRPV1 channels by pungent compounds in gingers." Br J Pharmacol **176**(17): 3364-3377.
Yonghak, P., S. Miyata and E. Kurganov (2020). "TRPV1 is crucial for thermal homeostasis in the mouse by heat loss behaviors under warm ambient temperature." Scientific Reports **10**(1): 8799.
Yu, F. H. and W. A. Catterall (2004). "The VGL-Chanome: A Protein Superfamily Specialized for Electrical Signaling and Ionic Homeostasis." Science's STKE **2004**(253): re15.
Zhang, K., D. Julius and Y. Cheng (2021). "Structural snapshots of TRPV1 reveal mechanism of polymodal functionality." Cell **184**(20): 5138-5150. e5112.
Zheng, J. and L. Ma (2014). Chapter Nine - Structure and Function of the ThermoTRP Channel Pore. Current Topics in Membranes. L. D. Islas and F. Qin, Academic Press. **74:** 233-257.

Figures and legends

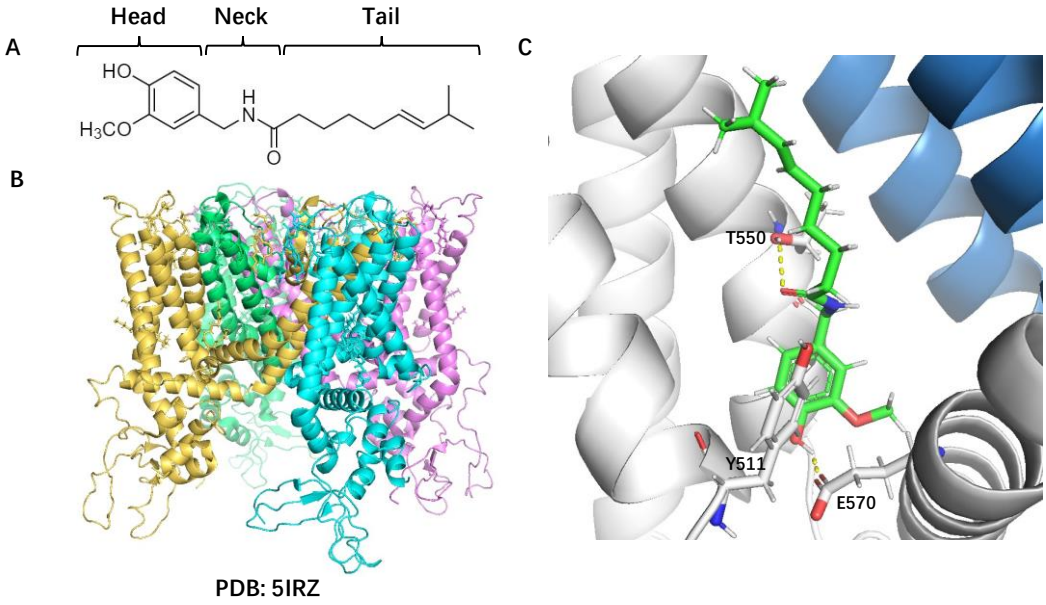

Figure 1. Molecular interactions between capsaicin and TRPV1. A. Molecular structure of capsaicin. B. Cryo-EM structure of rat TRPV1 determined in lipid nanodisc (PDB entry code 5IRZ). Each subunit is colored differently. C. The vanilloid binding pocket with a bound capsaicin. Key interacting residues are highlighted. Hydrogen bonds are indicated by a yellow dash line.

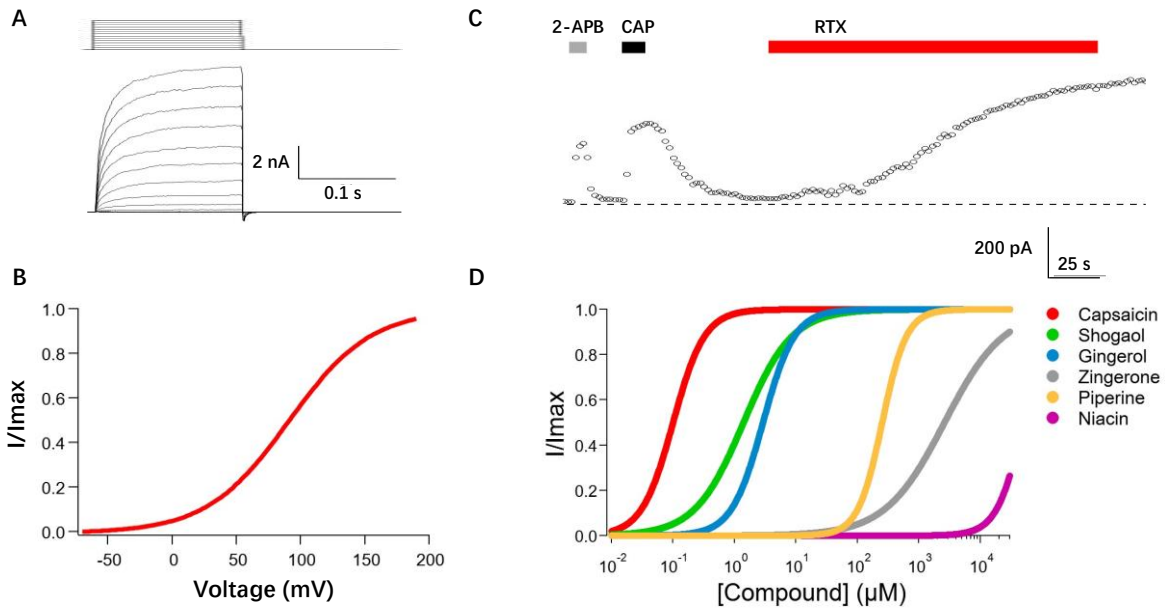

Figure 2. Ligand and voltage activation of TRPV1. A. Whole-cell recording of mouse TRPV1 activated by depolarization from a -80 mV holding potential up to +200 mV in 20 mV steps. B. G-V curve of voltage-dependent activation. C. An inside-out patch-clamp recording of mouse TRPV1 activated by 30 mM 2-APB, 10 μM capsaicin, and 100 nM RTX, at +80 mV. Current induced by 2-APB and capsaicin are fully reversible, whereas RTX-induced current is irreversible. Dash line indicates the zero current level. D. Concentration dependence of several TRPV1 agonists from natural products.

Chapter II: Opening of capsaicin receptor TRPV1 is Stabilized Equally by Its Four Subunits

Shisheng Li, Phuong Tran Nguyen, Simon Vu, Vladimir Yarov-Yarovoy, Jie Zheng

Abstract: Capsaicin receptor TRPV1 is a nociceptor for vanilloid molecules such as capsaicin and resiniferatoxin (RTX). Even though cryo-EM structures of TRPV1 in complex with these molecules are available, how their binding energetically favors the open conformation is not known. Here we report an approach to control the number of bound RTX molecules (0-to-4) in functional rat TRPV1. The approach allowed direct measurements of each of the intermediate open states under equilibrium conditions at both macroscopic and single-molecule levels. We found that RTX binding to each of the four subunits contributes virtually the same activation energy, which we estimated to be 1.70-to-1.86 kcal/mol and found to arise predominately from destabilizing the closed conformation. We further showed that sequential bindings of RTX increase open probability without altering single-channel conductance, confirming that there is likely a single open-pore conformation for TRPV1 activated by RTX.

Introduction: Allosteric coupling links structurally separate function domains together through a global conformational rearrangement which, in protein complexes, introduces cooperativity (1). Cooperative activation can substantially enhance the sensitivity to a stimulus, hence bestows a significant functional advantage to multi-subunit complexes. Indeed, multi-subunit complex formation is a common phenomenon in biology (2). Even though diverse models have been satisfactorily used to describe the overall cooperative behavior in protein complexes (3, 4), it remains a major challenge to directly access cooperative activation among subunits as it occurs, limiting our understanding of the underlying mechanism. The Monod-Wyman-Changeux (MWC) model proposed over half a century ago (3) postulates that ligand binding to individual subunits

promotes a concerted activation transition by an identical cooperative factor, f, which reflects energetic contribution by each subunit (Fig. 1A). However, exactly because of cooperative activation, the intermediate states (shaded in Fig. 1A) are rapidly traversed; their energetic contributions are rarely determined individually. Reflecting this challenge, a common practice has been to fit observed overall activities to a Hill function, yielding a slope factor estimate that is neither the cooperative factor nor the number of subunits but their combined contribution (5).

Biological ion channels are usually made of multiple, functionally coupled subunits or repeating domains (6, 7). The capsaicin (CAP) receptor TRPV1 is a representative multi-subunit ion channel (8, 9) whose activation exhibits allosteric properties (10-13). TRPV1 is known to serve as a polymodal nociceptor; its activation by vanilloids has been investigated in both functional and structural studies (14). Vanilloid compounds occupy a binding pocket within the transmembrane region surrounded by multiple transmembrane segments and the S4-S6 linker (9). In a typical recording of the mouse TRPV1 activated by CAP, current amplitude reached over 90% maximum within hundreds of milliseconds (Fig. S1). Even though this activation process is slow among ion channels, the intermediate states were swiftly traversed and could not be individually identified and studied (15). Methods to slow down activation and to fix gating transition in individual subunits were developed in this study, which allowed direct assessment of the property of intermediate states and subunit coupling at equilibrium under physiological conditions.

Results: We first used resiniferatoxin (RTX), a potent TRPV1 activator (8), to replace CAP as the agonist. RTX binds in the same vanilloid binding pocket as CAP (9) but activates the channel with an extremely slow (in minutes) time course; RTX-induced activation is also irreversible (Fig. 1B). The slow activation time course revealed a clear transition phase of increasing open probability in single-channel recordings (Fig. 1C and 1F), indicating sojourns in unstable intermediate open

states as suggested by the MWC model. However, these transient and stochastic events were observed under non-equilibrium conditions, hence were still difficult to analyze.

From the RTX-TRPV1 complex structures (9, 16), we identified key channel residues that directly interact with a bound RTX (Fig. S2). Mutations to these residues in most cases either exerted minor gating effects or eliminated function (Fig. S3). Mutating Y512 to alanine retained the slow activation property of the wild-type channel but noticeably made RTX activation completely reversible (Fig. 1D). We have previously suggested that Y512 serves to physically block a bound vanilloid molecule from exiting the binding pocket (17), in agreement with structural (16) and functional (18) observations. Molecular docking of RTX to TRPV1 structures in the closed (C1 and C2) and open (O1) states using RosettaLigand (19, 20) suggested reductions in Rosetta binding energy by this point mutation, in supportive of weakening of RTX binding (Fig. S4). After washing off RTX, Y512A channels could be activated by 2-APB, CAP and RTX similar to naïve channels without detectable desensitization (under the Ca2+-free condition). Single-channel recordings confirmed that Y512A traversed the transition phase during both activation and deactivation time courses (Fig. 1E&G; see also Fig. S5).

Taking advantage of the reversibility property of the Y512A mutant, we studied rat TRPV1 concatemers containing different numbers of wildtype and Y511A mutant (equivalent to Y512A in mouse TRPV1) subunits (Fig. 2A). These concatemer channels were previously shown to respond to CAP in a concentration-dependent manner, with the CAP potency progressively decreased as the number of mutant protomers increased (21). We confirmed that the spontaneous open probability of each concatemer matched that of wildtype channels (Fig. 2D&E). We observed with macroscopic (Fig. 2B) and single-channel recordings (Fig. S6) that RTX could fully activate all concatemer channels. Importantly, currents from these concatemers exhibited gradually

enhanced reversibility upon washing off RTX, with channels containing all or three wildtype subunits (YYYY and YYYA, respectively) exhibiting little current deactivation, whereas those with all Y511A subunits (AAAA) exhibiting complete deactivation like channels formed by unlinked monomeric mouse Y512A subunits (see Fig. 1D). We further confirmed that the remaining currents were not due to an unstable patch (Fig. 2B) but instead represented steady intermediate open probabilities (Fig. 2C; see also Fig. S6). These behaviors are expected as RTX binding to the Y511A subunits in concatemers is reversible, but irreversible when bound to the wildtype subunits. Therefore, after extended washing, the concatemer channels contained a fixed number (zero to four) of bound RTX molecules.

The concatemers allowed us to characterize each vertical equilibrium of the MWC model (Fig. 1A) in isolation. For example, after fully activating the YYAA channels and washing off RTX from the mutant subunits, each channel contained two RTX molecules (the third column of the model). The open probability (Po) value of these channels could be determined from both macroscopic currents (77 ± 3% of the maximum response; Fig. 2D) and single-channel currents (62 ± 10%; Fig. 2E) at the steady state. Po estimates for YYYY and AAAA channels matched those from channels made of wildtype and mutant monomeric subunits, respectively (Fig. 2D&E). The Po measurements from all concatemers could be satisfactorily fitted to a general formula derived from the MWC model that describes the relationship between Po and the number of bound ligands (Fig. 2F). Transformation of the formula yields a linear function that allows easy estimation of the equilibrium constant of unliganded channels, L0, and the cooperative factor, f. Fig. 2G shows results from the single-channel data. We estimated the L0 value to be 0.007, equivalent to a resting Po of 0.7%, which is consistent with experimental observations from wildtype channels (22); we

estimated the f value to be 23.1, equivalent to an activation energy of 1.86 kcal/mol per RTX binding (Fig. 2G).

It is noticed that a linear fit agreed with experimental measurements remarkably well, suggesting that subunit contributions to activation are indeed equal, as postulated by the MWC theorem. The position of wildtype and mutant subunits within the concatemers had no obvious influence on the activation energy, as data from concatemers YAYA and AYAY agreed reasonably well with that from YYAA (Fig. 2G; see also Fig.S7), an observation consistent with the new cryo-EM data showing that RTX binding has no position preference (16).

Where does the 1.86 kcal/mol activation energy arise from? For the isolated transition shown in Fig. 2F, the equilibrium can be altered at either the closed or the open state, both of which could contribute to an increased equilibrium constant. To quantify energetic effects of RTX binding to the closed and open state, we analyzed single-channel dwell-time distributions of the concatemers at steady state (Fig. 3). When results from all concatemers were compared, we found that the mean dwell-time of the closed state decreased exponentially with an increasing number of bound RTX, whereas the mean dwell-time of the open state increased exponentially (Fig. 3B). Equilibrium constant values estimated from dwell-time measurements matched closely with those estimated from open probability measurements (Fig. 3C). From linear fittings of the log-transformed dwell-times (Fig. 3B), we estimated that each RTX binding destabilized the closed state by 1.17 kcal/mol, stabilized the open state by 0.53 kcal/mol, therefore producing a total of 1.70 kcal/mol of activation energy. Therefore, activation of TRPV1 by RTX originates predominately from destabilization of the closed state.

Measurements from the concatemers revealed the Po values with 0-to-4 bound RTX molecules. Using this information, we could tentatively identify the intermediate open states produced by

sequential bindings of RTX during the course of activation. A typical time course of the wildtype channel single-channel activation exhibited distinct open states with low, moderate, and high Po values, corresponding to one, two, and three or four bound RTX molecules, respectively (Fig. 4A). All these open states, observed in the same single-channel recording, exhibited identical amplitudes (Fig. 4B&C). Similar observations were made from the concatemers. This finding is consistent with the classic MWC model in which the multi-subunit complex exists in two (tense and relaxed) conformations, with ligand binding progressively shifting the equilibrium towards the relaxed, a.k.a. open, conformation (3). Our results suggest that TRPV1 activated by RTX has a single open pore conformation.

Discussion: Previously we reported that structurally related natural vanilloids from chili peppers and gingers as well as synthetic capsaicin derivatives induce similar conformational changes of the vanilloid binding pocket of TRPV1, even though they may bind in different poses (23-25). We now present data suggesting that the activated channel pore adopts the same open conformation when a varying number of vanilloid binding pockets are occupied by RTX, consistent of pore opening being a concerted transition. Putting together, these observations support the general assumption that TRPV1 behaves as an allosteric protein (10-13). By fixing the number of bound RTX molecules, we were able to directly quantify equilibrium properties from otherwise unstable intermediate states at both macroscopic and single-molecule resolutions. We observed binding of RTX to each of the four subunits yielded an equal activation energy, as predicted by the classic MWC model for homotropic cooperativity. A recent structural study of RTX-TRPV1 complexes indeed suggested non-preference in RTX binding to the four subunits (16). The activation energy, estimated at 1.70-to-1.86 kcal/mol per liganded subunit, is comparable to that of other channels such as CNG channels (0.84-to-1.3 kcal/mol) determined indirectly from overall ligand activation

behaviors (26, 27). The comparable maximal Po of capsaicin-activated channels indicates that capsaicin binding is expected to produce a similar activation energy (17). Combining the activation energies from multiple subunits contributes to an exponential increase in open probability (the 1.86 X 4 = 7.44 kcal/mol activation energy shifts the closed-to-open equilibrium toward the open state by over 280000 folds) (Fig. 4D). For TRPV1 activated by RTX, the shift in equilibrium originates mostly from destabilization of the closed state.

Energetic contributions from the four subunits represent substantial activation cooperativity in TRPV1. Indeed, cooperative activation is a common phenomenon for diverse allosteric proteins. However, a general challenge for studying a cooperative process is to capture the intermediate states with either functional or structural methods. In the absence of direct information concerning the intermediate states, a mechanistic interpretation is often speculative. The Monod-Wyman-Changeux (MWC) model for allosteric proteins made of identical subunits (3) has been successfully applied to a wide variety of proteins including those made of different subunits. Nonetheless, equivalence in subunit contributions, a key feature distinguishing it from a Koshland-Némethy-Filmer (KNF)-type sequential model (28), remains a postulation. One key validation of the MWC theorem—measuring directly from the intermediate activation states—has been lacking, due to cooperativity among subunits that makes transitional states intrinsically unstable. Here we designed methods locking TRPV1 in each of the intermediate activation states with varying ligand occupations, which allowed direct measurements of their thermodynamic properties under physiological conditions at equilibrium. Near-perfect equivalence in subunit contribution to allosteric coupling was confirmed.

All RTX-induced open states are found to produce identical single-channel current amplitudes, suggesting the activated pore adopts near identical conformations. Therefore, pore opening by

RTX appears to be driven by a concerted conformational change. Our functional data hence suggest that structural asymmetry of the activated states occurs mainly in the vanilloid binding pockets, consistent with the recently reported RTX-TRPV1 complex structures (16). Based on the 1.86 kcal/mol/subunit activation energy, channels with 1-to-4 bound RTX molecules are expected to exhibit an open probability of 13.9%, 78.9%, 98.8% and 99.9%, respectively. Channels with two bound RTX molecules already spend two-third of the time in the open state under physiological conditions. Only the fully RTX-bound channels exhibited an open pore conformation in cryo-EM studies (16, 29), suggesting a shift in stability of the closed and/or open conformation under these experimental conditions, such as lower temperatures (22).

Concerted pore opening has been previously proposed for other channel types including Kv channels, for which independent voltage-sensor movements in the four subunits precede channel activation (30, 31). Very brief (microseconds) subconductance states were found to be associated with asymmetrical subunit activations by voltage, hence representing intermediate gating states (32, 33). It was proposed that subconductance states could arise from filtering effects on very rapid flickering events—representing likely a concerted transition—between the fully open state and the closed state, with voltage-dependent subunit activations progressively shifting the equilibrium towards the open state (32). While TRPV1 activation by RTX exhibited similar progressive shifting towards the open state, dwell-times in the closed and open states appeared to be long enough to skip the filtering effect on current amplitude. The allosteric behavior described in the present study may help correlate published high-resolution channel structures (16, 34) with distinct functional states towards a better understanding of the activation mechanism of TRPV1 and other ion channels.

Materials and Methods

Cell culture and molecular biology

The mouse TRPV1 wildtype and Y512A mutant cDNAs were constructed into pEYFP-N3 vector, where the C-terminus of the channel was fused with the cDNA encoding enhanced yellow fluorescent protein (eYFP) to help to identify transfected cells during patch clamp experiments, as previously described (35). The Y512A point mutation was introduced using a mutagenesis kit (Agilent Technologies) and confirmed by sequencing. Concatemers YYYY, YYYA, YYAA, YAYA, AYAY, YAAA, and AAAA represent tandem tetrameric cDNA constructs of rat TRPV1 wildtype (Y) and Y511A (A, equivalent to Y512A in mouse channel), were generous gifts from Dr. Avi Priel and have been previously described (21).

HEK293T cells (purchased from American Type Culture Collection) were cultured in a DMEM medium (Hyclone or Gibco) supplemented with 10% (v/v) fetal bovine serum (FBS) (Corning or GenClone), 1% (v/v) penicillin/streptomycin (Fisher Scientific) and 1% (v/v) MEM Non-Essential Amino Acids Solution (Hyclone) at 37°C with 5% CO2. Cells were cultured onto 25 mm glass coverslips (Fisher Scientific) in 35 mm chambers 18-24 h before transfection. Transient transfection was conducted 18-24 h before patch-clamp recording using Lipofectamine 2000 (Invitrogen) according to the manufacturer's instructions. For macroscopic recordings, 1 μg plasmid was used for transfection for each chamber; for single-channel recordings, 0.1 μg plasmid was used. For concatemers channels without a fluorescent tag, the YFP plasmid was co-transfected (0.2 μg) for each chamber.

Electrophysiology

Patch-clamp recordings were done using an EPC10 amplifier controlled with PatchMaster software (HEKA) in configurations as specified in the Results. All single-channel recordings were from inside-out patches; most of the macroscopic recordings were also from inside-out patches; whole-cell recordings were collected to increase the macroscopic current level, especially for mutants such as E571A mTRPV1, E571AT551A mTRPV1, E571AI574A mTRPV1, due to their poor expression levels. Patch pipettes were pulled from borosilicate glass (A-M systems or Sutter Instrument) using Sutter Instrument P-97 micropipette puller and fire-polished to 2-to-6 MΩ for macroscopic recordings, or 8-to-15 MΩ for single-channel recordings. For whole-cell recordings, serial resistance was compensated by 60%. Current signal was filtered at 2.3-to-2.9 kHz and sampled at 10.0-to-12.5 kHz. All recordings were conducted at room temperature. Ruthenium red (10 μM) and/or Ba2+ (100 mM) were used to block channel current for checking leak. A holding potential of 0 mV was used, from which a 300-ms step to +80 mV followed by a 300-ms step to -80 mV was applied. The durations of the +80 mV and -80 mV steps were between 300 ms and 2 s, adjusted according to experimental needs. The voltage was held at +80 mV for long continuous single-channel recordings. Standard symmetrical bath and pipette solutions contained (mM) 140 NaCl, 0.2 EGTA, 10 glucose (optional) and 15 HEPES (pH 7.2-to-7.4). Solution switching was achieved with a Rapid Solution Changer (RSC-200, Biological Science Instruments). 2-APB was dissolved in DMSO to make 1 M stock solution and diluted to working concentrations using the bath solution; capsaicin was dissolved in DMSO to make 50 mM stock solution and diluted to working concentrations using the bath solution; RTX was dissolved in ethanol to make 1 mM stock solution and diluted to working concentrations using the bath solution. To obtain single-channel recordings with a fixed number of RTX molecules in the concatemers (YYYY, YYYA, YYAA, YAYA, AYAY, YAAA and AAAA), 3 mM 2-APB was first perfused onto an inside-out patch to

confirm the number of channels in the patch. A 100 nM RTX solution was then perfused onto the patch until Po reached the stable maximal level to make sure all the binding sites were saturated by RTX. The bath solution was perfused to wash off the reversibly bound RTX until Po reached a stable level. This Po level was regarded as the Po value when the channel was bound with 0-to-4 RTX molecules according to different concatemers (4 for YYYY; 3 for YYYA; 2 for YYAA, YAYA, AYAY; 1 for YAAA; 0 for AAAA).

Rosetta modeling of RTX binding to mutant TRPV1 channels

To evaluate RTX binding to TRPV1, we used the cryoEM structures of TRPV1 solved in complex with RTX in the open (O1 state, PDB:7l2l) and closed (C1 state, PDB: 7l2n; C2 state, PDB:7mz5) states to model RTX interaction. RosettaLigand(19) was used to dock RTX to wild-type and Y511A mutant structures for each state. We generated 2,000 RTX conformers for the docking process using BioChemical Library (BCL) (20). The detail of the docking algorithm has been described elsewhere (19) (see Appendix for Rosetta docking scripts and command lines). A total of 10,000 docking models were generated and the top 1,000 models ranked by total_score were selected for analysis. Binding energy is represented by the interface_delta_X term reported in Rosetta Energy Unit (R.E.U). All-atom root-mean-square deviation (RMSD) was used to compare the generated docking RTX models to the RTX binding conformations captured in the cryoEM structures.

Data analysis

Patch-clamp data were exported and analyzed using Igor Pro 8. Statistical analyses were done using GraphPad Prism 8. Macroscopic current amplitude was calculated by measuring the difference between ligand-activated current and the baseline current level before any ligand

perfusion. A digital filter at 0.4 kHz was used for analyzing single-channel amplitude and open probability. Single-channel recordings were analyzed using all-point histograms and fitted to a double-Gaussian function; single-channel amplitude was measured as the difference between the two gaussian peaks; single-channel open probability was measured by calculating the portion of open events over the total time recorded. Only true single-channel recordings (n = 22) or two-channel recordings (n = 2) were used. Open probability of two-channel recordings was calculated using the equation $Po = \frac{t_1+2t_2}{2T}$, where t1 is the total time of one-channel opening events observed, t2 is the total time of two-channel opening events observed, T is the total recording time. Spontaneous open probability was measured using the equation $Po = \frac{t}{NT}$, where t is the total time of the open events observed at room temperature in bath solution, N is the total number of channels in the patch which was determined by calculating the amplitude ratio between maximum current and the average single-channel current, T is the total recording time. There were no overlapping open events in these recordings. To analyze single channel dwell-times, the recorded single-channel traces were processed using the single-channel search function in Clampfit to generate dwell-time histograms (36).

Model fitting was conducted in Igor, using the global fitting procedure when needed. Statistical analysis was done using GraghPad Prism 8. Student's t-test was used when comparing between two groups. For comparisons within the same recordings, paired t-test was used. For comparison between multiple groups, one-way ANOVA with Tukey's multiple comparisons test was used.\

References:

1. J. Monod, F. Jacob, Teleonomic mechanisms in cellular metabolism, growth, and differentiation. Cold Spring Harb Symp Quant Biol 26, 389-401 (1961).

2. A. V. Hill, A. Paganini-Hill, The possible effects of the aggregation of the molecules of haemoglobin on its dissociation curves. The Journal of Physiology 40, 4-7 (1910).
3. J. Monod, J. Wyman, J. P. Changeux, On the Nature of Allosteric Transitions: A Plausible Model. J Mol Biol 12, 88-118 (1965).
4. D. E. Koshland Jr, G. Némethy, D. Filmer, Comparison of experimental binding data and theoretical models in proteins containing subunits. Biochemistry 5, 365-385 (1966).
5. J. N. Weiss, The Hill equation revisited: uses and misuses. The FASEB Journal 11, 835 - 841 (1997).
6. B. Hille, Ion channels of excitable membranes (Sinauer, Sunderland, Mass., ed. 3rd, 2001), pp. xviii, 814 p.
7. J. Zheng, M. C. Trudeau, Handbook of ion channels (Crc Press, 2015).
8. M. J. Caterina et al., The capsaicin receptor: a heat-activated ion channel in the pain pathway. Nature 389, 816-824 (1997).
9. E. Cao, M. Liao, Y. Cheng, D. Julius, TRPV1 structures in distinct conformations reveal activation mechanisms. Nature 504, 113-118 (2013).
10. R. Latorre, S. Brauchi, G. Orta, C. Zaelzer, G. Vargas, ThermoTRP channels as modular proteins with allosteric gating. Cell calcium 42, 427-438 (2007).
11. J. A. Matta, G. P. Ahern, Voltage is a partial activator of rat thermosensitive TRP channels. The Journal of physiology 585, 469-482 (2007).
12. A. Jara-Oseguera, L. D. Islas, The role of allosteric coupling on thermal activation of thermo-TRP channels. Biophys J 104, 2160-2169 (2013).
13. X. Cao, L. Ma, F. Yang, K. Wang, J. Zheng, Divalent cations potentiate TRPV1 channel by lowering the heat activation threshold. Journal of General Physiology 143, 75-90 (2014).
14. F. Yang, J. Zheng, Understand spiciness: mechanism of TRPV1 channel activation by capsaicin. Protein & cell 8, 169-177 (2017).
15. K. Hui, B. Liu, F. Qin, Capsaicin activation of the pain receptor, VR1: multiple open states from both partial and full binding. Biophys J 84, 2957-2968 (2003).
16. K. Zhang, D. Julius, Y. Cheng, Structural snapshots of TRPV1 reveal mechanism of polymodal functionality. Cell 184, 5138-5150. e5112 (2021).
17. F. Yang et al., Structural mechanism underlying capsaicin binding and activation of the TRPV1 ion channel. Nature chemical biology 11, 518-524 (2015).
18. A. Hazan, A. Basu, N. Zalcman, H. Matzner, A. Priel, Tyrosine residue in the TRPV1 vanilloid binding pocket regulates deactivation kinetics. Journal of Biological Chemistry 291, 13855-13863 (2016).
19. S. DeLuca, K. Khar, J. Meiler, Fully Flexible Docking of Medium Sized Ligand Libraries with RosettaLigand. PLoS One 10, e0132508 (2015).
20. B. P. Brown et al., Introduction to the BioChemical Library (BCL): An Application-Based Open-Source Toolkit for Integrated Cheminformatics and Machine Learning in Computer-Aided Drug Discovery. Front Pharmacol 13, 833099 (2022).
21. A. Hazan, R. Kumar, H. Matzner, A. Priel, The pain receptor TRPV1 displays agonist-dependent activation stoichiometry. Scientific reports 5, 1-13 (2015).
22. F. Yang et al., The conformational wave in capsaicin activation of transient receptor potential vanilloid 1 ion channel. Nature communications 9, 1-9 (2018).
23. S. Vu, V. Singh, H. Wulff, V. Yarov-Yarovoy, J. Zheng, New capsaicin analogs as molecular rulers to define the permissive conformation of the mouse TRPV1 ligand-binding pocket. Elife 9 (2020).
24. Y. Yin et al., Structural mechanisms underlying activation of TRPV1 channels by pungent compounds in gingers. Br J Pharmacol 176, 3364-3377 (2019).
25. Y. Dong et al., A distinct structural mechanism underlies TRPV1 activation by piperine. Biochemical and Biophysical Research Communications 516, 365-372 (2019).

26. J. Schirmeyer et al., Thermodynamic profile of mutual subunit control in a heteromeric receptor. Proceedings of the National Academy of Sciences 118 (2021).
27. S. E. Gordon, W. N. Zagotta, Localization of regions affecting an allosteric transition in cyclic nucleotide-activated channels. Neuron 14, 857-864 (1995).
28. D. E. Koshland, Jr., G. Némethy, D. Filmer, Comparison of Experimental Binding Data and Theoretical Models in Proteins Containing Subunits*. Biochemistry 5, 365-385 (1966).
29. Y. Gao, E. Cao, D. Julius, Y. Cheng, TRPV1 structures in nanodiscs reveal mechanisms of ligand and lipid action. Nature 534, 347-351 (2016).
30. T. Hoshi, W. N. Zagotta, R. W. Aldrich, Biophysical and molecular mechanisms of Shaker potassium channel inactivation. Science 250, 533-538 (1990).
31. N. E. Schoppa, F. J. Sigworth, Activation of Shaker potassium channels. II. Kinetics of the V2 mutant channel. J Gen Physiol 111, 295-311 (1998).
32. J. Zheng, L. Vankataramanan, F. J. Sigworth, Hidden Markov model analysis of intermediate gating steps associated with the pore gate of shaker potassium channels. The Journal of General Physiology 118, 547-564 (2001).
33. J. Zheng, F. J. Sigworth, Selectivity Changes during Activation of Mutant Shaker Potassium Channels. Journal of General Physiology 110, 101-117 (1997).
34. D. H. Kwon, F. Zhang, J. G. Fedor, Y. Suo, S.-Y. Lee, Vanilloid-dependent TRPV1 opening trajectory from cryoEM ensemble analysis. Nature communications 13, 1-12 (2022).
35. W. Cheng, F. Yang, C. L. Takanishi, J. Zheng, Thermosensitive TRPV channel subunits coassemble into heteromeric channels with intermediate conductance and gating properties. The Journal of general physiology 129, 191-207 (2007).
36. F. Sigworth, S. Sine, Data transformations for improved display and fitting of single-channel dwell time histograms. Biophysical journal 52, 1047-1054 (1987).

Figures and legends

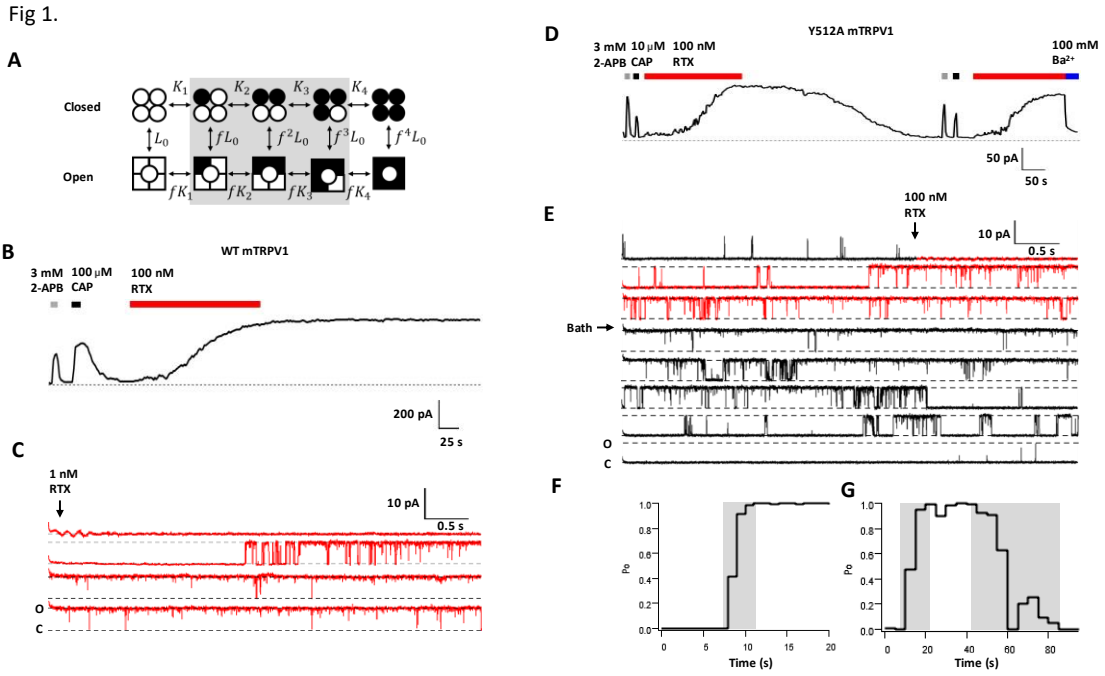

Figure 1. Intermediate open states of wildtype and Y512A mutant channels.

A: A classic MWC-type allosteric model for TRPV1 activation; circles and squares indicate a resting and activated subunit, respectively; open and filled symbols represent apo and RTX-bound subunits, respectively. L0, Kn, fnKn and fnL0 are equilibrium constants for each transition (n = 1 to 4). B: A representative macroscopic inside-out patch-clamp current trace of wildtype mTRPV1 at +80 mV. C: A representative inside-out single-channel recording of wildtype mTRPV1 activated by RTX. D: A representative inside-out macroscopic current trace of Y512A. Ba2+ was used to block channel current. E: A representative inside-out single-channel recording of Y512A activated by RTX. F&G: Po versus time plots for the recording shown in C and E, respectively. Transitional Po phases are highlighted by grey shading. Red segments in C and E indicate duration of RTX application.

Fig 2.

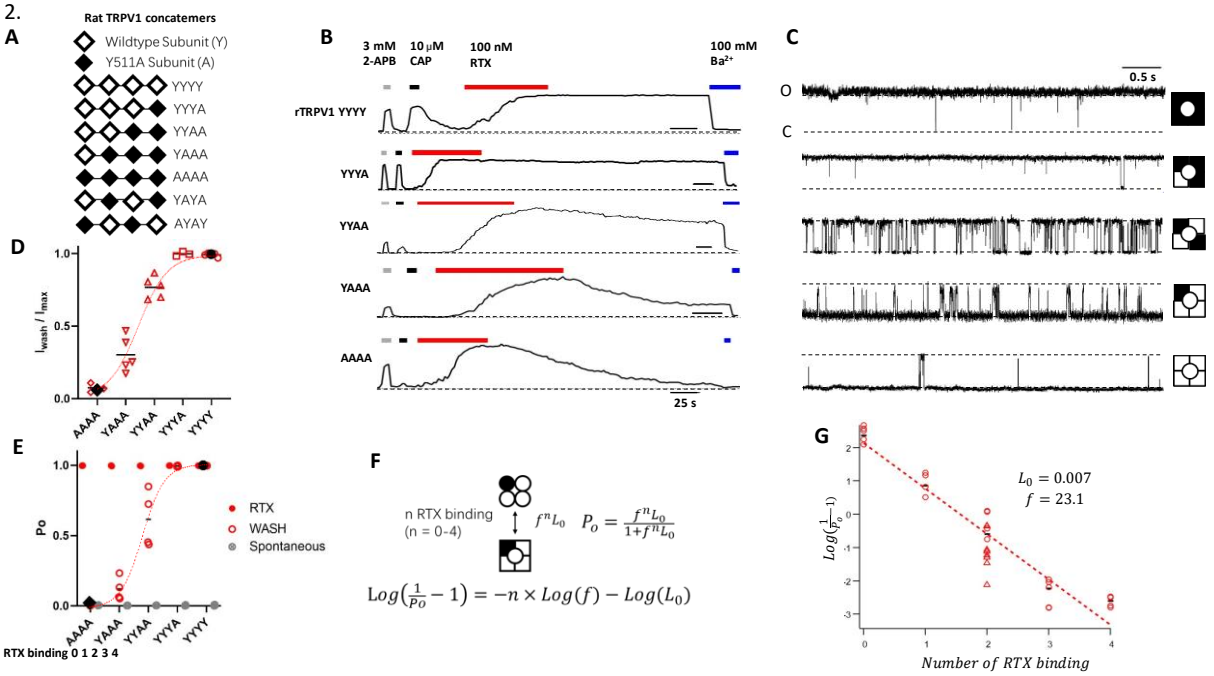

Figure 2. Equilibrium measurements of transition states.

A: Illustration of concatemer cDNA constructs. B&C: Representative inside-out current traces from concatemer channels. RTX activation reached near 100% Po and was partially or fully reversible, depending on the number of mutant subunits. The Y511A mutation did not affect 2-APB activation and, as expected, shifted the concentration dependence for capsaicin activation to the right (17, 21). D: Normalized remaining currents after complete wash (Iwash/Imax) can be well-fitted to the function Po=(fnL0)/(1+fnL0). E: Spontaneous (filled grey circles), maximal (filled red circles) and remaining Po (open red circles) measurements from single-channel recordings fitted to the same function as in D. For D&E, black diamonds and circles represent the level of the spontaneous activity of the apo state and maximal activity of the fully RTX-bound state, respectively, of the wildtype channel. F: The simplified MWC model when the number of

bound RTX is fixed. G: Estimation of Lo and f using the model in F. Data points from YAYA and AYAY are presented in red triangles.

Fig 3.

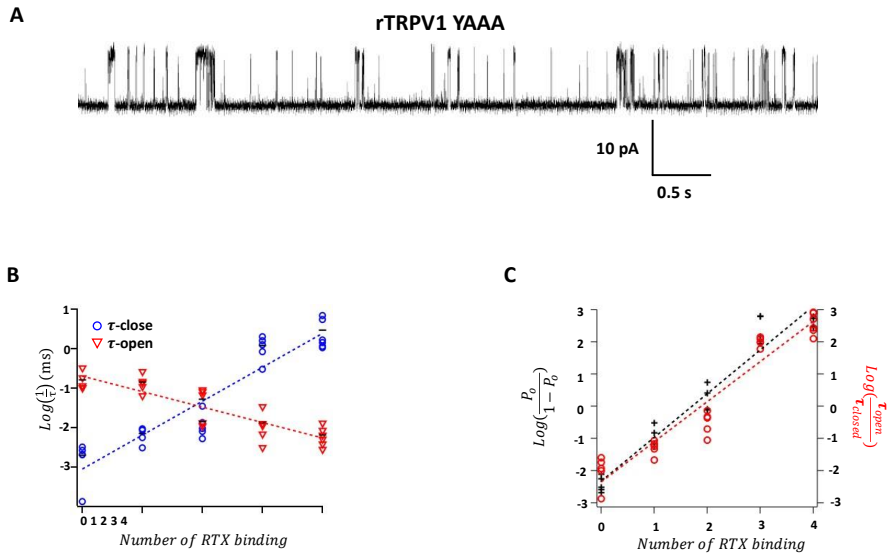

Figure 3. Single-channel dwell-time analysis reveals energetic effects on the closed and open states. A. An example inside-out single-channel trace from the YAAA channel. B. Relationship between dwell-time in the closed or open state and the number of RTX binding. Dotted lines represent linear fits of the log-transformed data, with a slope factor of 0.86 for the closed state and -0.39 for the open state. The mean values are shown as black bars. n = 3-5. C. Comparison between log-transformed lifetime ratios (red) and open probabilities (black). Dash lines represent linear fits, with slope factor values of 1.36 (Po) and 1.25 (lifetime ratio).

Fig 4.

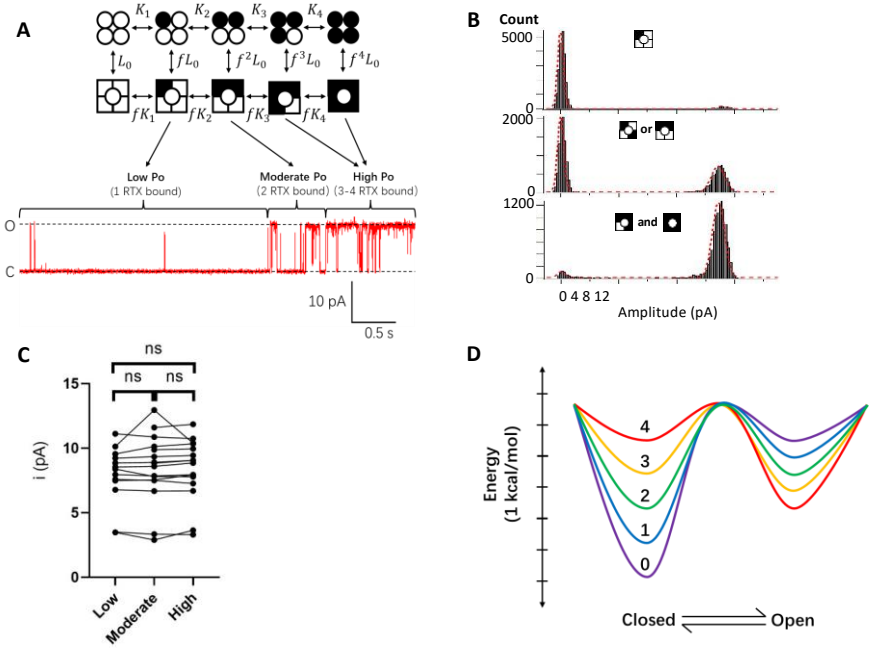

Figure 4. RTX-induced open states exhibit identical single-channel conductance. A: A representative inside-out single-channel trace from the wildtype TRPV1 activated by RTX. Distinct states with varying numbers of bound RTX were assigned according to Po. B: All-point histograms (with double-Gaussian fitting) of the three phases shown in panel A; only the open probabilities, represented by the relative areas of the two Gaussian functions, changed but not the single-channel amplitude. C. Comparison of single-channel amplitudes of distinct phases measured from 16 individual patches. One way ANOVA with Tukey's multiple comparisons test, p = 0.9025; ns, no significant difference. D. Eyring energy plots for channels with varying numbers of bound RTX. Ligand binding shifts the closed state energy more substantially than the open state; the four ligand binding steps shift these energies by the same amount; the energy wells for the closed and open states remain at the same locations along the reaction coordinate. The level of energy barrier is artificially set and unchanged.

Fig.S1

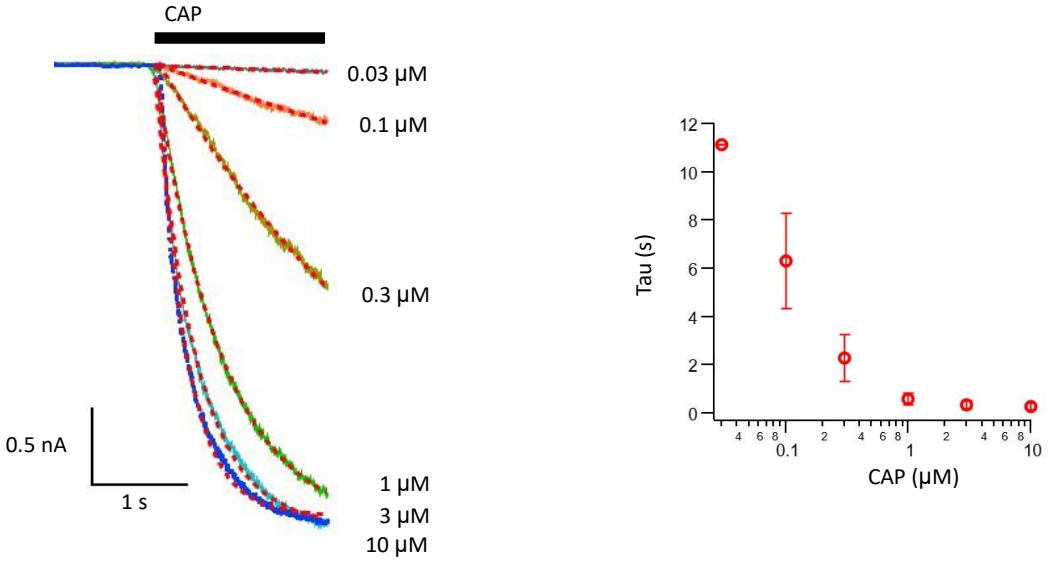

Fig. S1. Left: Representative mouse TRPV1 current traces from the same whole-cell recording activated by different concentrations of capsaicin. Superimposed are fits of an exponential function. A slight delay at the beginning of capsaicin perfusion can be seen but ignored from fitting. Right: Summarized time constant values from exponential fittings at different capsaicin concentrations. Error bar indicates mean and one standard deviation (mean ± SD, n = 6).

Fig. S2a-c. RTX-TRPV1 complex structures in different conformations (a, PDB: 7L2N; b, PDB: 7MZ5; c, PDB: 7L2L). The distances between RTX and potential interacting residues in TRPV1 are highlighted.

Fig.S2a

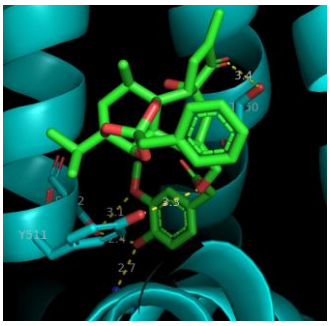

Polar interactions:

S512: 3.1 Å, 2.4 Å with head

R557: 2.7 Å with head

E570: no interaction with head

Y511: 3.3 Å with neck

T550: 3.4 Å with tail

7L2N: Full-length TRPV1 with RTX bound, in state C_1

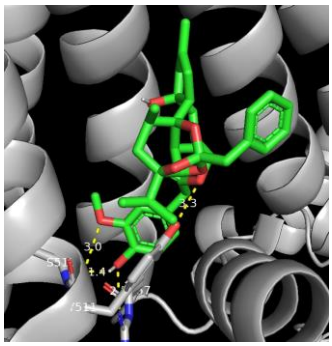

Polar interactions:

S512: 3.0 Å, 1.4 Å with head

R557: 2.9 Å with head

E570: no interaction with head

Y511: 3.3 Å with neck

T550: no interaction with tail

7L2L: Full-length TRPV1 with RTX bound, in state O_1

Fig.S2b

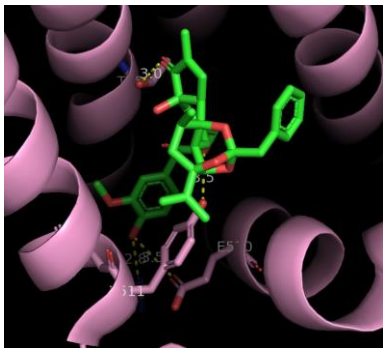

Polar interactions:

S512: no interaction with head

R557: 2.8 Å with head

E570: 3.5 Å with head

Y511: 3.5 Å with neck

T550: 3.0 Å with tail

7MZ5: Full-length TRPV1 with RTX bound, in state C_2

Fig.S3

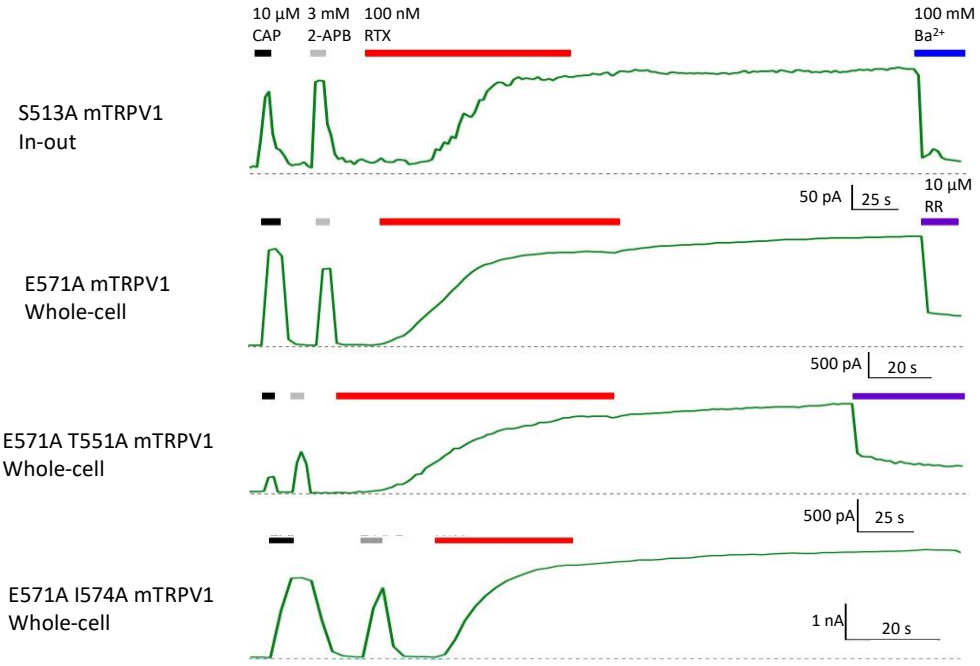

Fig. S3. Representative traces from mouse TRPV1 S513A (equivalent to S512A in rat TRPV1), E571A (equivalent to E570A in rat TRPV1), and E571A T551A double mutant (equivalent to E571A T551A in rat TRPV1) and E571A I574A double mutant (equals to E570A I573A in rat TRPV1). These mutants did not change the RTX behaviors dramatically. Representative recordings from n = 3-to-6. Ruthenium Red (RR, purple bar) or Ba2+ (blue bar) was used at the end of recording to block channel current and check for leak.

Fig.S4

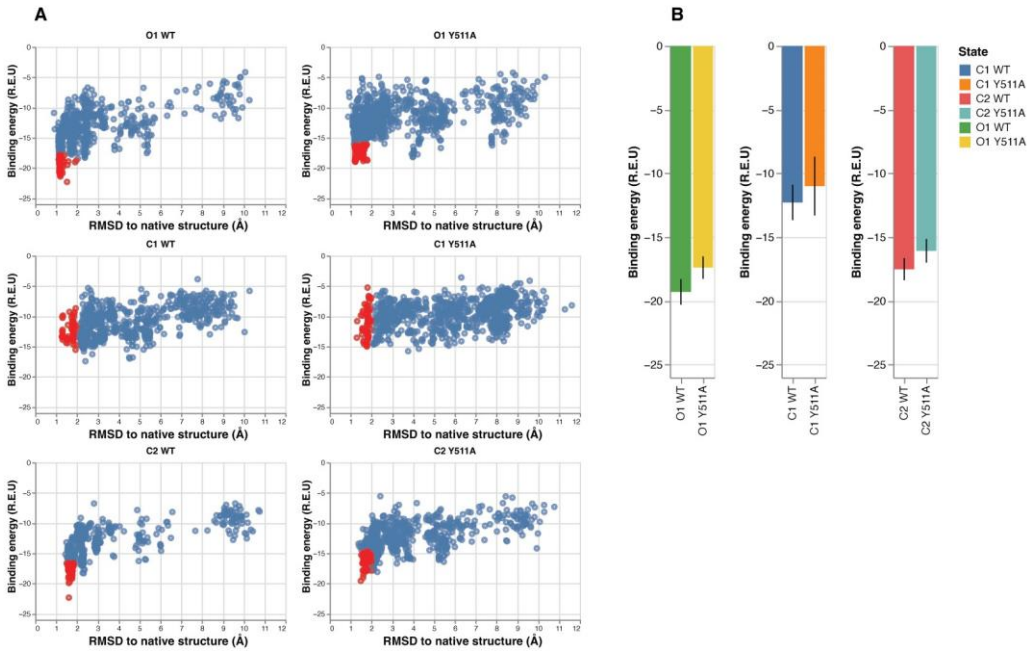

Fig. S4. RosettaLigand docking of RTX to TRPV1 wildtype and Y511A mutant structures. (A) RTX docking energy landscape is represented by the Rosetta binding energy versus the all-atom root-mean-square deviation (RMSD) to the native structure. Energy is reported in Rosetta Energy Unit (R.E.U). The data for near-native docking models (top 100 models with RMSD less than or equal to 2 Å) are shown in red. (B) Binding energy (in R.E.U.) for the top 100 near-native docking models for the wildtype (WT) and Y511A mutant in the closed (C1 and C2), and open (O1) states. Bar graph indicates the mean and one standard deviation (mean ± SD).

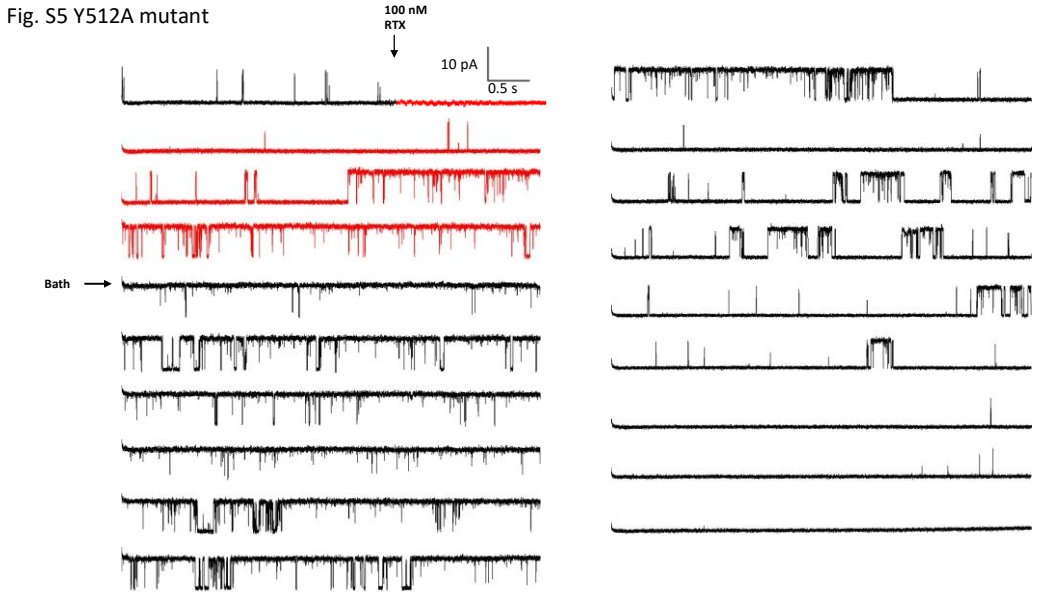

Fig. S5. Continuous inside-out single-channel recording of Y512A mTRPV1 activated by 100 nM RTX and subsequently wash-off. Events of RTX application and wash-off are indicated by arrows with current during RTX application in red. Recordings in Figure 1E originated from this recording.

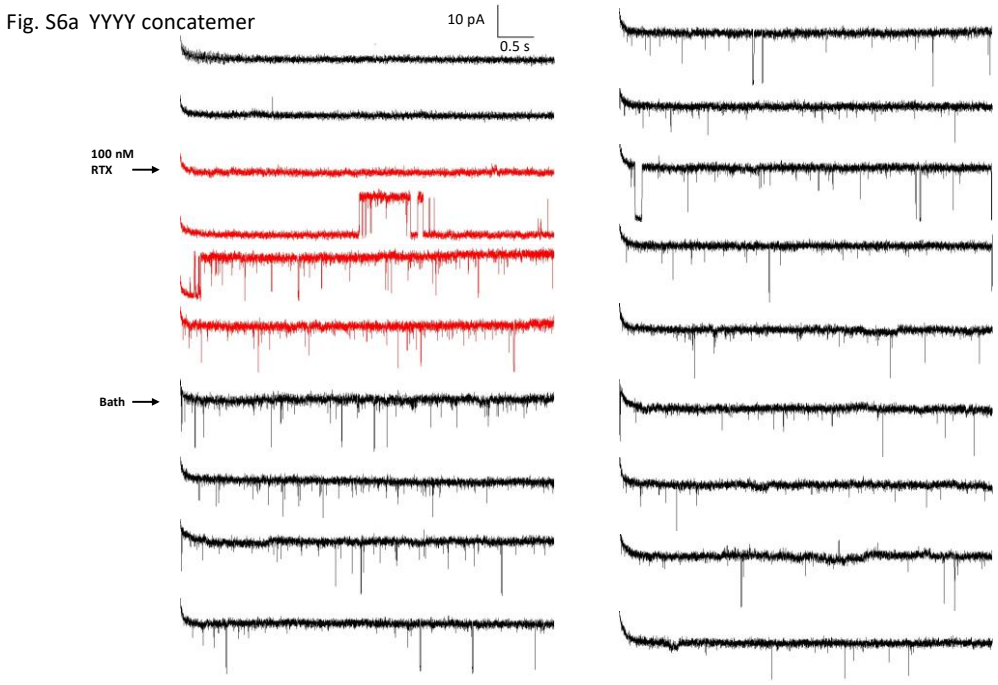

Fig. S6b YYYA concatemer

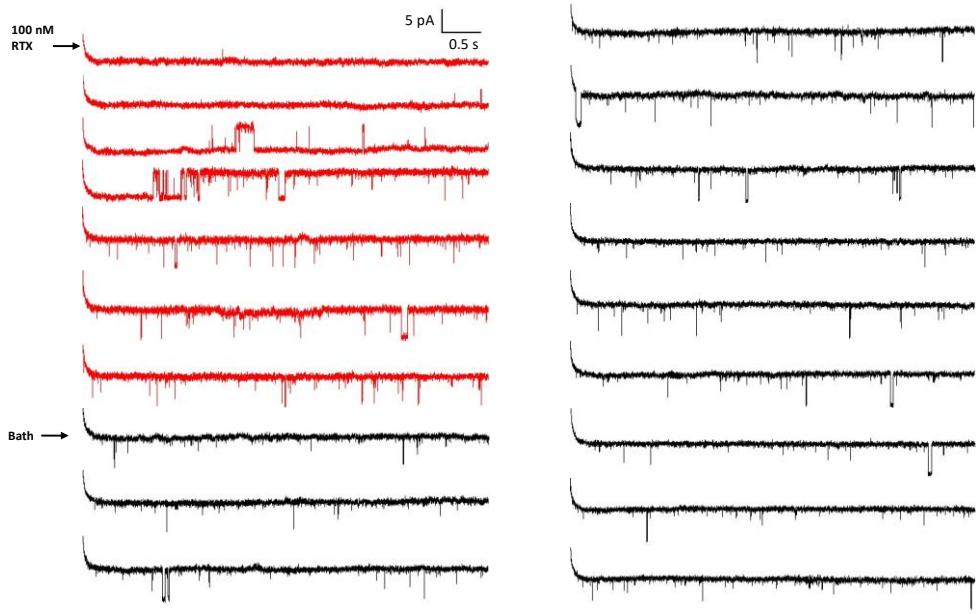

Fig. S6c YYAA concatemer

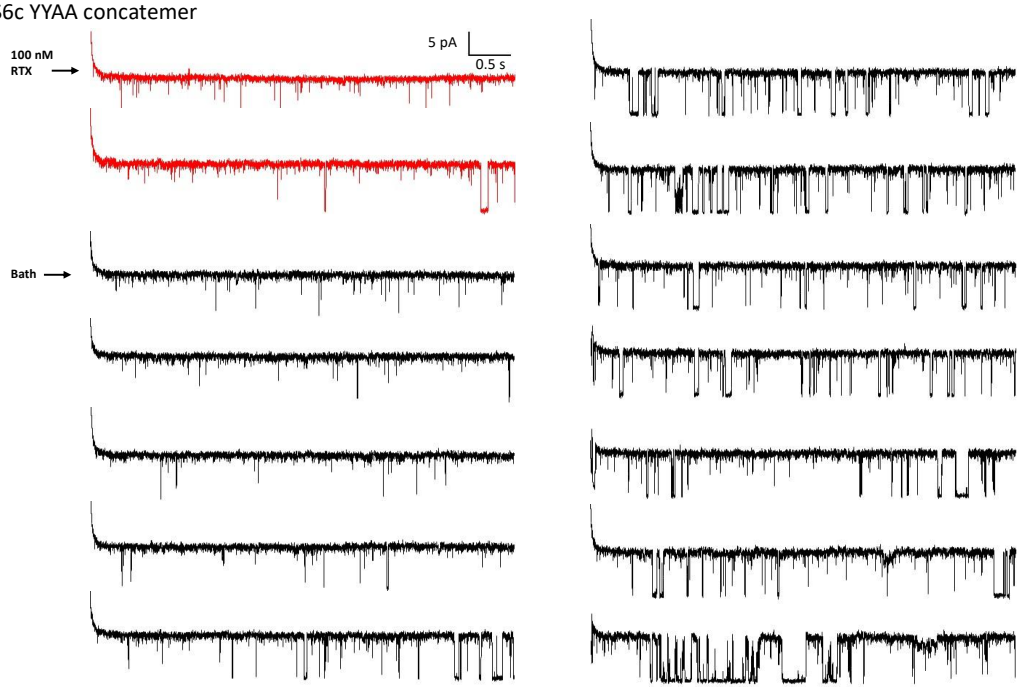

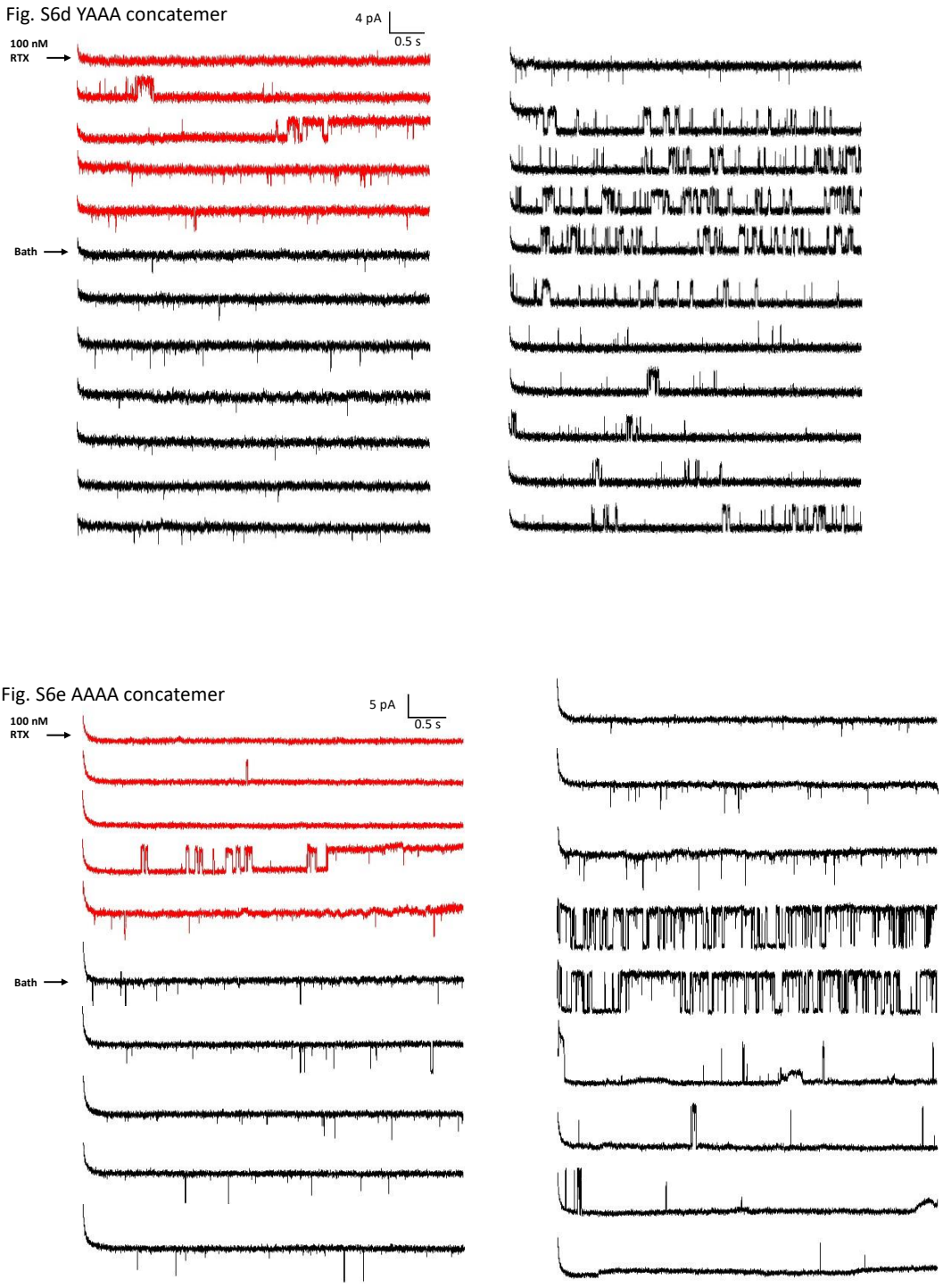

Fig. S6a-e. Representative continuous inside-out single-channel recordings of YYYY (a), YYYA (b), YYAA (c), YAAA (d), and AAAA (e) concatemer. Events of RTX application and wash-off are marked by arrows with current during RTX application in red.

Fig. S7 Comparison between YYAA, YAYA and AYAY concatemers

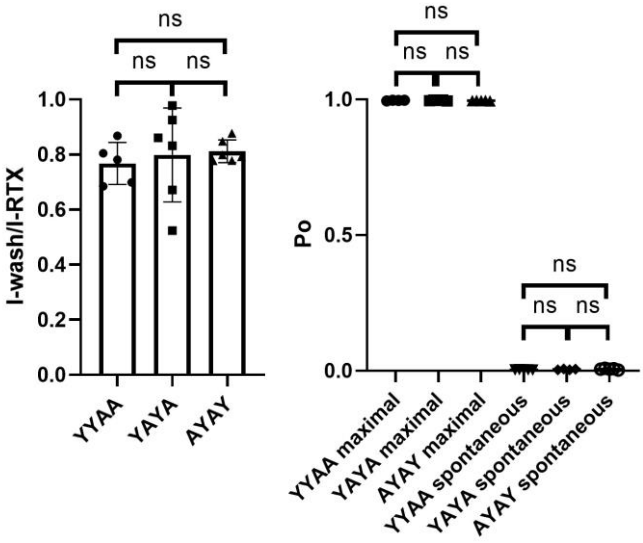

Fig. S7. Comparison between concatemers containing two wildtype and two mutant subunits with different subunit positionings. (left) Fraction of remaining current in macroscopic recordings. Bar graphs indicate mean and standard deviation (mean ± SD, n = 5 – 6). One way ANOVA with Tukey's multiple comparisons test, $P > 0.05$. n.s., not significant (right) Spontaneous and maximal open probabilities measured from single-channel recordings. One way ANOVA with Tukey's multiple comparisons test, $P > 0.05$. n.s., not significant.

Chapter III: The Capsaicin Binding Affinity of Wild-Type and Mutant TRPV1 Ion Channels

Shisheng Li and Jie Zheng

Abstract

Vanilloids such as capsaicin and resiniferatoxin (RTX) are highly selective and potent activators for TRPV1, a nociceptor for heat and pain perception. However, the intrinsic vanilloid binding affinity, key for understanding TRPV1 function, remains unknown despite intensive investigations by electrophysiological, structural, and computational methods. In this study, we determined capsaicin binding affinity under physiological conditions by isolating individual binding steps with concatemers. We estimated the capsaicin association constant of a wildtype subunit to be in the order of 106 M-1, and that of the Y511A mutant subunit to be a hundred times lower, in the order of 104 M-1. The Y511A mutation, located at the entrance of the vanilloid binding pocket, reduces binding affinity without a noticeable effect on activation gating. We further affirmed that there is little cooperativity between vanilloid binding steps. Models based on independent binding and equally cooperative subunit gating can accurately describe capsaicin activation.

Introduction

Capsaicin receptor TRPV1 ion channel is a pivotal sensor of harmful heat and protons, as well as the piquant sensation linked to spicy foods (1, 2). Its activation by vanilloids such as capsaicin and resiniferatoxin (RTX) underlines an important form of nociception, and offers a pathway for developing new analgesics (3). Vanilloids bind to the vanilloid binding pocket located within the transmembrane domain of the channel, formed by S3, S4, and the S4-S5 linker from one subunit and S5 and S6 from a neighbor subunit (4, 5) (Figure 1A). As a homotetramer, each TRPV1

channel can accommodate four vanilloid molecules that cooperatively activate the channel(1, 4, 5). Vanilloid-induced TRPV1 activation has been serving as an outstanding model system for elucidating the energetics and kinetics of ligand activation, thanks to extensive structural (4-9), functional (10-19), and computational investigations (20, 21). Nonetheless, a fundamental feature of TRPV1 activation—the binding affinity of capsaicin and other vanilloids—has not been determined. The EC50 value, a descriptive term combining binding and activation (22), has been generally used.

Activation of TRPV1 by vanilloids is an allosteric process for which the classic Monod-Wyman-Changeux (MWC) model can be applied (23, 24) (see Supplementary Figure 1). The MWC model is defined by three key parameters: the apo-state equilibrium constant (L0), activation energy from each ligand binding represented by the cooperative factor (f), and the ligand association constant (K). A quantitative understanding of the vanilloid activation process requires knowledge of these three parameters. L0, reflecting the resting activity level, has been measured by many groups; our estimates from mouse TRPV1 channels range from 0.005 to 0.007 (12, 24). In a recent study, we confirmed that the activation energies for the four vanilloid-binding steps are virtually the same, and determined the value to be 1.70-to-1.86 kcal/mol for RTX (24). The present study aimed to determine the value for ligand binding affinity.

Capsaicin is an extremely pungent compound. It activates TRPV1 in sub-micromolar concentrations under physiological conditions (3). To define the capsaicin binding process entails answering three essential and closely interconnected questions: 1) What is the binding affinity of capsaicin for each subunit? 2) Does binding of capsaicin to the four subunits occur independently or cooperatively? 3) How do residues in the vanilloid binding pocket contribute to capsaicin binding? Addressing these questions is a challenging task. With four (wildtype or mutant) binding

sites per channel and the possibility of cooperative binding and activation, a general binding model would contain up to 32 states, each with a distinct binding affinity. To overcome this challenge, our approach was to first preload some of the binding sites in an irreversible manner, allowing us to measure capsaicin binding to one or two remaining binding sites.

Preventing capsaicin binding in individual subunits can be potentially achieved by introducing mutations to the binding site. However, no such mutation has been found. Moreover, the approach would completely obliterate the binding site and, more importantly, have a potential global impact to activation. To circumvent these confounding issues, we took advantage of the irreversible binding of RTX and its derivatives to block out selected subunits (whose functional contribution to activation could still be quantified). Previous studies have demonstrated that the rat TRPV1 Y511A mutation (equivalent to Y521A in mouse TRPV1) could convert RTX binding from irreversible to reversible without significantly altering activation gating (12, 16, 24, 25). In an earlier study, it has been shown that different combinations of wild-type and Y511A subunits in concatemers would allow faithful introduction of these phenotypes in a stoichiometric manner (25). Building upon these findings, we developed a method to block two or three binding sites in order to quantify capsaicin binding affinity to the remaining binding site(s) with single-channel measurements of channel open probability. Once capsaicin binding affinity to the Y511A subunit was known, we could then determine the capsaicin binding affinity to a wild-type subunit. The possibility of cooperative bindings was examined and ruled out in the process.

Results

Direct functional measurement of capsaicin binding affinity to a single subunit

In a previous study, we found that RTX binds irreversibly to wild-type (Y) TRPV1 subunits but can be washed off Y511A (A) mutant subunits (24). Therefore, if we first treat YYYA concatemeric channels with RTX and then wash thoroughly, RTX will occupy the vanilloid binding sites of the three wild-type subunits. We can then directly measure association constant (K) and energy contribution (f) of capsaicin from the single mutant binding site (Figure 1B). However, when three RTX molecules were bound in a YYYA concatemeric channel, its open probability (Po) already approached approximately 99% (24). There was hardly any observable change for the subsequent capsaicin binding step. Hence, we searched for an alternative to RTX that retains the irreversible binding property but functions as a weaker TRPV1 activator. This search led us to the RTX derivative 6'-iodo-RTX (hereafter called 6'-iRTX), with an iodine atom at the 6' position of the vanillyl group (Supplementary Figure 2), which is known as a weak partial agonist for TRPV1 (26).

In both macroscopic and single-channel recordings, we confirmed that 6'-iRTX binds irreversibly to the wild-type subunits (Figure 1C, also see Supplementary Figure 3). This is evident from the observation that, after perfusing 6'-iRTX to wild-type mTRPV1 channels—which produced weak channel activities, as anticipated for a partial agonist—capsaicin lost its activation effect whereas 2-APB could still activate these channels (Figure 1C, top panels). In contrast, 6'-iRTX could be washed off Y512A mTRPV1 mutant channels, after which capsaicin was able to reactivate them (Figure 1C, bottom panels; also see Supplementary Figure 4). With three 6'-iRTX molecules bound in a YYYA concatemer, the channel was barely activated. This allowed us to observe a subsequent increase in Po in a capsaicin concentration-dependent manner as capsaicin bound to

the single remaining site (Figure 1D&E, also see Supplementary Figure 5). By fitting the concentration dependence of Po to a simple four-state model (indicated by a dashed box in Figure 1B), we obtained the association constant for capsaicin in the Y511A mutant subunit to be 2.6x104 M-1. This value is in agreement with the EC50 value of 1.3x10-5 M observed from the Y512A mutant mTRPV1 channels (12).

Functional measurement of capsaicin binding affinity to two subunits

The same approach described above for a single binding site can be applied to two binding sites offered by the YYAA concatemer, as illustrated in Figure 2A. Indeed, whereas the range of Po change we could observe from capsaicin binding to a single subunit in YYYA was relatively narrow—from about 1% to 15% (Figure 1E), the range became much broader when capsaicin bound to two subunits in YYAA to increase channel activity, from about 1% to 50% (Figure 2B, also see Supplementary Figures 6 & 7). Using the six-state model with an independent binding assumption shown in Figure 2A, we estimated the K value to be 6.2x104 M-1 (Figure 2C). This value is very close to the K value estimated for the single binding site in YYYA (Figure 1E).

With only two wildtype subunits in YYAA, we had the option to preload the wild-type binding sites with the more potent agonist RTX, producing an initial Po level of approximately 50% (Figure 2B). Application of capsaicin at varying concentrations further increased Po up to nearly 100%. Measurements from RTX-loaded channels served as a nice internal control as they were done at otherwise identical conditions as those with 6'-iRTX (see Supplementary Figure 7). Using the same six-state model, we estimated the K value to be 3.7x104 M-1 for RTX-preloaded channels. This value is in close agreement with the independently obtained values with 6'-iRTX from YYAA and YYYA. Therefore, we conclude that the Y511A mutant subunit has a capsaicin association constant of 2.6x104 – 6.2x104 M-1.

Are capsaicin binding steps independent or cooperative?

The nearly identical K estimates from one or two binding sites strongly indicate that capsaicin bindings to different subunits of a TRPV1 channel are likely independent events. To test this hypothesis, we relaxed the independence assumption for the six-state system and assigned the capsaicin binding steps with two separate association constants, K' and aK' (Figure 3A); here K' is equivalent to 2K in Figure 2A. For independent bindings, the a value would be 0.25 (see Figure 2A); a > 0.25 or a < 0.25 would indicate bindings with positive or negative cooperativity, respectively. Simultaneously fitting the data from YYAA channels with preloaded RTX or 6'-iRTX using the new model yielded satisfactory concentration dependence predictions (Figure 3B). The fitting residuals (differences between model and data) exhibited no detectable difference from those using the model with independent binding steps (Figure 3C), even though the new model has one additional free parameter. A value of 0.27 for the a factor yielded the best fitting results, confirming that cooperativity between capsaicin binding steps, if existed, was too weak to be detected, and an independent model is sufficient to describe capsaicin activation.

To further check for potential binding cooperativity, we performed global fittings of the data from both YYYA and YYAA concatemers assuming the same K value for capsaicin binding, that is, binding of capsaicin was independent of what had been preloaded in the other binding sites (RTX or 6'-iRTX) and independent of the number of pre-loaded ligands per channel. As shown in Figure 3D, the approach yielded fitting results nearly indistinguishable from the individual fittings in Figures 1E and 2D. The K value estimated this way is also in close agreement with those determined individually. These observations suggest that binding of capsaicin is insensitive to what and how many ligands bind to the other subunits. Indeed, a global fitting with capsaicin binding being dependent on what were in the other subunits did not significantly improve the

fitting outcome (Figure 3E&F), even though four additional free parameters were added. It is further noticed that the binding affinity estimates for the three cases differ by less than three folds from each other and from estimates using previous methods (Figure 3E).

In summary, our observations suggest that there is no detectable cooperativity between bindings of vanilloid to the TRPV1 subunits.

Binding affinity of capsaicin to a wildtype subunit

Since models with independent ligand binding steps could accurately predict the behavior of concatemeric channels, it is possible to determine the binding affinity of capsaicin to a wildtype subunit. We approach this goal by globally fitting capsaicin activation data from concatemers with all possible combinations of wild-type and mutant subunits, without pre-treatment by RTX or 6'-iRTX. For the global fitting, there were two capsaicin association constants, one for the wildtype subunit (KY) and another for the mutant subunit (KA). The 32-state independent binding model (Figure 4A) contains only four free parameters: in addition to KY and KA, L0 represents the equilibrium constant for spontaneous opening of an unliganded channel (which has been determined in our previous study (24)), and f represents the folds increase of the closed-to-open equilibrium constant due to each capsaicin binding. Fitting of this simple model simultaneously to capsaicin concentration-dependent Po curves for YYYY, YYYA, YYAA, YAAA, AAAA concatemers yielded satisfactory results (Figure 4B, also see Supplementary Figure 8). We found that relaxing the model to incorporate different f factors for wild-type and mutant subunits would not improve fitting outcome even with the additional free parameter (Figure 4C), in agreement with the prediction that Y511 participates mainly in ligand binding but not activation gating (12, 16). The estimate for KA is 2.0x104 M-1, which is again in close agreement with results for the Y511A subunit discussed earlier. The estimate for capsaicin binding affinity to the wild-type

subunits, KY, is 2.4x106 M-1. It is two orders of magnitude higher than KA, consistent with the observation that the Y511A mutation substantially shifted capsaicin responses to higher concentrations in a mutant number dependent manner (25).

Discussion

Ligand activation of an ion channel has two basic yet functionally linked aspects: how tight the ligand binds and how strong ligand binding promotes activation. These two properties, together with the level of channel activity in the apo state, define the response of an ion channel to ligands (27). In a recent study, we utilized subunit concatenation and irreversible binding of RTX to measure and compare the activation energies from ligand binding to each of the four subunits (24). We found each subunit contributes the same amount of activation energy, which is 1.70-to-1.86 kcal/mole for RTX. With the binding affinity values obtained in the present study, we are now in the position to make quantitative predictions of the equilibrium properties of TRPV1 activated by capsaicin. With just three parameters (L0, K, f), the model shown in Figure 5A satisfactorily predicts concentration-dependent activation of both the wild-type and Y511A mutant channels (Figure 5B). In comparison, the Hill function can describe the high Po data but deviates substantially at the low Po range, as the Hill function yields a straight line in the log transformed plot but the experimental data exhibit a clear plateau at low capsaicin concentrations, due to unliganded channel openings (Figure 5C). In the middle range of capsaicin concentrations, Hill function yields a more sluggish response, which is more obvious in the wildtype channels.

Successful reproduction of capsaicin activation with the elegantly simple MWC model confirms that TRPV1 is indeed an allosteric protein, as the TRPV1 research community has correctly assumed (28-31). An allosteric protein exists in a perpetual equilibrium between two functional states—Monod, Wyman and Changeux used Tense (T) and Relaxed (R) states to describe

hemoglobin (23); for an ion channel the corresponding states are Closed (C) and Open (O). Keeping an allosteric protein in a quiescent state under the "resting" physiological condition means that the equilibrium constant for the T←→R balance, L0, is sufficiently small. For TRPV1, the L0 value under near-physiological conditions (but at room temperature) is in the order of 10-4, corresponding to a resting open probability of the same order that has been experimentally confirmed (12, 24). Binding of vanilloids shifts the C←→O balance towards the open state, by a factor of 17.6-to-23.1 per RTX binding (24), and about 12 per capsaicin binding (Figure 5B). The 1.4-to-1.8 kcal/mol activation energy contributed by each bound ligand explains the high potency of these vanilloid molecules; combination of the contributions from four subunits (yielding 4.8-to-7.2 kcal/mol) is the origin of activation cooperativity. The vanilloid binding steps however occur in a near-independent manner. Being a polymodal nociceptor, it appears TRPV1 may response to other stimuli (e.g., protons, animal peptide toxins) in a similar manner (32).

Most multi-subunit ion channels examined so far exhibit strong cooperativity in their responses to a stimulus (33). Depending on the origin of cooperativity—stimulus sensing versus activation gating—a channel's sensitivity to the stimulus can be quite different(27) . Our results from TRPV1 are consistent with the MWC theorem (23) that strong cooperativity can be present even when ligand binding steps are independent: cooperativity of TRPV1 activation originates from the concerted transition, which is promoted equally by each subunit (24). Structures of hemoglobin (34, 35) and TRPV1 (5) reveal that their ligand binding sites are indeed separated. No direct structural interaction is seen in either the apo or liganded state. The ligand-binding domains of many ion channels exhibit similar structural features. Cyclic nucleotide-gated (CNG) channels for example contain four structurally separated intracellular ligand-binding domains(36) . Recent studies in the Chanda lab found the cyclic nucleotide-binding steps being independent (37) despite

functional asymmetry among subunits (38, 39). There are nonetheless ligand-gated ion channels whose ligand-binding domains directly associate. The glutamate receptors, for example, contain four extracellular ligand-binding domains that combine into two structural and functional dimers (40).

Determining L0, K, and f for TRPV1 moves one step closer towards understanding the structural mechanism of vanilloid activation. Here the role of residue Y511 offers a good example. When the first high-resolution TRPV1 structures were solved by the Cheng and Julius labs, it was noticed that this aromatic residue, located at the entrance of the vanilloid binding pocket (see Figure 1A), switches from a downward position in the apo state to an upward position in the capsaicin- or RTX-bound state (4, 5). Prior mutational studies already identified this residue being highly sensitive in determining capsaicin activation (14, 15). However, despite its close proximity to a bound RTX (9), mutations of Y511 shift capsaicin dependence without substantially reducing the maximal activity (16) or the activation energy exerted by vanilloid binding (12, 24). These observations led us to propose that the upward position of Y511 in the ligand bound state physically prevents a bound vanilloid molecule from falling out (12). Indeed, mutating Y511 to an amino acid with a smaller side-chain such as alanine makes RTX binding reversible (24) and speeds up reversal of capsaicin activation (16); mutating Y511 to a phenylalanine or tryptophan (with a large, non-polar side-chain) does not have as much an effect as changing to a cystine (with a small yet polar side-chain) (15, 16), indicating that direct, hydrogen bond-type interactions with the bound ligand or nearby residues may not be needed. We showed in this study that Y511A produces a two-order of magnitude shift in the capsaicin activation curve by reducing the binding affinity of capsaicin and progressively shifting the concentration dependence for activation (Figure 5); no major effect on activation energy was detected. It is clear that Y511 functions like a turnstile

(revolving gate) to secure vanilloid binding. The knowledge on L0, K, and f would open the door to reliably identify the functional role of other channel residues lining the vanilloid binding pocket. Similarly, it is now possible to start investigating how different vanilloid molecules exert distinct functional effects on TRPV1 activity (full or partial agonists, or antagonists). For example, whereas RTX is a full agonist, 6'-iRTX is a weak agonist despite their highly similar overall molecular structures (Supplementary Figure 2).

Method and Materials

Molecular biology

The wildtype mouse TRPV1 cDNA was constructed into the pEYFP-N3 plasmid backbone. The cDNA of enhanced yellow fluorescent protein (eYFP) was fused to the C-terminus of TRPV1 cDNA to indicate the transfected cells during patch-clamp recordings. The Y512A point mutation was introduced using mutagenesis kit purchased from Agilent Technologies, as previously described (12, 24). All the sequences of these plasmids were confirmed by sequencing. Plasmids of the TRPV1 concatemers (YYYY, YYYA, YYAA, YAAA and AAAA) were generated by Dr. Avi Priel as previously described (25). Briefly, rat TRPV1 wildtype and Y511A (equivalent to Y512A in the mouse TRPV1 channel) cDNA segments were linked with sequences encoding flexible peptide linkers to build the tandem tetrameric channel plasmids. It was observed that the activation profile of channels with four concatenated wildtype subunits closely mimicked that of channels made with monomeric wildtype subunits(25).

Cell culture

TSA201 (HEK293T) cells were purchased from American Type Culture Collection and used for mouse and rat TRPV1 expression and patch-clamp recordings. Cells were cultured in DMEM high

glucose medium (Gibco) with 10% (v/v) fetal bovine serum (FBS) (GenClone) at 37°C with 5% CO2. Cells grown to 30%-to-50% confluence on 25 mm glass coverslips in 30 mm dishes (Fisher Scientific) were used for transient transfection using Lipofectamine 2000 (Invitrogen) according to the manufacturer's instructions. Patch-clamp experiments were conducted 18-to-24 hours after transfection. For macroscopic recordings, 1 μg plasmids were used for each 30 mm dish; for single-channel recordings, 0.1 μg plasmids were used for each 30 mm dish. Because the TRPV1 concatemer plasmids did not contain the fluorescent tag, 0.2 μg YFP plasmids were co-transfected to identify transfected cells for patch-clamp experiments.

Chemical solutions

Symmetrical bath and pipette solutions were used for patch-clamp recordings, which contained (in mM) 140 NaCl, 2 EDTA, 15 HEPES (pH 7.4). Capsaicin (Sigma-Aldrich) was dissolved in DMSO to make the 1 mM stock solution and diluted to working concentrations (0.01-to-100 μM) using bath solution. Since it is known that high concentrations of capsaicin produce non-specific effects on membrane and embedded proteins (41), higher concentrations of capsaicin were not attempted in this study. 2-Aminoethoxydiphenyl borate (2-APB, purchased from Sigma-Aldrich) was dissolved in DMSO to make the 1 M stock solution and diluted to the 3 mM working concentration using the bath solution. 6′-Iodo-resiniferatoxin (6-iRTX, purchased from Sigma-Aldrich) and resiniferatoxin (RTX, purchased from Alomone Labs) were dissolved in ethanol to make the 1 mM stock solution and diluted to working concentrations (10-to-200 nM) using the bath solution. A 100 mM BaCl2 solution with 15 mM HEPES was used to block TRPV1 current from the intracellular side.

Electrophysiology

Patch-clamp pipettes were pulled from borosilicate glass tubes (Sutter Instrument) using a Sutter Instrument P-97 micropipette puller and fire-polished to create resistances of 2-to-6 MΩ for macroscopic recordings, or 8-to-15 MΩ for single-channel recordings. An EPC 10 USB patch-clamp amplifier controlled by PatchMaster software was used. The current signal was sampled at 10 kHz and filtered at 2.25 kHz. The holding potential was set at 0 mV, followed by a 500-ms step to +80 mV and then a 500-ms step to -80 mV. The durations of the +80 mV and -80 mV steps were adjusted between 300 ms to 2 s as per experimental requirements. For continuous single-channel recordings, the voltage was held at +80 mV throughout the entire recording. Perfusion was gravity-driven, and solution switching was executed using a Rapid Solution Changer (RSC-200, Biological Science Instruments).

Data Analysis

Patch-clamp data were exported from the PatchMaster software and analyzed using Igor Pro 8 (WaveMetrics). Statistical analyses were performed using GraphPad Prism 8. The Student's t-test was employed when comparing two groups. Paired t-tests were used for comparisons within the same recordings. For comparison among multiple groups, one-way ANOVA was utilized.

Macroscopic current amplitude was calculated by measuring the difference between ligand-activated current and the baseline current level before any ligand perfusion. A digital filter at 0.4 kHz was used for analyzing single-channel amplitude and open probability. Single-channel recordings were analyzed using all-point histograms and fitted to a double-Gaussian function; single-channel open probability was measured by calculating the portion of open events over the total time recorded. Only true single-channel recordings or two-channel recordings were used.

Open probability of two-channel recordings was calculated using the equation $Po = \frac{t_1+2\times t_2}{2\times T}$, where t_1 is the total time of one-channel opening evens observed, t_2 is the total time of two-channel opening evens observed, T is the total recording time. Spontaneous open probability was measured from single-channel recordings without perfusing any ligands, and a saturating concentration of 2-APB (3 mM) or capsaicin (10 to 100 μM) was used to determine the number of channels in the patch.

For the YYYA concatemer channels pre-loaded with three 6'-iRTX molecules in the Y subunits, the single-channel open probability data were fitted with the MWC model shown in Figure 1B, using the equation $Po = \frac{L_3+fK[C]L_3}{1+K[C]+L_3+fK[C]L_3}$, in which L_3 is the equilibrium constant before capsaicin application, f is the cooperative factor describing the folds increase of the equilibrium constant by capsaicin, K is the capsaicin association constant for the A subunit, $[C]$ is the concentration of capsaicin.

For the YYAA concatemer channels pre-loaded with two RTX molecules in the Y subunits, the single-channel open probability data were fitted with the MWC model shown in Figure 2A, using the equation $Po = \frac{L_2+2fK[C]L_2+f^2K^2[C]^2L_2}{1+L_2+2K[C]+K^2[C]^2+2fK[C]L_2+f^2K^2[C]^2L_2}$, where L_2 is the equilibrium constant before capsaicin application, f, K, $[C]$ are the same as defined above. Alternatively, two separate associate constants K1 and K2 were assumed for the first and seconding binding steps. The Po data were fitted with the MWC model shown in Figure 3A, using the equation $Po = \frac{L_2+fK'[C]L_2+f^2aK'^2[C]^2L_2}{1+L_2+K'[C]+aK'^2[C]^2+fK'[C]L_2+f^2aK'^2[C]^2L_2}$, where the factor a would be 0.25 when the two binding steps are independent. Global fittings were conducted in Igor Pro using the equations described above, with each fitting parameter(s) being either specific to one dataset or shared among datasets.

For YYYY, YYYA, YYAA, YAAA, AAAA concatemer channels activated by capsaicin without pre-treatment with RTX or 6'-iRTX, the single-channel open probability data were fitted with the MWC model shown in Figure 4A. Given that each capsaicin binding step is independent, capsaicin binding to a wildtype subunit was assumed to have the same association constant K_Y, whereas binding to a mutant subunit was assumed to have the same binding affinity K_A. A global fitting routine was conducted in Igor Pro, using the following equation:

$$Po = \frac{\left(1 + \sum_{i=1}^{4} f K_i[C] + \sum_{1\le i<j\le 4} f^2 K_i K_j [C]^2 + \sum_{1\le i<j<l\le 4} f^3 K_i K_j K_l [C]^3 + f^4 K_1 K_2 K_3 K_4 [C]^4\right) L}{\left(1 + \sum_{i=1}^{4} f K_i[C] + \sum_{1\le i<j\le 4} f^2 K_i K_j [C]^2 + \sum_{1\le i<j<l\le 4} f^3 K_i K_j K_l [C]^3 + f^4 K_1 K_2 K_3 K_4 [C]^4\right) L + 1 + \sum_{i=1}^{4} K_i[C] + \sum_{1\le i<j\le 4} K_i K_j [C]^2 + \sum_{1\le i<j<l\le 4} K_i K_j K_l [C]^3 + K_1 K_2 K_3 K_4 [C]^4}$$

in which L is the equilibrium constant without capsaicin, K_1, K_2, K_3, K_4 are the association constant for the first, second, third and fourth subunit, respectively, f and $[C]$ are as defined above. For the YYYY concatemer, $K_1 = K_2 = K_3 = K_4 = K_Y$; for the YYAA concatemer, $K_1 = K_2 = K_W, K_3 = K_4 = K_A$; etc.

Figures and legends

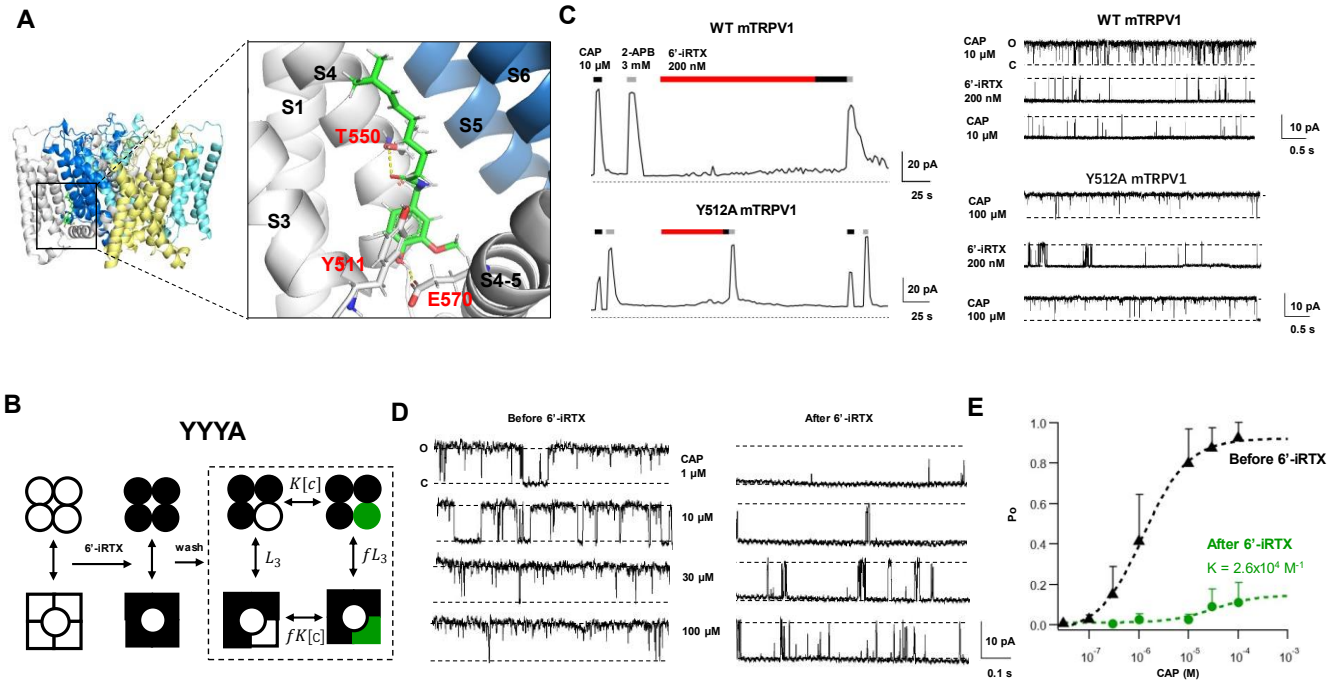

Figure 1. Direct measurement of capsaicin binding affinity to the Y511A mutant binding site. A. Structure of the rat TRPV1 (based on PDB entry 3J5R), with a zoom-in view of the vanilloid binding pocket, capsaicin (green), and key interacting residues. Yellow dash lines indicate a hydrogen bond. B. Illustration of the experimental scheme for the YYYA concatemer. A solution of 200 nm 6'-iRTX was first perfused to a membrane patch containing a single YYYA channel to occupy all the binding sites; after washing off the reversibly bound 6'-iRTX from the Y subunits, capsaicin solutions at varying concentrations were perfused to occupy the available binding site in the mutant A subunit. The dash box highlights an allosteric model for capsaicin binding to the single binding site. L_3, K[c], fL_3, fK[c] are equilibrium constant for the respective transition. C. Representative macroscopic (left panel) and single-channel (right panel) inside-out patch-clamp recordings from wildtype and Y512A mutant mouse TRPV1 (equivalents to Y511A rat TRPV1).

D. Representative capsaicin responses of a YYYA channel before (left) and after (right) loading the channel's Y subunits with 6'-iRTX. E. Summarized capsaicin-dependent Po with or without 6'-iRTX in the Y subunits, data are reported as mean ± S.D.. Black triangles: capsaicin responses without 6'-iRTX, fitted to a Hill equation with the following parameters: EC_{50} = 1.2x10^{-6} M, Hill slope = 0.96. N = 5 to 9. Green circles: capsaicin responses with preloaded 6'-iRTX in the Y subunits, fitted to the allosteric model derived for panel B with the following parameters: L3 = 0.1, f = 15.4, K = 2.6x10^{4} M^{-1}. N = 5.

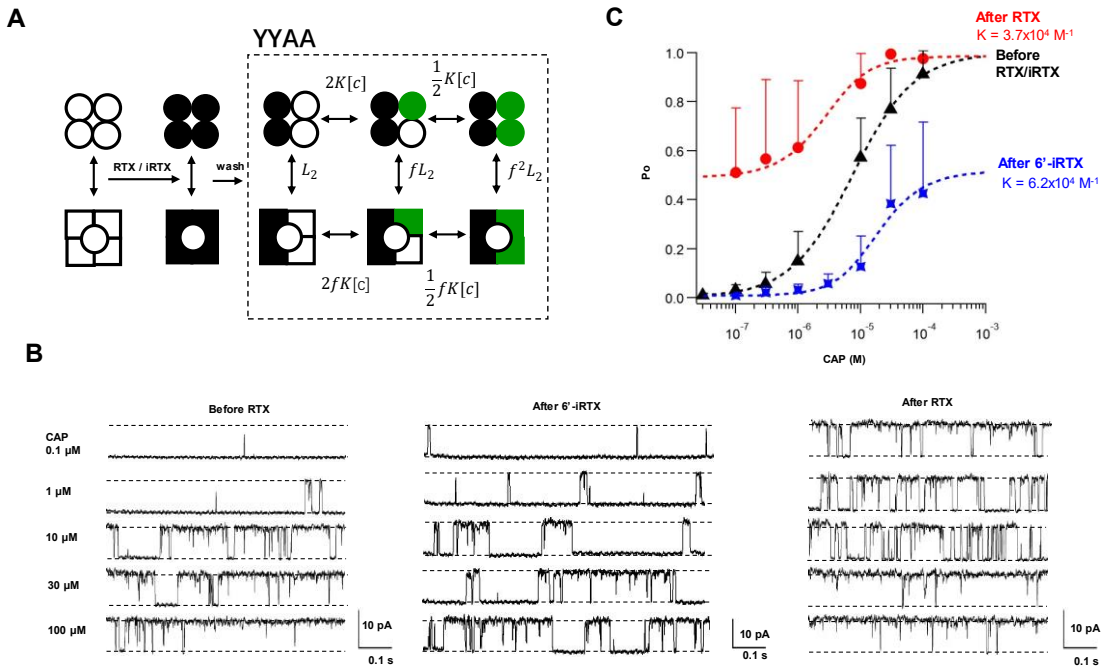

Figure 2. Measurement of capsaicin binding affinity from two Y511A mutant subunits in the channel. A. Illustration of the experimental scheme for the YYAA concatemer. A solution of 200 nm 6'-iRTX or RTX was first perfused to occupy all the binding sites; after washing off the reversibly bound 6'-iRTX or RTX from the Y subunits, capsaicin solutions were perfused to occupy the available binding sites in the A subunits. The dash box highlights an allosteric model

for capsaicin binding to the two A subunits. The equilibrium constants for each transition are labeled. B. Representative inside-out patch-clamp recordings from a YYAA channel before (left) and after loading the Y subunits with 6'-iRTX (middle) or RTX (right). C. Summarized Po of a YYAA channel with or without RTX/6'-iRTX. Data are reported as mean ± S.D. Black triangles: capsaicin responses without 6'-iRTX or RTX, fitted to a Hill equation with the following parameters: EC_{50} = 7.4x10-6 M, Hill slope = 0.88. N = 4 to 7. Red circles: capsaicin responses with preloaded RTX in the two Y subunits, fitted to the allosteric model derived from panel A with the following parameters: L_2 = 0.96, f = 8.9, K = 3.7 x 10^4 M^{-1}. N = 5. Blue squares: capsaicin responses with preloaded 6'-iRTX in the Y subunits, fitted with the following parameters: L_2 = 0.008, f = 11.8, K = 6.2 x 10^4 M^{-1}. N = 5.

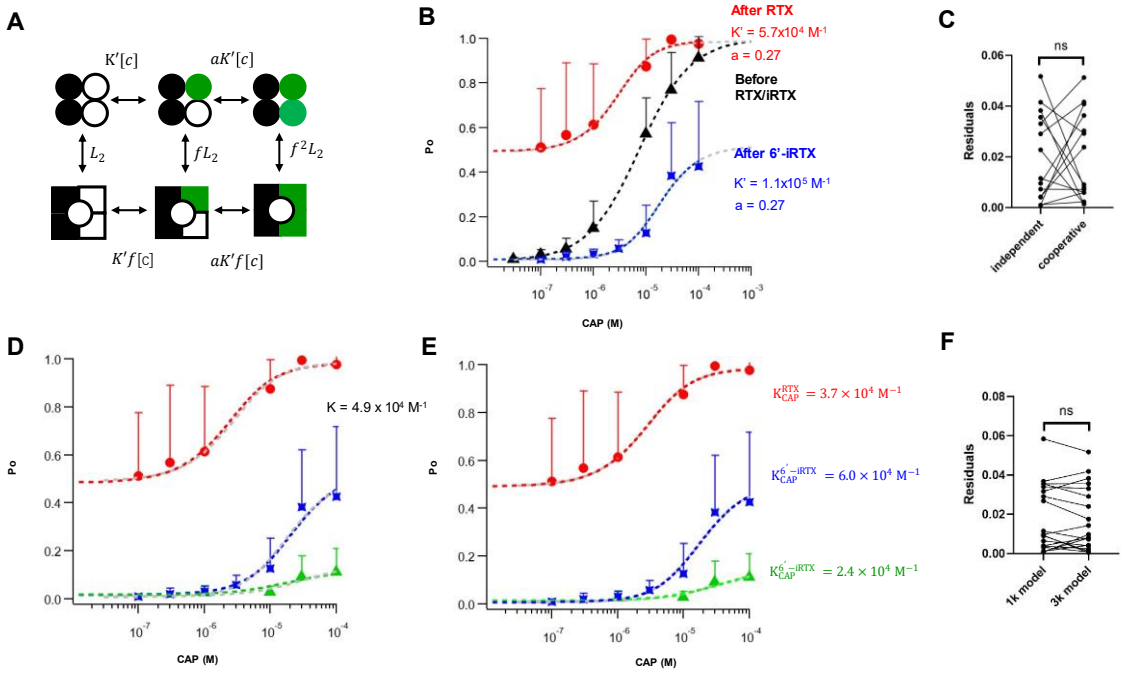

Figure 3. Testing cooperativity in capsaicin bindings. A. An allosteric model for the YYAA concatemer, with the two capsaicin binding steps having independent association constants. B.

Global fitting of YYAA channel's capsaicin responses using the model shown in panel A, assuming that the f and a values are identical when the wildtype binding sites are occupied by RTX (red circles) or 6'-iRTX (blue squares). L_2 = 0.97 (for RTX), L_2 = 0.01 (for 6'-iRTX), f =10.3. Gray curves represent fitting results with the independent binding model in Figure 2A. C. Paired Student's t test for the residuals from independent binding model and cooperative binding model. P = 0.98. ns: no significant difference. D. Global fitting of capsaicin concentration-dependent Po changes measured from YYYA preloaded with 6'-iRTX (green triangles), YYAA preloaded with RTX (red circles) or 6'-iRTX (blue asterisks). The K value for capsaicin binding was assumed to be the same with for all these cases. K = $4.9x10^5$ M^{-1}, f = 8.0, L with two pre-bound RTX = 0.94, L with two pre-bound 6'-iRTX = 0.02, L with three pre-bound 6'-iRTX = 0.02. Gray curves represent fitting results with the independent binding model in Figure 1B & 2A. E. Global fitting for capsaicin concentration dependent Po changes assuming that the K value for capsaicin binding is different in each case. With two pre-bound RTX: K = 3.7 $x10^4$ M-1, f = 8.9, L = 0.96; with three pre-bound 6'-iRTX: K = 2.4 $x10^4$ M^{-1}, f = 12.1, L = 0.01; with two pre-bound 6'-iRTX: K = 6.0 $x10^4$ M^{-1}, f = 10.7, L = 0.01. Gray curves represent fitting results with the independent binding model in Figure 1B & 2A. F. Paired Student's t test for the fitting residuals from the two assumptions (1K model vs 3K model). P = 0.36. ns: no significant difference.

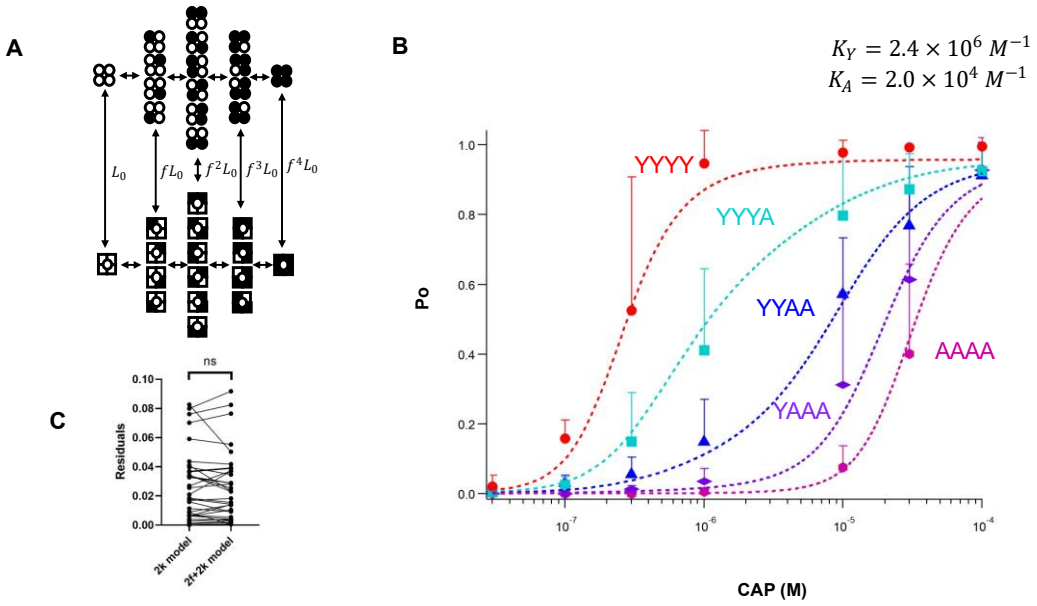

Figure 4. Determining capsaicin binding affinity to the wildtype binding site. A. A 32-state allosteric activation model, with reversible binding for capsaicin in both mutant and wildtype subunits. B. Global fitting of capsaicin concentration-dependent Po values from YYYY, YYYA, YYAA, YAAA and AAAA concatemers. Data are reported as mean ± S.D.. Independent binding and identical f factor for Y and A subunit were assumed; the association constants for the Y and A subunit, KY and KA, are distinct. L_0 = 0.001, K_Y = 2.4 x10^6 M^{-1}, K_A = 2.0 x10^4 M^{-1}, f = 12.1. N = 5 – 13. C. Paired Student's t test between the residuals from fitting a 2K model and those from fitting a 2f + 2K model (in which the f factors for Y and A subunits were assumed to be different). P = 0.49. ns: no significant difference. For fitting this 2f + 2K model, the following parameters were used: L_0 = 0.002, K_Y = 2.4 x10^6 M^{-1}, K_A = 1.5 x10^4 M^{-1}, f_Y = 10.7, f_A = 12.9.

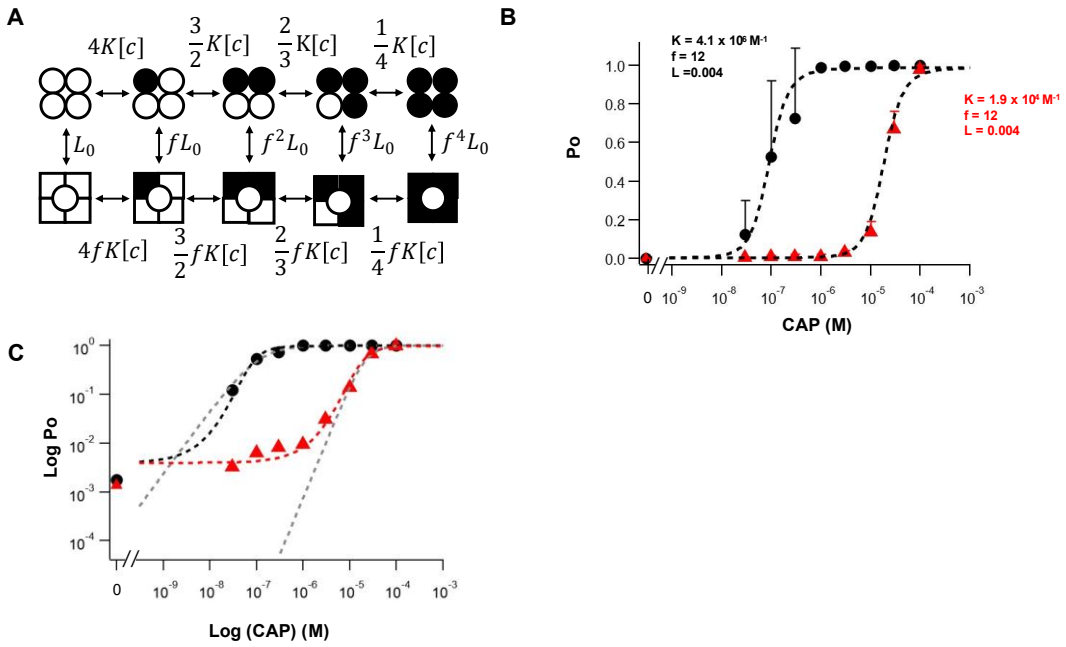

Figure 5. Quantitative description of capsaicin activation of the mouse TRPV1 wild-type and mutant channels. A. A complete MWC model with independent ligand binding steps. B. Concentration dependent Po data for the wild-type and mutant channels (black and red symbols, respectively) measured at the single-channel level, Data are reported as mean ± S.D., fitted to the MWC model (dash curves) with the following parameters: L_0 = 0.004, K_Y = 4.1 x10^6 M^{-1}, K_A = 1.9 x10^4 M^{-1}, f = 12. C. Log-transformation of the plot shown in B and overlapping Hill functions (gray dash curves) with the following parameters (EC50, slope factor): wild-type, 1.1 X10^{-7} M and 1.3; mutant, 2.2 X10^{-5} M and 2.3. The resting Po values, estimated from spontaneous activities, are shown on the left, at zero concentration.

SF1. MWC allosteric model

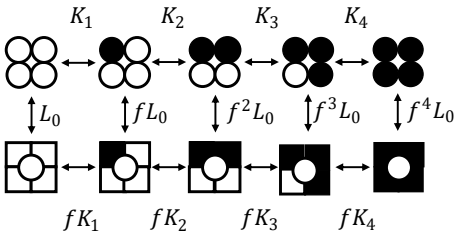

SF1. A classic MWC model for a tetrameric ion channel. The open and filled symbols represent an apo and ligand-bound subunit, respectively. L_0, apo-state equilibrium constant; f, cooperative factor that reflects the activation energy originated from each ligand binding; K, ligand association constant.

SF2. Structure comparison between 6' -iRTX and RTX

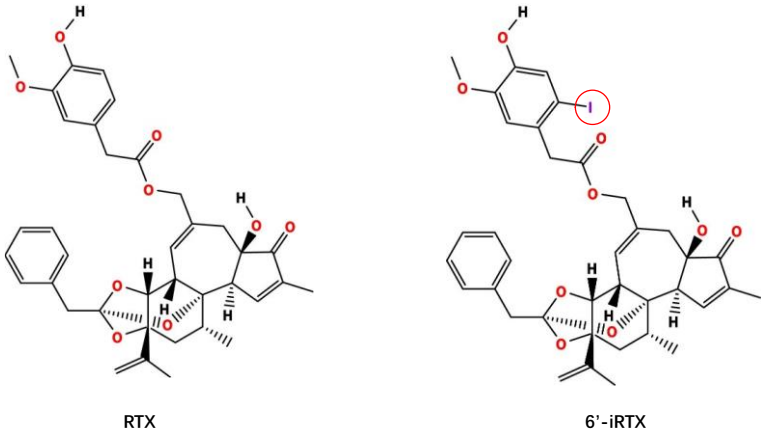

SF2. Molecular structure of resiniferatoxin (RTX) and 6'-iRTX. The iodine atom at the 6' position of the vanillyl group is highlighted.

SF3. 6’-iRTX irreversibly bound to WT mouse TRPV1 in single channel recording

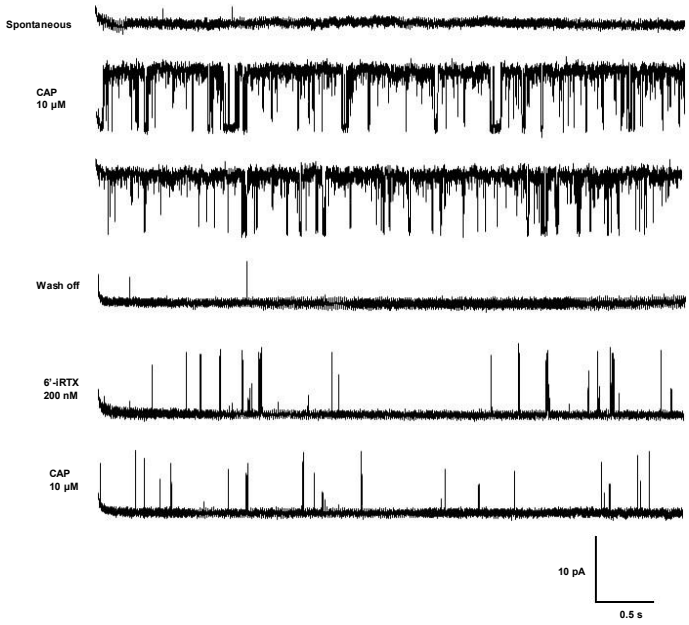

SF3. A representative single channel inside-out patch clamp recording for wildtype mouse TRPV1 activated by capsaicin and then irreversibly bound with 6’-iRTX.

SF4. 6’-iRTX reversibly bound to Y512A mouse TRPV1 in single channel recording

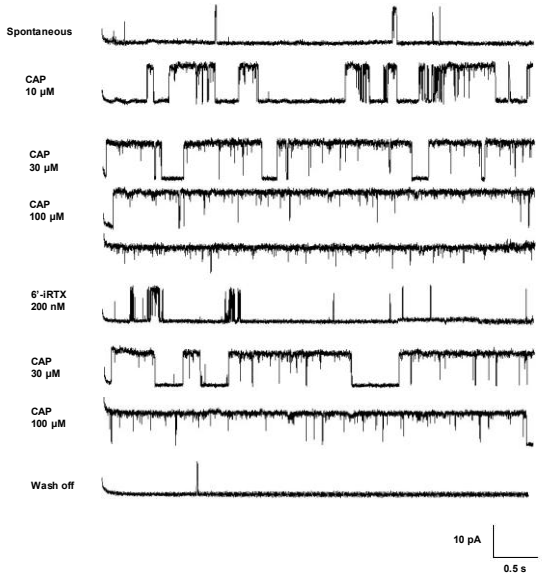

SF4. A representative single channel inside-out patch clamp recording for wildtype Y512A mouse TRPV1 activated by capsaicin and then reversibly bound with 6'-iRTX.

SF5. Capsaicin response in YYYA rat TRPV1 with preloaded 3 6' -iRTX molecules in single channel recording

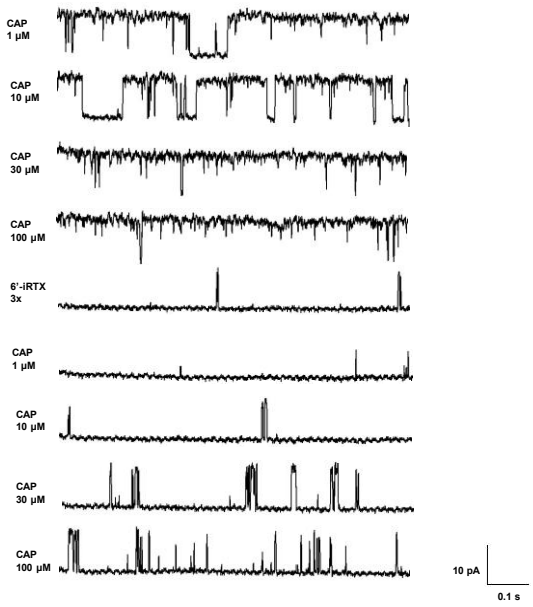

SF5. A representative single channel inside-out patch clamp recording for YYYA rat TRPV1 activated by capsaicin and loaded with 3 6'-iRTX molecules and tested capsaicin response again.

SF6. Capsaicin response in YYAA rat TRPV1 with preloaded 2 RTX molecules in single channel recording

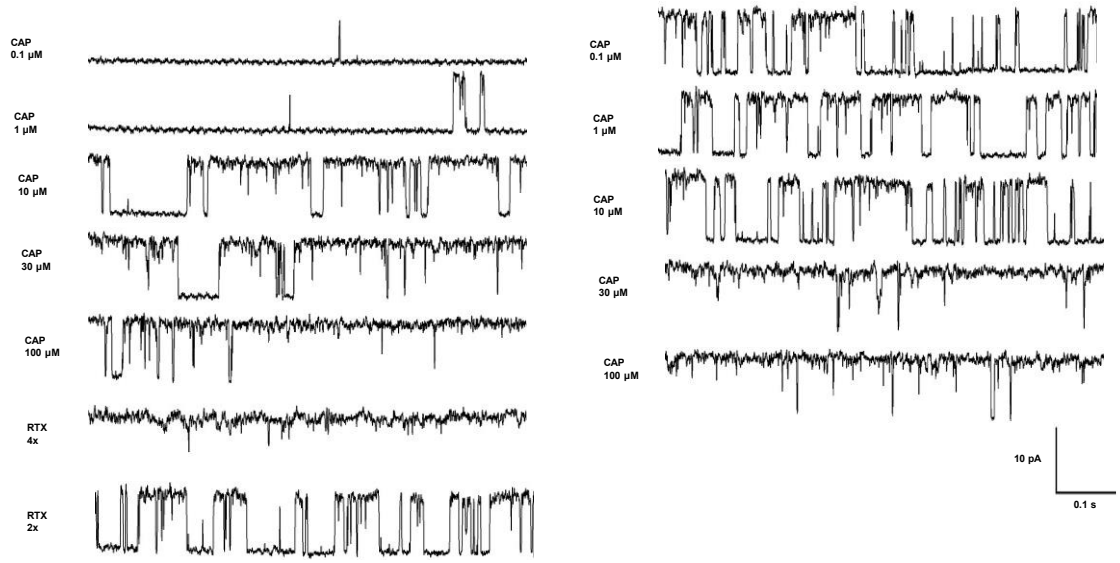

SF6. A representative single channel inside-out patch clamp recording for YYAA rat TRPV1 activated by capsaicin and loaded with 2 RTX molecules and tested capsaicin response again.

SF7. Capsaicin response in YYAA rat TRPV1 with preloaded 2 RTX or 6' -iRTX molecules in single channel recording

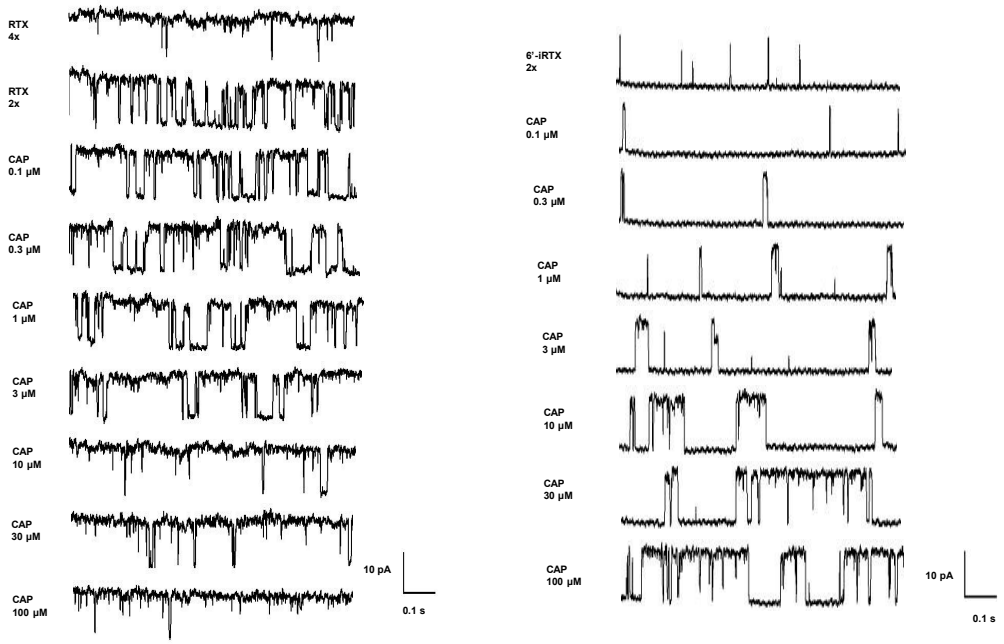

SF7. A representative single channel inside-out patch clamp recording for YYAA rat TRPV1 activated by capsaicin and loaded with 2 6'-iRTX molecules and tested capsaicin response again.

SF8a. Capsaicin response in rat TRPV1 concatemers in single channel recording

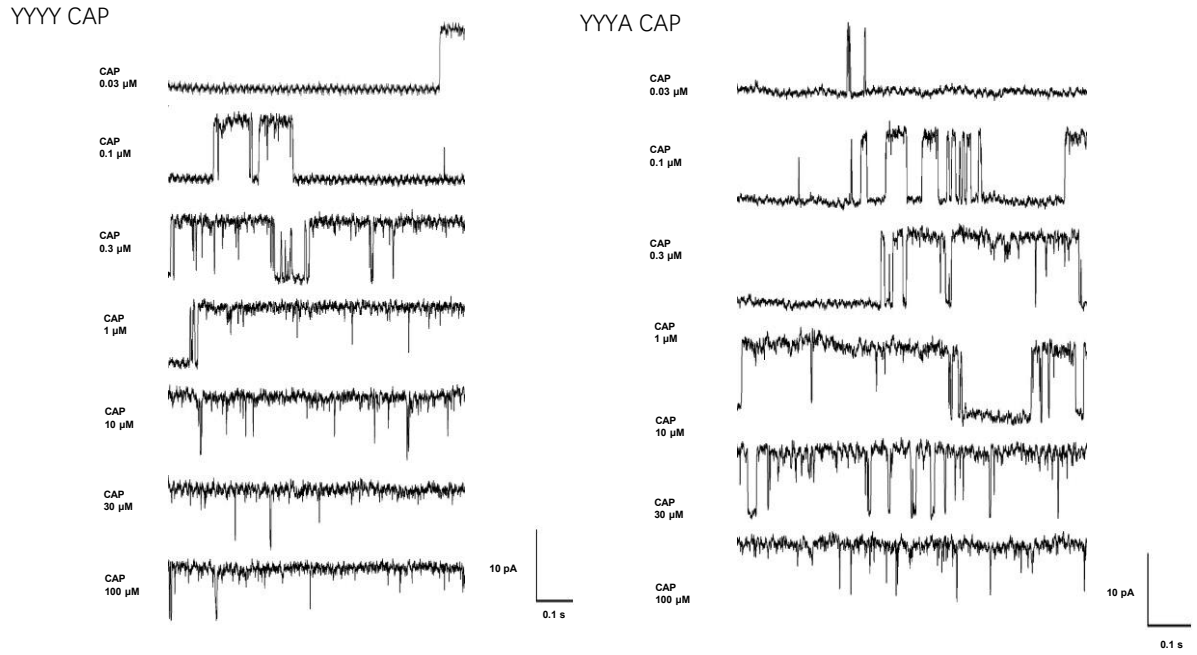

SF8b. Capsaicin response in rat TRPV1 concatemers in single channel recording

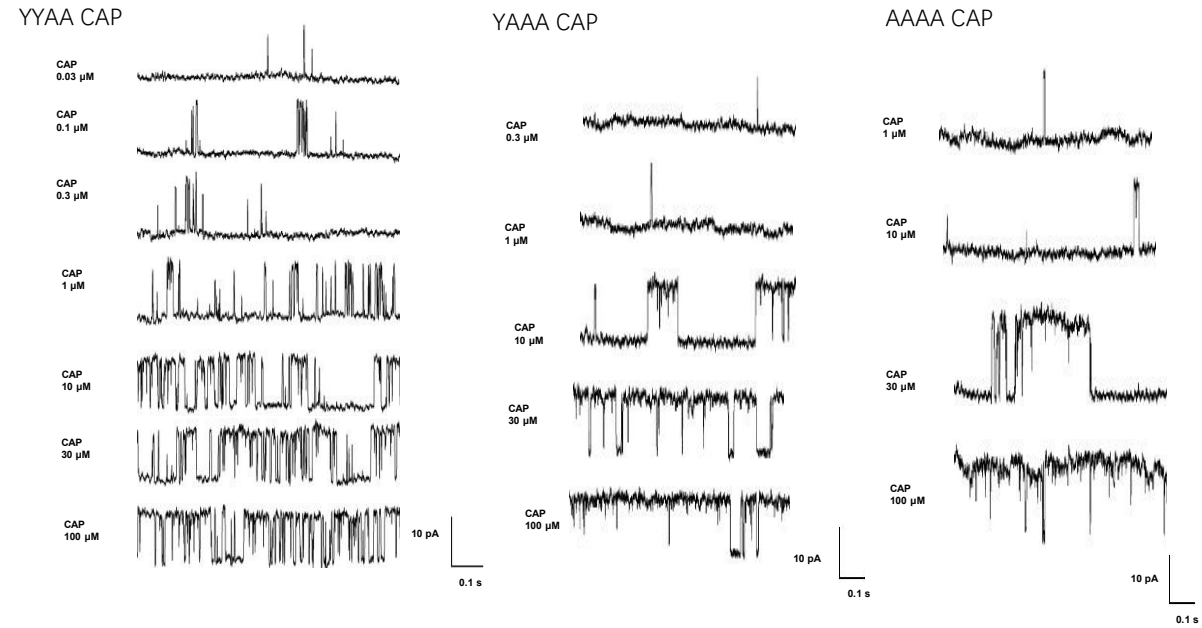

SF8. Capsaicin response in rat TRPV1 concatemers

References

1. M. J. Caterina *et al.*, The capsaicin receptor: a heat-activated ion channel in the pain pathway. *Nature* **389**, 816-824 (1997).
2. M. Tominaga *et al.*, The cloned capsaicin receptor integrates multiple pain-producing stimuli. *Neuron* **21**, 531-543 (1998).
3. F. Yang, J. Zheng, Understand spiciness: mechanism of TRPV1 channel activation by capsaicin. *Protein & cell* **8**, 169-177 (2017).
4. E. Cao, M. Liao, Y. Cheng, D. Julius, TRPV1 structures in distinct conformations reveal activation mechanisms. *Nature* **504**, 113-118 (2013).
5. M. Liao, E. Cao, D. Julius, Y. Cheng, Structure of the TRPV1 ion channel determined by electron cryo-microscopy. *Nature* **504**, 107-112 (2013).
6. K. Zhang, D. Julius, Y. Cheng, Structural snapshots of TRPV1 reveal mechanism of polymodal functionality. *Cell* **184**, 5138-5150. e5112 (2021).
7. D. H. Kwon, F. Zhang, J. G. Fedor, Y. Suo, S.-Y. Lee, Vanilloid-dependent TRPV1 opening trajectory from cryoEM ensemble analysis. *Nature Communications* **13**, 2874 (2022).
8. A. Neuberger *et al.*, Human TRPV1 structure and inhibition by the analgesic SB-366791. *Nature Communications* **14**, 2451 (2023).
9. Y. Gao, E. Cao, D. Julius, Y. Cheng, TRPV1 structures in nanodiscs reveal mechanisms of ligand and lipid action. *Nature* **534**, 347-351 (2016).
10. K. Hui, B. Liu, F. Qin, Capsaicin activation of the pain receptor, VR1: multiple open states from both partial and full binding. *Biophysical journal* **84**, 2957-2968 (2003).
11. F. Yang *et al.*, The conformational wave in capsaicin activation of transient receptor potential vanilloid 1 ion channel. *Nature communications* **9**, 1-9 (2018).
12. F. Yang *et al.*, Structural mechanism underlying capsaicin binding and activation of the TRPV1 ion channel. *Nat Chem Biol* **11**, 518-524 (2015).
13. H. Salazar *et al.*, Structural determinants of gating in the TRPV1 channel. *Nature Structural & Molecular Biology* **16**, 704-710 (2009).
14. N. R. Gavva *et al.*, Molecular determinants of vanilloid sensitivity in TRPV1. *J Biol Chem* **279**, 20283-20295 (2004).
15. S.-E. Jordt, D. Julius, Molecular basis for species-specific sensitivity to “hot” chili peppers. *Cell* **108**, 421-430 (2002).
16. A. Hazan, A. Basu, N. Zalcman, H. Matzner, A. Priel, Tyrosine residue in the TRPV1 vanilloid binding pocket regulates deactivation kinetics. *Journal of Biological Chemistry* **291**, 13855-13863 (2016).
17. Y. Yin *et al.*, Structural mechanisms underlying activation of TRPV1 channels by pungent compounds in gingers. *British Journal of Pharmacology* **176**, 3364-3377 (2019).
18. S. Vu, V. Singh, H. Wulff, V. Yarov-Yarovoy, J. Zheng, New capsaicin analogs as molecular rulers to define the permissive conformation of the mouse TRPV1 ligand-binding pocket. *Elife* **9**, e62039 (2020).
19. Y. Dong *et al.*, A distinct structural mechanism underlies TRPV1 activation by piperine. *Biochemical and biophysical research communications* **516**, 365-372 (2019).
20. K. Elokely *et al.*, Understanding TRPV1 activation by ligands: Insights from the binding modes of capsaicin and resiniferatoxin. *Proceedings of the National Academy of Sciences* **113**, E137-E145 (2016).
21. L. Darré, C. Domene, Binding of capsaicin to the TRPV1 ion channel. *Molecular pharmaceutics* **12**, 4454-4465 (2015).

22. D. Colquhoun, Binding, gating, affinity and efficacy: the interpretation of structure-activity relationships for agonists and of the effects of mutating receptors. *Br J Pharmacol* **125**, 924-947 (1998).
23. J. Monod, J. Wyman, J. P. Changeux, On the Nature of Allosteric Transitions: A Plausible Model. *J Mol Biol* **12**, 88-118 (1965).
24. S. Li, P. T. Nguyen, S. Vu, V. Yarov-Yarovoy, J. Zheng, Opening of capsaicin receptor TRPV1 is Stabilized Equally by Its Four Subunits. *Journal of Biological Chemistry*, 104828 (2023).
25. A. Hazan, R. Kumar, H. Matzner, A. Priel, The pain receptor TRPV1 displays agonist-dependent activation stoichiometry. *Scientific reports* **5**, 1-13 (2015).
26. M. E. McDonnell, S.-P. Zhang, A. E. Dubin, S. L. Dax, Synthesis and in vitro evaluation of a novel iodinated resiniferatoxin derivative that is an agonist at the human vanilloid VR1 receptor. *Bioorganic & medicinal chemistry letters* **12**, 1189-1192 (2002).
27. W. N. Zagotta, "Ligand-dependent gating mechanism" in Textbook of Ion Channels Volume I. (CRC Press, 2023), pp. 45-60.
28. R. Latorre, S. Brauchi, G. Orta, C. Zaelzer, G. Vargas, ThermoTRP channels as modular proteins with allosteric gating. *Cell calcium* **42**, 427-438 (2007).
29. J. A. Matta, G. P. Ahern, Voltage is a partial activator of rat thermosensitive TRP channels. *The Journal of physiology* **585**, 469-482 (2007).
30. A. Jara-Oseguera, L. D. Islas, The role of allosteric coupling on thermal activation of thermo-TRP channels. *Biophys J* **104**, 2160-2169 (2013).
31. X. Cao, L. Ma, F. Yang, K. Wang, J. Zheng, Divalent cations potentiate TRPV1 channel by lowering the heat activation threshold. *Journal of General Physiology* **143**, 75-90 (2014).
32. J. Zheng, Molecular mechanism of TRP channels. *Comprehensive Physiology* **3**, 221-242 (2013).
33. J. Zheng, M. C. Trudeau, *Textbook of Ion Channels: Three Volume Set* (CRC Press, 2023).
34. W. Bolton, M. Perutz, Three dimensional Fourier synthesis of horse deoxyhaemoglobin at 2.8 Å resolution. *Nature* **228**, 551-552 (1970).
35. B. Shaanan, Structure of human oxyhaemoglobin at 2· 1resolution. *Journal of molecular biology* **171**, 31-59 (1983).
36. M. D. Varnum, D. Gucan, "Cyclic nucleotide-gated channels" in Textbook of Ion Channels Volume II. (CRC Press), pp. 163-180.
37. D. S. White *et al.*, cAMP binding to closed pacemaker ion channels is non-cooperative. *Nature* **595**, 606-610 (2021).
38. D. T. Liu, G. R. Tibbs, P. Paoletti, S. A. Siegelbaum, Constraining ligand-binding site stoichiometry suggests that a cyclic nucleotide–gated channel is composed of two functional dimers. *Neuron* **21**, 235-248 (1998).
39. J. Schirmeyer *et al.*, Thermodynamic profile of mutual subunit control in a heteromeric receptor. *Proceedings of the National Academy of Sciences* **118**, e2100469118 (2021).
40. A. Plested, Ionotropic glutamate receptors. *Textbook of Ion Channels Volume II: Properties, Function, and Pharmacology of the Superfamilies* **255**, 239 (2023).
41. H. I. Ingólfsson *et al.*, Phytochemicals perturb membranes and promiscuously alter protein function. *ACS chemical biology* **9**, 1788-1798 (2014).

Chapter IV: How Much Does TRPV1 Deviate from An Ideal MWC-Type Protein

Shisheng Li and Jie Zheng

Abstract

Many ion channels are known to behave as an allosteric protein, coupling environmental stimuli captured by specialized sensing domains to the opening of a central pore. The classic Monod-Wyman-Changeux (MWC) model, originally proposed to describe binding of gas molecules to hemoglobin, has been widely used as a framework for analyzing ion channel gating. Here we address the issue of how accurate the MWC model predicts activation of the capsaicin receptor TRPV1 by vanilloids. Taking advantage of a concatemeric design that makes it possible to lock TRPV1 in states with zero-to-four bound vanilloid molecules, we showed quantitatively that the overall gating behavior is satisfactorily predicted by the MWC model. There is however a small yet detectable subunit position effect: ligand binding to two kitty-corner subunits is 0.3 to 0.4 kcal/mol more effective in inducing opening than binding to two neighbor subunits. This difference—less than 10% of the overall energetic contribution from ligand binding—might be due to the restriction on subunit arrangement imposed by the planar membrane; if this is the case, the position effect is not expected in hemoglobin, in which each subunit is related equivalently to all the other subunits.

Significance

The MWC model, proposed more than 50 years ago, is elegantly simple yet powerful in predicting the behavior of allosteric proteins like hemoglobin. Its prediction power for ion channel gating has been beautifully demonstrated in the studies of BK channels. Our present work aims to determine how accurate the MWC model predicts TRPV1 activation induced by vanilloids. Our findings

support the notion that the evolutionary drive upon allosteric proteins applies generally to multi-subunit proteins including ion channels.

Introduction

In the landmark study of neuronal action potential, Hodgkin and Huxley found that the entities controlling transmembrane conductance for sodium and potassium ions—which are now known as voltage-gated sodium (Nav) channels and voltage-gated potassium (Kv) channels—operate with high voltage sensitivities (Hodgkin and Huxley 1952). In their empirical equations describing the voltage dependence of sodium and potassium conductance, this high sensitivity is reflected by the exponents assigned to the probability terms. Modern expansions of the H&H ideas incorporating knowledge of Nav and Kv channel structures reveal that high voltage sensitivity is partially rooted in the highly cooperative nature of voltage-dependent activation. In the 1990s, Zagotta, Hoshi and Aldrich (Zagotta, Hoshi, and Aldrich 1994) and Schoppa and Sigworth (Schoppa and Sigworth 1998) identified a late cooperative transition that would be needed in an otherwise independent subunit gating scheme to satisfactorily describe the course of activation in Shaker potassium channels. It is thought that the voltage sensors of Shaker, as well as many other voltage-gated ion channels, operate in a mostly independent manner, whereas some of the conformational changes in the channel pore must be concerted (Zheng and Trudeau 2023).

BK potassium channels are activated by not just transmembrane voltage but also intracellular calcium. Their activation also exhibits cooperativity (Rothberg and Magleby 1998). In a comprehensive investigation of BK channel macroscopic currents, single-channel currents, and gating currents, Horrigan, Cui and Aldrich revealed that the voltage sensor and calcium sensor operate separately, and they both influence the channel pore opening allosterically (Horrigan and Aldrich 1999; Horrigan, Cui, and Aldrich 1999; Horrigan and Aldrich 2002). The kinetic model

that could satisfactorily describe BK activation behaviors thus contains two branches of allosteric coupling. In each branch of the model, the four sensors (for voltage or calcium) contribute an equal amount of energy towards influencing the pore opening. Cooperativity among subunits is rooted in this joint influence of open pore stability.

This type of allosteric coupling has been previously proposed to govern another protein, the oxygen carrier hemoglobin. Hemoglobin is a protein complex made of two α subunits and two β subunits; each of these subunits contains a structurally and functionally similar binding pocket for gas molecules (Bolton and Perutz 1970). Oxygen binding to these four sites in hemoglobin is highly cooperative (Edsall 1972). Monod, Wyman and Changeux postulated that the cooperativity comes from a concerted conformational change that affects all gas binding sites equally (Monod, Wyman, and Changeux 1965). Hemoglobin serves as a carrier for gas molecules; there is no function equivalent to ion conduction in an ion channel that can be used as a direct indicator of the concerted transition. Studies of hemoglobin therefore focused on the ligand binding process. It was proposed that, there is an equal energetic contribution to the concerted transition by each gas molecule binding step, and these binding steps per se are independent (Monod, Wyman, and Changeux 1965). Introducing interactions at the binding steps, such as those seen in the sequential model, yields good performance but also adds complexity (Koshland, Némethy, and Filmer 1966).

Equal and independent contribution to gating by each subunit is assumed for BK channels in the study by Horrigan, Cui and Aldrich, and for many other ion channels studied subsequently. The MWC-type models in general worked well in predicting channel behaviors and provided important guidance for mechanistic investigations in the following decades. Many mechanistic predictions from these studies are nicely confirmed when ion channel structures became available (Zheng and Trudeau 2023). In recent studies of the capsaicin receptor TRPV1 (Li et al. 2023; Li and Zheng

2023), we realized that a set of concatemers previously designed by Priel and colleagues (Hazan et al. 2015) would allow us to lock a TRPV1 channel in each of the intermediate ligand-bound states, hence presenting a unique opportunity to directly test applicability of the MWC model to the TRPV1 channel. This is possible because the concatemers, made of various combinations of wildtype and Y511A mutant protomers, would trap a vanilloid molecule such as resiniferatoxin (RTX) when it binds to a wildtype subunit but allow it to fall off a mutant subunit. Isolating intermediate binding states for equilibrium measurements has been challenging for hemoglobin bound with small gas molecules; it is, to our best knowledge, not done with any concatemeric ion channels. In the present study, we took advantage of this powerful system to address the question: how close does TRPV1 resemble an ideal MWC-type allosteric protein?

Materials and Methods

Molecular Biology

The plasmids used in this study were made in the Priel laboratory (Hazan et al. 2015). Briefly, wild-type rat TRPV1 (Y) cDNAs were joined with the Y511A mutant (A) cDNAs in various combinations: YYYY, YYYA, YYAA, YAYA, AYAY, YAAA, and AAAA. Their functional properties have been carefully tested and described in previous publications; no noticeable change in gating behavior was detected in these studies (Hazan et al. 2015; Li et al. 2023; Li and Zheng 2023). Representative single-channel recordings for each concatemer are presented in Supplementary Figures. Y511 locates near the entrance of the vanilloid binding pocket (Liao et al. 2013). Its long-side chain points downward in the apo state; binding of a vanilloid ligand causes the side chain to flip upwards (Cao et al. 2013). In this up position, the side-chain would slow down a bound ligand from exiting the pocket (Yang et al. 2015a; Li and Zheng 2023). We recently found that the Y512A mutation (with a smaller side-chain) in the mouse TRPV1, or the equivalent

Y511A mutation in the rat TRPV1, makes binding of RTX and 6'-iRTX reversible (Li et al. 2023; Li and Zheng 2023). Exit of a bound capsaicin, which has the same vanillyl head group as RTX but is much small in overall size, is apparently also facilitated by the mutation (Hazan et al. 2016).

Cell Culture

TSA201 cells (HEK293T variant from American Type Culture Collection) served as the expression system for patch-clamp assays. These cells were cultivated on 25-mm glass coverslips in 30-mm dishes (from Fisher Scientific) until reaching 30% - 50% confluence, then transiently transfected. Transfection was carried out using Lipofectamine 2000 (Invitrogen) 24 hours prior to patch-clamp recording, following the manufacturer's guidelines. For single-channel recordings, a combination of 0.1 μg concatemer plasmid and 0.2 μg eYFP plasmid was utilized per transfection.

Chemical Solutions

For inside-out patch-clamp recordings, we used symmetric bath and pipette solutions containing 140 mM NaCl, 15 mM HEPES, 2 mM EDTA, with a pH of 7.4. Capsaicin (from Sigma-Aldrich) was dissolved in dimethyl sulfoxide (DMSO) to prepare a 1 M stock, then further diluted to concentrations ranging from 0.01 μM to 100 μM using the bath solution. Both resiniferatoxin (Alomone Labs) and 6'-iodoresiniferatoxin (6'-iRTX, Sigma-Aldrich) were dissolved in ethanol to create a 1 mM stock and subsequently diluted to a 200 nM working concentration with the bath solution. Lastly, 2-aminoethoxydiphenyl borate (2-APB, Sigma-Aldrich) was dissolved in DMSO to produce a 1 M stock, which was then diluted to a 3 mM working solution.

Electrophysiology

Pipettes for patch-clamp recordings were pulled from borosilicate glass capillaries (Sutter Instrument) using a P-97 micropipette puller (Sutter Instrument) and fire-polished to achieve

resistances 8-15 MΩ for single-channel recordings. We employed an EPC 10 USB patch-clamp amplifier (Warner Instruments), operated by the PatchMaster software. Sampling and filtering frequencies were set at 10 kHz and 2.25 kHz, respectively. Patch-clamp configurations were primarily inside-out, unless specifically stated otherwise. The holding potential began at 0 mV and proceeded to steps of +80 mV and –80 mV. Step durations were adjusted as required. A gravity-driven perfusion system, controlled by the Rapid Solution Changer (RSC200, Biological Science Instrument), facilitated solution perfusion and changes.

Data Analysis

Patch-clamp data, exported from PatchMaster in the Igor format, were analyzed using Igor Pro 8 (WaveMetrics). Statistical analyses were conducted in Graphpad Prism 8. Two-way ANOVA tests were done to detect difference between YYAA (ligand binding in neighboring subunits) versus YAYA or AYAY (ligand binding in kitty-corner subunits). Detailed results for the two-way ANOWA test are included in supplementary tables. Data are presented as mean $\pm$ SEM.

Single-channel open probabilities were determined by creating all-point histograms from single-channel current traces. For recordings from a single channel, the histogram contained two peaks whose area represented the total time spent in the closed state, tc, and the open state, to, respectively. The open probability was calculated as $Po = \frac{t_o}{t_o + t_c}$. For patches containing two channels, the histogram contained two open-state peaks corresponding to one and two channels in the open state. The areas under them, t1 and t2, respectively, were used to determine the open probability using the equation $Po = \frac{t_1 + 2 \times t_2}{2 \times T}$. Here, T the total area of the histogram. Recordings with more than two channels were discarded.

Model fitting

As an initial analysis, capsaicin responses of concatemeric channels were fitted to a Hill equation

$$Po = P_{o\_base} + \frac{(P_{o\_max} - P_{o\_base})}{1 + \left(\frac{EC50}{[Cap]}\right)^{n}}$$

where EC50 is the concentration for 50% activity, [Cap] is the capsaicin concentration, n is the Hill slope factor. Capsaicin responses of concatemeric channels pretreated with RTX or 6'-iRTX were further fitted to models with specific modifications of the MWC model (shown in Figure 2). The goal of these analyses was to obtain an upper limit estimate for the free energy representing the deviation from an ideal MWC system. For these analyses, a global fitting routine was applied simultaneously to data from all three concatemers pretreated with either RTX or 6'-iRTX. The global fitting package in Igor Pro 8 was used to fit these single-channel Po data.

To obtain free energy estimates, we considered two extreme situations. For the first situation, we assumed that the observed position effect was solely due to differences in capsaicin binding affinity. This could be reflected by assigning a cooperativity coefficient to the first ligand binding step in the MWC-type model for a two-site system, while keeping the other parameters unchanged. Shown in Figure 3A&B are equilibrium constants for all the transitions, where L_2 is the equilibrium constant for channels pre-loaded with two RTX or 6'-iRTX molecules, $[c]$ is the concentration of capsaicin in the perfusion solution, K is the binding affinity parameter, a and a' are the cooperativity coefficient for binding, f is the gating parameter (fold change to L2 as a result of each capsaicin binding step). Solving this model under the equilibrium condition yields the following equation:

$$Po = \frac{L_2 + 2afK[c]L_2 + af^2K^2[c]^2L_2}{1 + 2aK[c] + aK^2[c]^2 + L_2 + 2afK[c]L_2 + af^2K^2[c]^2L_2}$$

Global fitting results using this model are shown in Figure 3C, where the same set of values for f, K were used, the values for L2, a (applied to the YYAA dataset) and a' (applied to the YAYA and AYAY datasets) were allowed to vary between different groups.

For the second extreme situation, we assumed that the observed position effect was solely due to a difference in the activation transition. This could be reflected by assigning a cooperativity coefficient to the first vertical gating transition (which would be carried on to the second gating transition and the first binding transition in the open state, to maintain microscopic reversibility), while keeping the other parameters unchanged. Shown in Figure 4A&B are equilibrium constants for all the transitions, where individual parameters are defined in the same way as described above, and b and b' are the cooperativity coefficient for gating (ratio factor between the two gating equilibrium constants following the first and second capsaicin binding steps). Solving this model under the equilibrium condition yields the following equation:

$$Po = \frac{L_2 + 2bfK[c]L_2 + bf^2K^2[c]^2L_2}{1 + 2K[c] + K^2[c]^2 + L_2 + 2bfK[c]L_2 + bf^2K^2[c]^2L_2}$$

Global fitting results using this model are shown in Figure 4C, where the same set of values for f, K were used, the values of L2, b (applied to the YYAA dataset) and b' (applied to the YAYA and AYAY datasets) were allowed to vary between different groups.

For comparison, a classic MWC model without a position effect was also used to fit the group data (gray curves in Figures 3C and 4C):

$$Po = \frac{L_2 + 2fK[c]L_2 + f^2K^2[c]^2L_2}{1 + 2K[c] + K^2[c]^2 + L_2 + 2fK[c]L_2 + f^2K^2[c]^2L_2}$$

To directly determine the position effect on free energy associated with the gating transitions, we measured the Po values when a different number of RTX molecules were bound to the channel. This was achieved by treating each of the YYYY, YYYA, YYAA, YAYA, AYAY, YAAA, and AAAA channel for an extended time, followed by thorough wash to remove the reversible binding of RTX to the A subunits, as previously described (Li et al. 2023). The following equations were used:

For AAAA (with none RTX bound): $Po = \frac{L_0}{1+L_0}$

For YAAA (with 1 RTX bound): $Po = \frac{f_1 L_0}{1+f_1 L_0}$

For YAYA and AYAY (with 2 RTX bound at diagonal sites): $Po = \frac{f_2 L_0}{1+f_2 L_0}$

For YYAA (with 2 RTX bound at adjacent sites): $Po = \frac{{f_1}^2 L_0}{1+{f_1}^2 L_0}$

For YYYA (with 3 RTX bound): $Po = \frac{f_1 f_2 L_0}{1+f_1 f_2 L_0}$

For YYYY (with 4 RTX bound): $Po = \frac{{f_2}^2 L_0}{1+{f_2}^2 L_0}$

In these equations, L_0 is the equilibrium constant for channels in the apo state, f_1 is the gating parameter when only one RTX bound in the diagonal pair of the binding sites, f_2 is the gating parameter when two RTX bound in the diagonal pair of the binding sites. The results of global fitting of these equations simultaneously to the corresponding datasets are shown in Figure 5B.

The classic MWC model would predict for this situation the following equation: $Po = \frac{f^n L_0}{1+f^n L_0}$, where L_0 is the equilibrium constant for channels in the apo state, f is the gating parameter for

each RTX bound to the channel, n is the number of bound RTX. Prediction of this model is included in Figure 5B for comparison.

Results

TRPV1 is an allosteric protein. In the absence of ligands such as capsaicin or RTX, TRPV1 can spontaneously transition from a closed state to an open state at a very low probability (with an equilibrium constant less than 0.01) (Li et al. 2023; Yang et al. 2018). As an increasing number of agonist molecules bind to TRPV1, the equilibrium progressively shifts towards the open state. Our previous study showed that, during RTX activation of TRPV1, sequential RTX bindings shift the equilibrium nearly exponentially, suggesting energy contributions from these RTX binding steps are approximately equal (Li et al. 2023), as the classic MWC model postulates (Monod, Wyman, and Changeux 1965). Binding of all four subunits with RTX molecules contributes a total energy of 6.8-to-7.4 kcal/mol towards activation (Li et al. 2023).

However, when we closely examined the capsaicin response curves for YAYA, AYAY, and YYAA concatemers—all producing channels with two wild-type subunits and two mutant subunits but with different subunit arrangements (Figure 1A)—a minor but apparent difference could be discerned. Both YAYA and AYAY (with two mutant subunits located at kitty-corners in the assembled channels) appeared to be slightly more sensitive to capsaicin than YYAA (with mutant subunits at neighbor positions) (Figure 1B). The small differences in the EC50 value, obtained from fitting with a Hill function, would translate into a free energy difference of about 0.66 kcal/mol between YYAA and YAYA, and 0.53 kcal/mol between YYAA and AYAY. The group data for YAYA and AYAY are significantly deviated from the group data for YYAA (P <

0.0001 and P = 0.005) (Supplementary Table). Nonetheless, at most specific capsaicin concentrations, a statistically significant difference in Po was hard to be confidently established *.

Given the uncertainty, we assessed the potential subunit positioning effect with a different approach. Taking advantage of the reversible binding of RTX to the A subunits and irreversible binding to the Y subunits, we first fully loaded each channel type with RTX, followed by thorough washing. As we reported previously (Li et al. 2023; Li and Zheng 2023), this procedure yielded channels containing two Y subunits bound with RTX and two A subunits available for subsequent binding by capsaicin. We measured the channel open probability at increasing concentrations of capsaicin. As shown in Figure 1C, a slightly higher capsaicin sensitivity in YAYA and AYAY concatemeric channels was again observed, which is reflected in the uplifted concentration-dependence curves, though this apparent difference wasn't statistically significant (P = 0.16 and 0.15) (Supplementary Table). Similar results were obtained using 6'-iRTX, a RTX derivative that is a much weaker TRPV1 agonist; a small yet statistically significant (P = 0.0009 and 0.015) upward shift in the capsaicin concentration dependence curves for AYAY and YAYA could be seen (Figure 1D).

Our results indicate that, when two ligands bind to a single TRPV1 channel, the diagonal ("kitty-corner") binding positions produce a higher open probability than the adjacent binding positions. This behavior is not aligned with the prediction of the classic MWC model, which assumes equality in subunit contributions (Figure 2A). To experimentally assess the magnitude of this position effect, we used a modified model incorporating distinct states for the two-ligand bound configurations,

* One of the five recordings from AYAY yielded an abnormal right-shifted capsaicin dependence curve, which was excluded from Figure 1B. While the cause of this abnormality is unknown, there are previous reports that a concatemeric construct may sometimes fail to constrain the subunit composition. Including this outlier recording would make the difference between AYAY and YYAA even smaller (see Supplementary Figure 4).

as shown in Figure 2B. In this expanded model, the increased cooperativity for the diagonal binding positions could arise either from the binding process (characterized by the K parameter) or the gating process (characterized by the f parameter). We evaluated these possibilities separately in the following two sets of experiments, using single-channel Po data in response to capsaicin after the two Y subunits in each channel were preloaded with RTX or 6'-iRTX molecules (the sub-system shown by the dash box in Figure 2B).

To assess a potential subunit position effect on binding affinity, we first assumed the gating effect (f) to be independent of the position effect (Figure 3A&B); that is, variation in gating cooperativity was assumed to originate solely from binding, hence potentially exaggerating the binding effect. We assigned the equilibrium constant for the last binding step the same K parameter, since this step is identical for all concatemers, as can be seen in Figure 3A&B. However, transitioning from a two-ligand-bound state to a three-ligand-bound state might show sensitivity to the initial positions of liganded subunits, leading us to introduce a coefficient factor a or a' to the binding parameter K. In the absence of a position effect, both a and a' would be 1 as expected from independent binding. However, if a position effect existed, a and a' would differ. As described earlier, we first treated each concatemeric channel with RTX or 6'-iRTX followed by thorough wash; this yielded channels in which the wildtype Y subunits were occupied (black filled symbols in Figure 3A&B) and the mutant subunits available for binding by capsaicin. Global fitting of the capsaicin response datasets from all concatemers pretreated with either RTX or 6'-iRTX (Figure 3C; Supplementary Figure 5, left panel) yielded values of a = 0.83 and a' = 1.37, suggesting the presence of a position effect, albeit one that is rather small. These factors represent a free energy difference from independence (a and a' = 1) by -0.11 kcal/mol and 0.19 kcal/mol, respectively. The kitty-corner bound subunits arrangement deviates more noticeably. The free energy difference

between the two subunit arrangements would be $\Delta\Delta\Delta G$ = 0.30 kcal/mol. Considering that our method likely overestimated binding cooperativity, the actual difference would be smaller.

To gauge the gating effect, we used a similar approach, assuming the binding steps were independent (Figure 4A&B). This would attribute any binding cooperativity to gating, potentially exaggerating the gating effect. For the reason discussed earlier, we assigned the same f factor when the channel transitioned from a three-ligand-bound state to a four-ligand-bound state. We introduced a coefficient factor b or b' to the gating parameter f for transitions from a two-ligand-bound state to a three-ligand-bound state. Without a position effect, b and b' would be 1; otherwise, they would differ. Global fitting of the same datasets yielded values of b = 1.07 and b' = 2.18, corresponding to a free energy deviation from equal subunit contribution (b and b' = 1) by 0.04 kcal/mol and 0.46 kcal/mol (Figure 4C; Supplementary Figure 5, right panel). Again, the kitty-corner bound subunits arrangement deviates more noticeably. The free energy difference between the two subunit arrangements would be $\Delta\Delta\Delta G$ = 0.42 kcal/mol.

Since both fitting methods could potentially skew the estimated position effect, we explored a direct approach to estimate the free energy difference associated with the position effect on gating. We have previously shown that, by fully loading each concatemer with RTX followed by thorough washing, we could isolate channels with one-to-four RTX-bound subunits (Li et al. 2023). Po measurements from these channels reflect only the gating equilibrium of each vertical transition seen in Figure 5A without confounding effects from binding. The difference between two-ligand-bound channels could be represented by introducing just one additional degree of freedom to the classic MWC model. We assigned f1 as the gating coefficient for a single independent binding site and hypothesized that each pair of diagonal binding sites would exhibit stronger cooperativity (f_2) than two independent sites (f_1^2). Using this model to fit the RTX-bound TRPV1 single-channel Po

data (Figure 5B), we found f_2 to be 107% larger than f_1^2, equivalent to a free energy difference $\Delta\Delta\Delta G$ = 0.43 kcal/mol. This result aligns nicely with our indirect estimates discussed earlier, suggesting that, while binding might contribute to the position effect (probably much less than 0.30 kcal/mol), gating plays a larger role, contributing approximately 0.4 kcal/mol. The position effect would favor traversing the diagonally liganded conformation over the adjacently liganded conformation in a roughly 2:1 ratio. Nonetheless, compared to the 6.8-to-7.4 kcal/mol total energetic contribution from ligand binding to activation, the position effect is small (less than 10%).

Discussion

The present paper is the third in a series of studies of TRPV1 activation by vanilloid molecules (Li et al. 2023; Li and Zheng 2023). Our collective results from these studies suggest that, as an allosteric protein, TRPV1 can exist in various conformations (closed versus open, and with various number of ligands) at any ligand concentration. A recent structural study has captured many of these conformations, including those with two bound ligands at either neighbor or kitty-corner positions (Zhang, Julius, and Cheng 2021). It remains unclear what might contribute to the small difference in stability between these two configurations. The cryo-EM structures reveal that a vanilloid molecule bound in its binding pocket does not belong strictly to one subunit: due to the domain-swapped arrangement, the vanilloid binding pocket is formed by the S3 and S4 segments and the S4-S5 linker from one subunit together with the S5 and S6 segments from a neighbor subunit (Liao et al. 2013). Whereas capsaicin forms hydrogen bonds with the S4 segment and the

S4-S5 linker of the same subunit, extensive hydrophobic interactions with the S5 and S6 segments are predicted from both the cryo-EM structures and computational modeling (Yang et al. 2015b). Polar interactions between capsaicin or other ligands and the S6 segment are also predicted (Yin et al. 2019; Vu et al. 2020; Dong et al. 2019). However, results from our recent study and the present study showed that capsaicin binding to the four TRPV1 subunits are independent events (Li and Zheng 2023), suggesting that the position effect might have a different origin (see below).

One intriguing question arises from the present study is, does hemoglobin exhibit position differences in ligand induced allosteric transition like what we have observed in TRPV1? To our best knowledge, no direct experimental evidence in support of such a possibility has been reported. The binding pockets for gas molecules in hemoglobin are formed within each of the four isolated gas molecule binding domain (Bolton and Perutz 1970). These binding pockets are positioned at the vertex corners of a tetrahedron, such that each pocket is related to all the other pockets nearly equally (Figure 5C, top panel). TRPV1 and other ion channels existing in a planar membrane do not share this symmetry. A vanilloid binding pocket in TRPV1 is related differently to its neighbor pockets and the kitty-corner pocket (Figure 5C, bottom panel). When two neighbor binding pockets are occupied by ligands, the channel complex lacks the rotational symmetry exhibited when the kitty-corner binding pockets are occupied. Our observations showed that diagonally liganded channels have a higher probability residing in the open state (corresponding to the relaxed state in the MWC model). The situation would not be found in hemoglobin.

Despite the geometric restriction imposed by the planar membrane, a centrally located ion permeation pore surrounded by three-to-five structurally similar subunits or domains evolves as the overwhelmingly dominant architecture for biological ion channels (Zheng and Trudeau 2023). An obvious benefit of this architecture is the possibility for cooperative control of ion permeation by the multiple subunits or domains, which bestows a much greater sensitivity compared to a monomeric functional unit. Simply combining functional units into a complex without cooperativity does not benefit from this advantageous feature. Heteromeric subunit combination offers further opportunities to yield a wider variety of channel types from limited genetic resource (Zheng and Trudeau 2023), while retaining the advantageous feature of cooperativity. The majority of ligand-gated ion channels have each subunit participating in ligand binding, a situation that would maximize the benefit of cooperativity. Intriguingly, many pentameric channels do not possess five ligand binding sites. Acetylcholine receptors, for example, often have only two ligand-binding sites (Bouzat and Chrestia 2023). In these cases, the ligand-bind sites are always separated across the channel protein complex, as if this arrangement would allow acetylcholine binding to exert the maximal energetic effect on channel activation.

Figures and legends

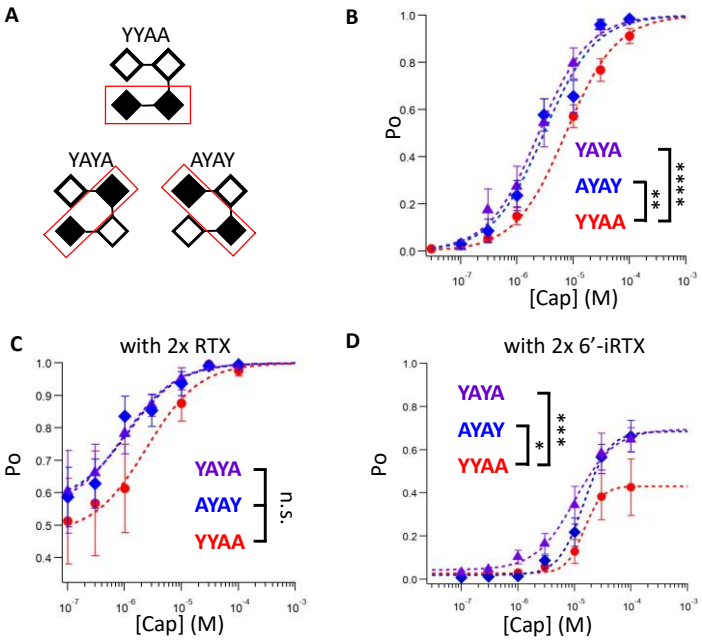

Figure 1. A. Expected subunit positioning for YYAA, YAYA and AYAY concatemers; open square represents a wildtype subunit; filled square represents a Y511A mutant subunit. B. Capsaicin concentration-dependent single-channel open probability curves for YYAA, YAYA and AYAY fitted to a Hill Equation using the following EC50 and Hill slope parameters: YYAA (red), 7.31 μM, 0.87, n = 12; AYAY (blue), 2.99 μM, 0.95, n = 4; YAYA (black), 2.42 μM, 0.97, n = 5. C. Capsaicin concentration-dependent single-channel open probability curve for YYAA, YAYA and AYAY with two preloaded RTX molecules in the wildtype protomers fitted to a Hill Equation: YYAA, 2.42 μM, 0.93, n = 5; AYAY, 0.97 μM, 0.94, n = 5; YAYA, 1.13 μM, 0.95, n = 5. D. Capsaicin concentration-dependent single-channel open probability curve for YYAA, YAYA and AYAY with two preloaded 6'-iRTX molecules in the wildtype protomers fitted to a Hill Equation: YYAA, 14.77 μM, 2.72, n = 4; AYAY, 14.61 μM, 1.95, n = 6; YAYA, 10.25 μM, 1.24, n = 8.

Two-way ANOVA with Sidak's multiple comparisons test; n.s., no significance; *, P < 0.05; **, P < 0.01; ***, P < 0.001; ****, P < 0.0001.

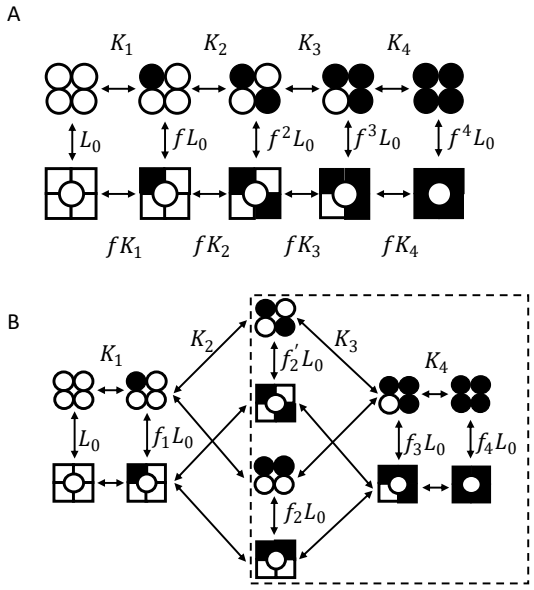

Figure 2. A. Illustration of a classic MWC model for a tetrameric ligand-gated ion channel with four identical ligand-binding sites. L0 represents the equilibrium constant for the apo state, f represents the cooperative factor which reflects the energy contribution by each ligand binding; K1 to K4 represent the ligand association constants. B. Illustration of a modified model with position effects. The dash box shows the sub-system examined in Figures 3 and 4.

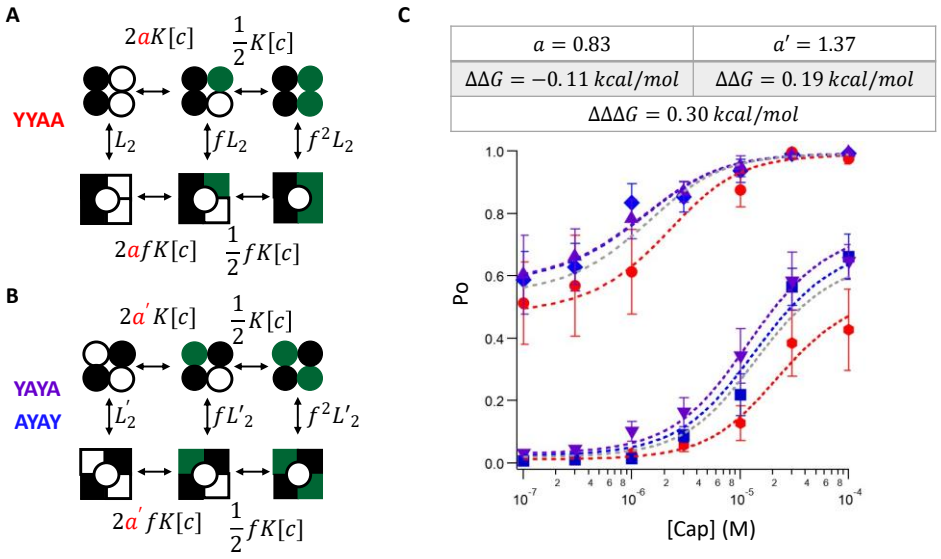

Figure 3. A&B. Illustration of the models used for fitting the capsaicin-dependent Po data with two pre-loaded RTX or 6'-iRTX, to test the contribution of binding to the position effect. L2 and L2' represent the equilibrium constant for the state with two preloaded RTX or 6'-iRTX (L2 for YYAA, L2' for YAYA and AYAY), before application of capsaicin; a and a' are coefficient factors for the position effect (a for YYAA, a' for YAYA and AYAY); when there is no position effect, a and a' should be 1 for independent bindings; f represents the cooperative factor which reflects the energy contribution by each ligand binding; K represents the ligand binding affinity constant for the Y511A mutant subunit, [c] is the capsaicin concentration. C: Global fitting results using the models shown in panels A and B with the following parameters: a = 0.83; a' = 1.37; K = 4.8x104 M-1, f = 10.3; YYAA: L (with 6'-iRTX) = 0.01, L (with RTX) = 0.92; YAYA: L (with 6'-iRTX) = 0.03, L (with RTX) = 1.38; AYAY: L (with 6'-iRTX) = 0.02, L (with RTX) = 1.35. Deviations of the a and a' values from 1 (for independent ligand binding) represent $\Delta\Delta G$ values of -0.11 kcal/mol (for YYAA) and 0.19 kcal/mol (for YAYA and AYAY). For model fitting with the

classic MWC model (gray line): K = 5.8x104 M-1, f = 10.4, L (with 6'-iRTX) = 0.02, L (with RTX) = 1.16.

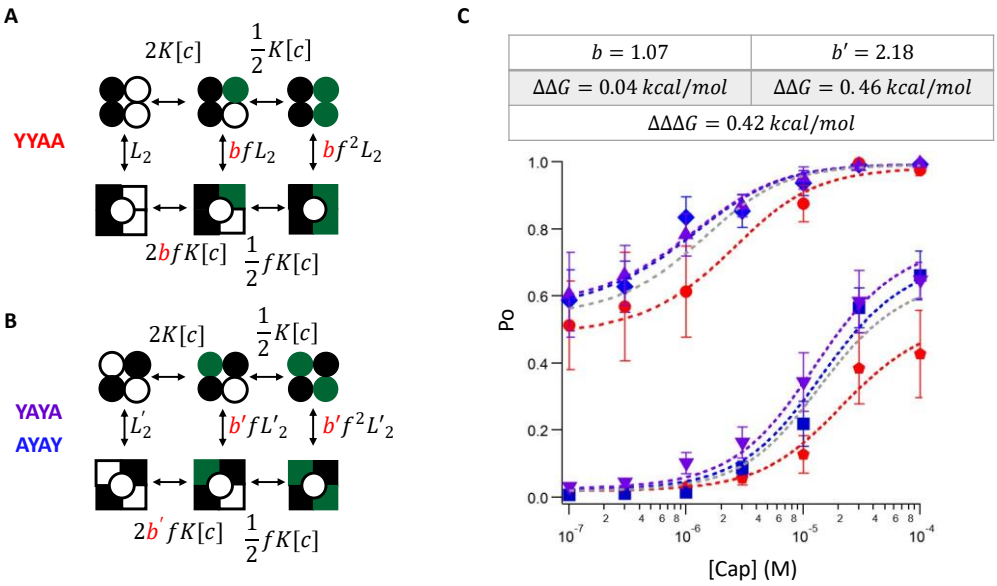

Figure 4. A&B. Illustration of the models for testing the contribution of gating to the position effect. L2 and L2' represent the equilibrium constant for the state with two preloaded RTX or 6'-iRTX (L2 for YYAA, L2' for YAYA and AYAY), before application of capsaicin; b and b' are coefficient factors for the position effect (b for YYAA, b' for YAYA and AYAY); when there is no position effect, b and b' should be 1; f represents the cooperative factor which reflects the energy contribution by each ligand binding; K represents the ligand binding affinity constant for the Y511A mutant subunit, [c] is the capsaicin concentration. C: Global fitting results using the models from panels A and B with the following parameters: b = 1.07; b' = 2.18. K = 4.6x104 M-1, f = 7.8; YYAA: L (with 6'-iRTX) = 0.02, L (with RTX) = 0.94; YAYA: L (with 6'-iRTX) = 0.02, L (with RTX) = 1.32; AYAY: L (with 6'-iRTX) = 0.02, L (with RTX) = 1.28. Deviations of the b and b' values from 1 (none position effect) represent $\Delta\Delta G$ values of 0.04 kcal/mol (for YYAA)

and 0.46 kcal/mol (for YAYA and AYAY). For model fitting with classic MWC model (gray line): K = 5.8x104 M-1, f = 10.4, L (with 6'-iRTX) = 0.02, L (with RTX) = 1.16.

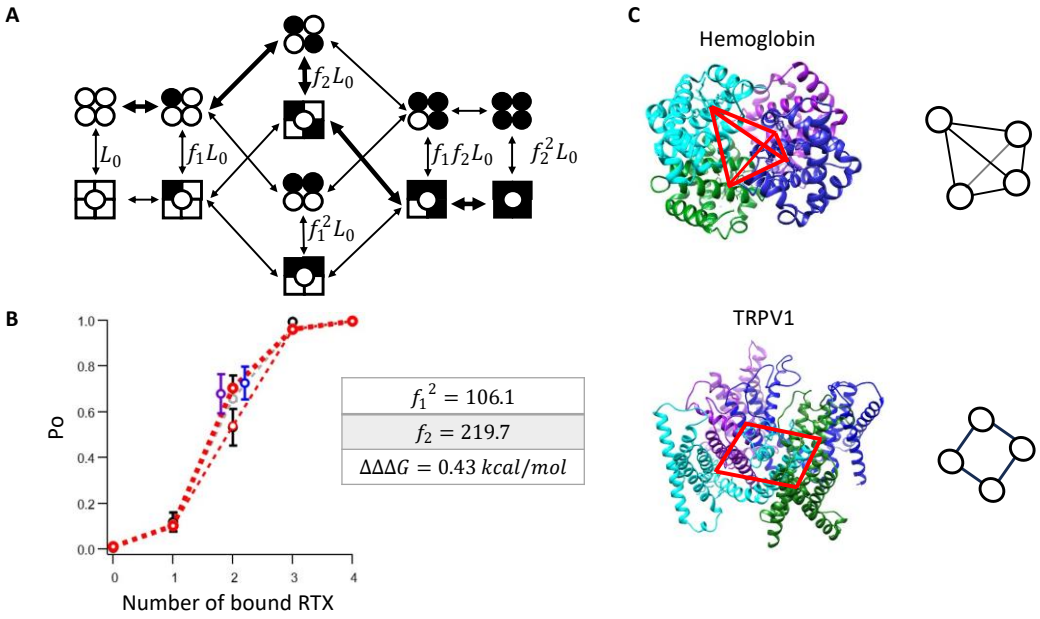

Figure 5. A. Illustration of a modified MWC model with position effects. L0 represents the equilibrium constant for the apo state, f1 represents the cooperative factor which reflects the energy contribution by one ligand binding in the pair of the two diagonal binding sites; f2 represents the cooperative factor which reflects the energy contribution by two ligands binding to the pair of the two diagonal binding sites; when there is no position effect, f2 should equal to f12, making the model equivalent to the classic MWC model. Thicker arrows indicate pathways with higher probabilities. B. Global fitting results for the Po data from AAAA, YAAA, YYAA, YAYA, AYAY, YYYA, YYYY concatemers, with the Y subunits loaded with RTX: L0 = 0.01, f1 = 10.3, f2 = 219.7, which produce $\Delta\Delta\Delta G$ = 0.43 kcal/mol between neighbor and kitty-corner positions, n = 4 to 10. Black circles represent the data points; red circles represent predictions of our modified MWC model; grey dash lines represent a classic MWC model with L0 = 0.01, f = 15.7. Purple

circle represents YAYA data point; blue circle represents AYAY data points. C. Relationships between ligand binding pockets in hemoglobin (PDB entry 2DHB, top panel) and tetrameric ligand-gated ion channels such as TRPV1 (transmembrane part of TRPV1, modified from PDB entry 3J5R, bottom panel). Positions of ligand binding sites are highlighted by red lines between them and illustrated by a diagram on the right.

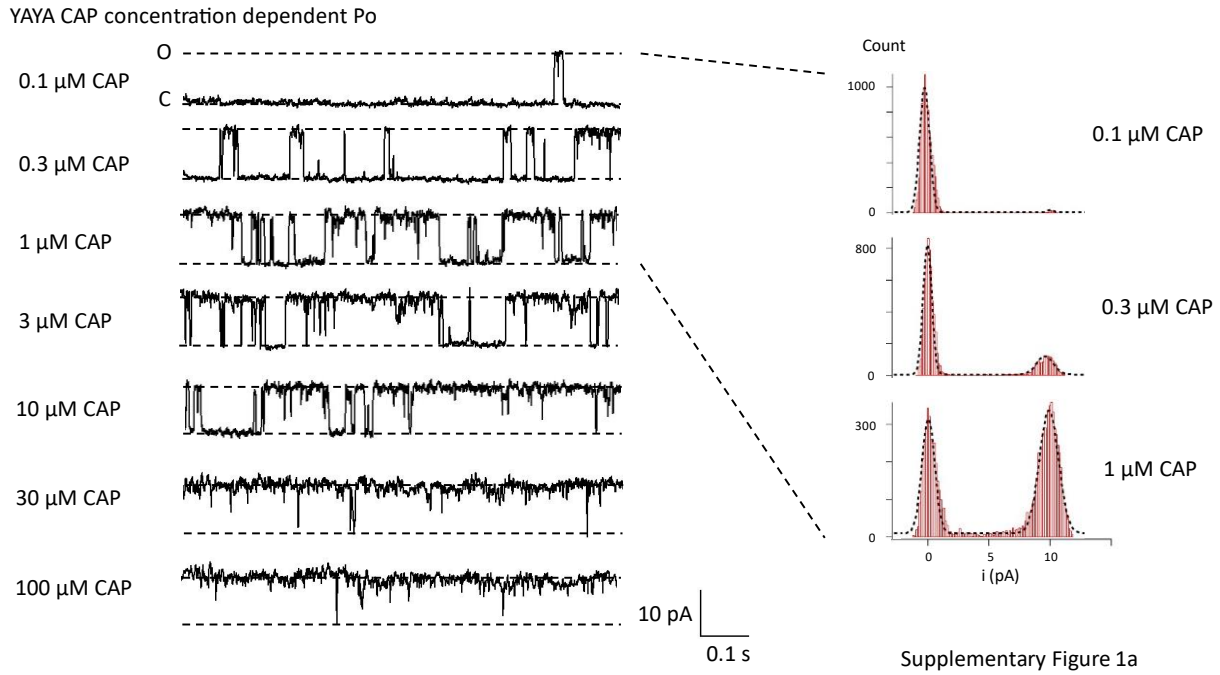

Supplementary Figure 1a

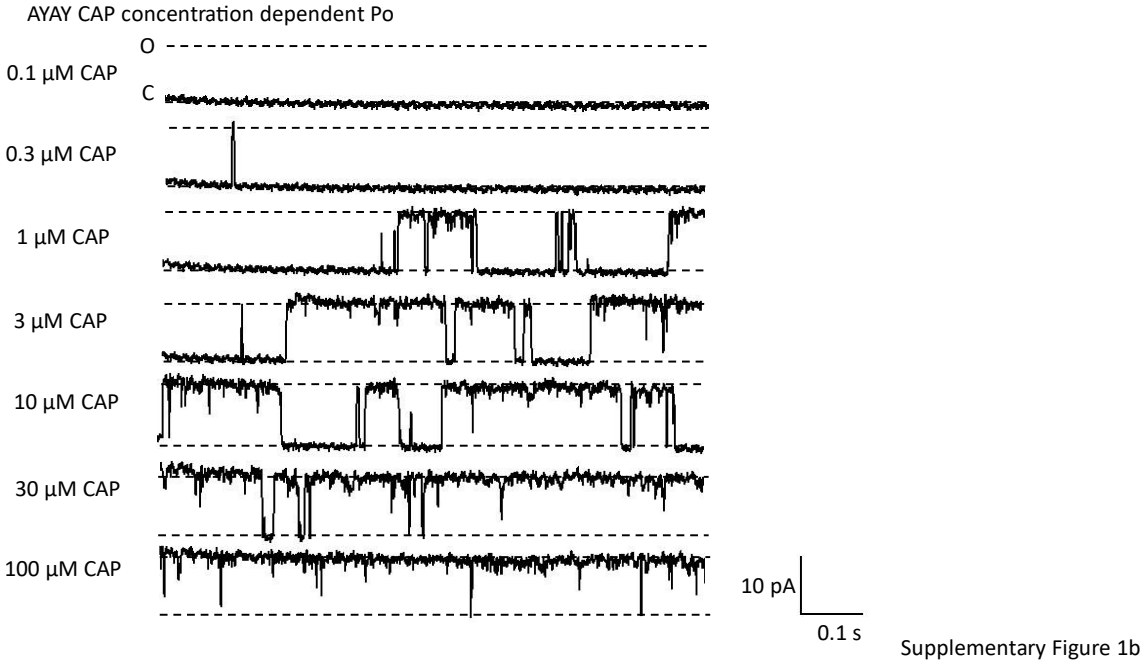

Supplementary Figure 1a-b

Representative single-channel current traces of YAYA and AYAY concatemers activated by different concentrations of capsaicin from the same inside-out patch. YYAA representative recording is already published in a previous study (Li and Zheng 2023). Representative all-point histogram plots for first three single channel current traces are shown.

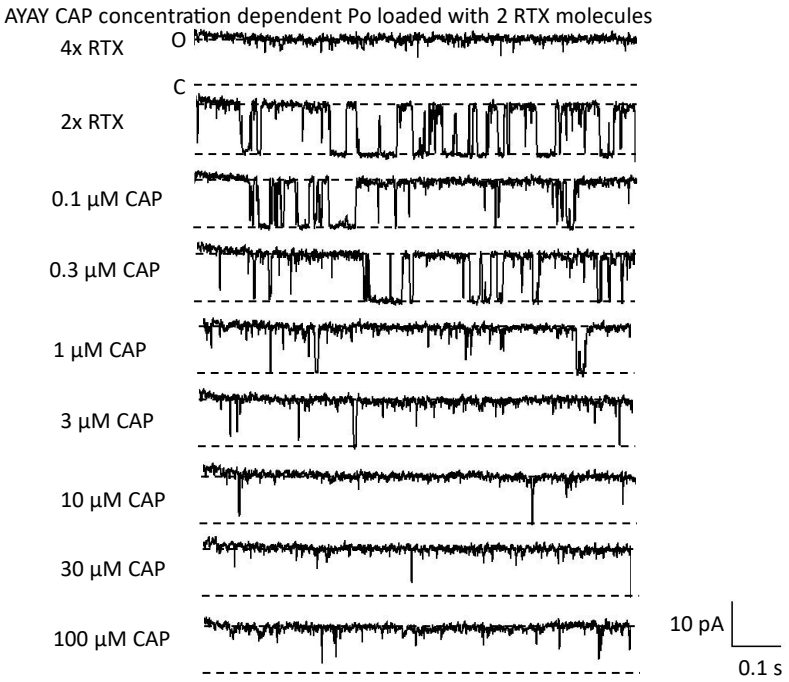

Supplementary Figure 2a

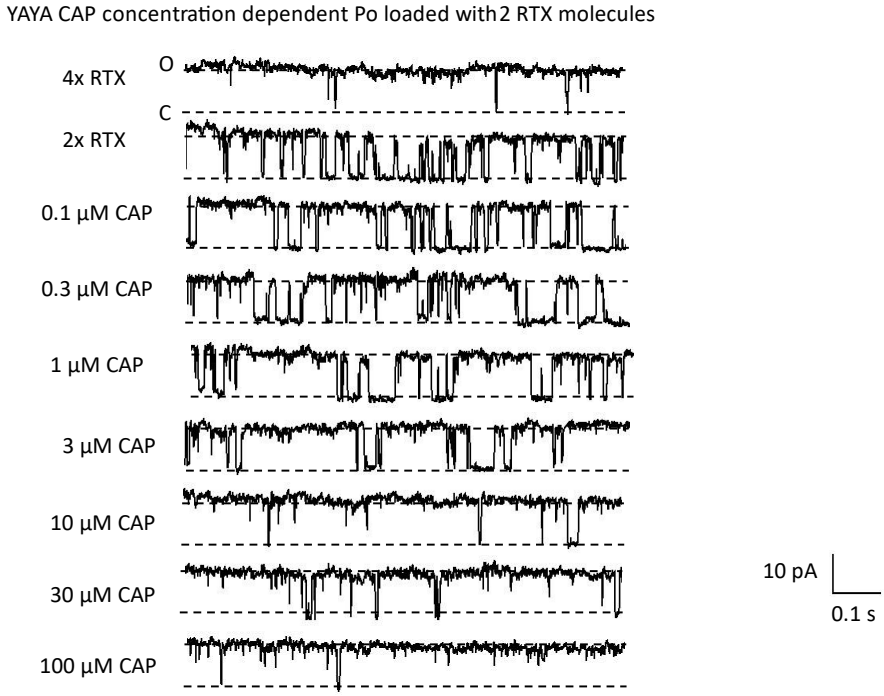

Supplementary Figure 2b

Supplementary Figure 2a-b

Representative single-channel current traces of YAYA and AYAY concatemers first loaded with two RTX molecules in the wildtype subunits then activated by different concentrations of capsaicin

from the same inside-out patch. YYAA representative recording is already published in a previous study (Li and Zheng 2023).

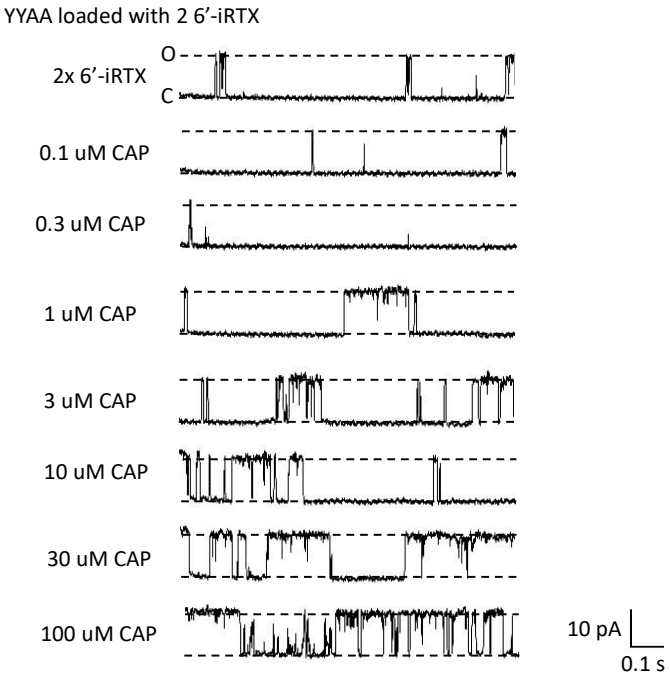

Supplementary Figure 3a

AYAY loaded with 2 6’-iRTX

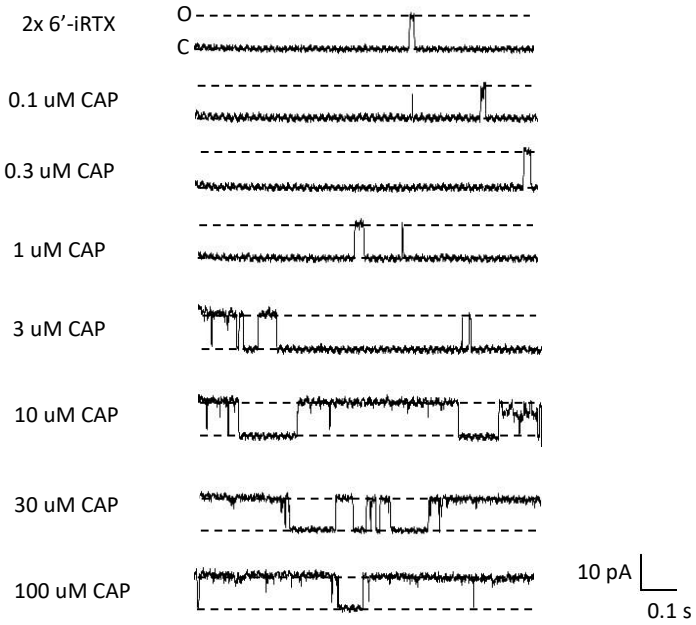

Supplementary Figure 3b

YAYA with 2x 6’-iRTX

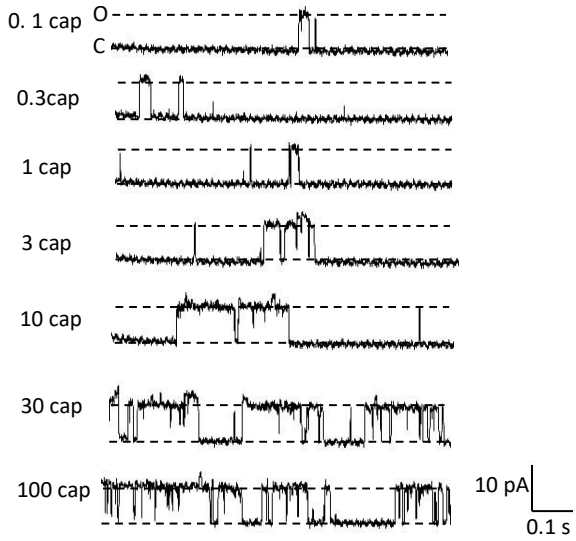

Supplementary Figure 3c

Supplementary Figure 3a-c

Representative single-channel current traces of YYAA, YAYA and AYAY concatemers first loaded with two 6'-iRTX molecules in the wildtype subunits then activated by different concentrations of capsaicin from the same inside-out patch.

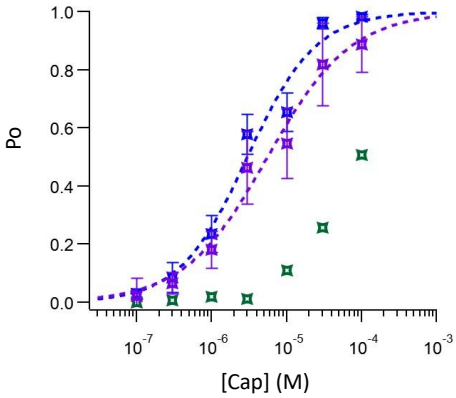

After excluding the outlier recording,
n = 4, EC50 2.99 μM, Hill slope 0.95

Before excluding the outlier recording,
n = 5, EC50 5.55 μM, Hill slope 0.95

One AYAY recording excluded as an outlier

Supplementary Figure 4

Supplementary Figure 4

Replot of Figure 1B by including the outlier recording from an AYAY channel.

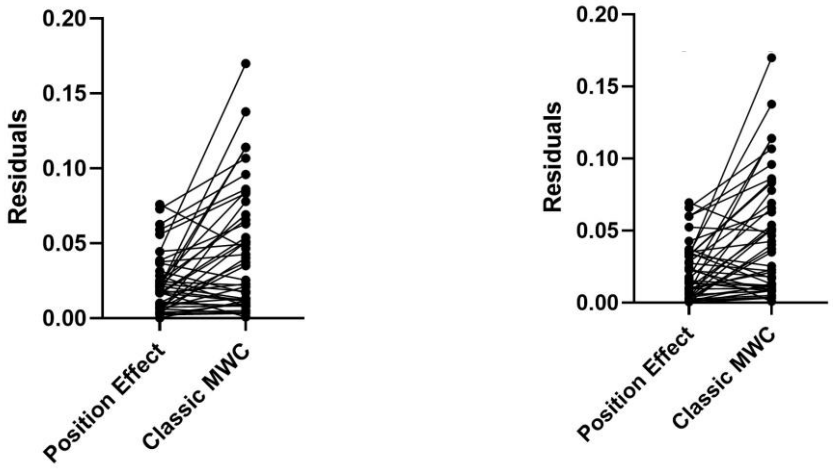

Supplementary Figure 5

Supplementary Figure 5

Comparison of residues between the classic and modified MWC models in Figure 3 (left) and Figure 4 (right).

References

Bolton, W., and M. F. Perutz. 1970. "Three Dimensional Fourier Synthesis of Horse Deoxyhaemoglobin at 2.8 Å Resolution." *Nature* 228 (5271):551-552. doi: 10.1038/228551a0.

Bouzat, Cecilia, and Juan Facundo Chrestia. 2023. "Acetylcholine Receptors." *Textbook of Ion Channels Volume II: Properties, Function, and Pharmacology of the Superfamilies*:223.

Cao, Erhu, Maofu Liao, Yifan Cheng, and David Julius. 2013. "TRPV1 structures in distinct conformations reveal activation mechanisms." *Nature* 504 (7478):113-118.

Dong, Yawen, Yue Yin, Simon Vu, Fan Yang, Vladimir Yarov-Yarovoy, Yuhua Tian, and Jie Zheng. 2019. "A distinct structural mechanism underlies TRPV1 activation by piperine." *Biochemical and Biophysical Research Communications* 516 (2):365-372. doi: https://doi.org/10.1016/j.bbrc.2019.06.039.

Edsall, John T. 1972. "Blood and hemoglobin: The evolution of knowledge of functional adaptation in a biochemical system." *Journal of the History of Biology* 5 (2):205-257. doi: 10.1007/BF00346659.

Hazan, Adina, Arijit Basu, Nomi Zalcman, Henry Matzner, and Avi Priel. 2016. "Tyrosine residue in the TRPV1 vanilloid binding pocket regulates deactivation kinetics." *Journal of Biological Chemistry* 291 (26):13855-13863.

Hazan, Adina, Rakesh Kumar, Henry Matzner, and Avi Priel. 2015. "The pain receptor TRPV1 displays agonist-dependent activation stoichiometry." *Scientific reports* 5 (1):1-13.

Hodgkin, A. L., and A. F. Huxley. 1952. "A quantitative description of membrane current and its application to conduction and excitation in nerve." *J Physiol* 117 (4):500-44. doi: 10.1113/jphysiol.1952.sp004764.

Horrigan, F. T., and R. W. Aldrich. 1999. "Allosteric voltage gating of potassium channels II. Mslo channel gating charge movement in the absence of Ca(2+)." *J Gen Physiol* 114 (2):305-36.

Horrigan, F. T., and R. W. Aldrich. 2002. "Coupling between voltage sensor activation, Ca2+ binding and channel opening in large conductance (BK) potassium channels." *J Gen Physiol* 120 (3):267-305.

Horrigan, F. T., J. Cui, and R. W. Aldrich. 1999. "Allosteric voltage gating of potassium channels I. Mslo ionic currents in the absence of Ca(2+)." *J Gen Physiol* 114 (2):277-304.

Koshland, D. E., Jr., G. Némethy, and D. Filmer. 1966. "Comparison of experimental binding data and theoretical models in proteins containing subunits." *Biochemistry* 5 (1):365-85. doi: 10.1021/bi00865a047.

Li, Shisheng, Phuong Tran Nguyen, Simon Vu, Vladimir Yarov-Yarovoy, and Jie Zheng. 2023. "Opening of capsaicin receptor TRPV1 is Stabilized Equally by Its Four Subunits." *Journal of Biological Chemistry*:104828.

Li, Shisheng, and Jie Zheng. 2023. "The Capsaicin Binding Affinity of Wild-Type and Mutant TRPV1 Ion Channels." *Journal of Biological Chemistry*:105268. doi: https://doi.org/10.1016/j.jbc.2023.105268.

Liao, Maofu, Erhu Cao, David Julius, and Yifan Cheng. 2013. "Structure of the TRPV1 ion channel determined by electron cryo-microscopy." *Nature* 504 (7478):107-112.

Monod, J., J. Wyman, and J. P. Changeux. 1965. "On the Nature of Allosteric Transitions: A Plausible Model." *J Mol Biol* 12:88-118. doi: 10.1016/s0022-2836(65)80285-6.

Rothberg, B. S., and K. L. Magleby. 1998. "Kinetic structure of large-conductance Ca2+-activated K+ channels suggests that the gating includes transitions through intermediate or secondary states. A mechanism for flickers." *J Gen Physiol* 111 (6):751-80. doi: 10.1085/jgp.111.6.751.

Schoppa, N. E., and F. J. Sigworth. 1998. "Activation of Shaker potassium channels. III. An activation gating model for wild-type and V2 mutant channels." *J Gen Physiol* 111 (2):313-42. doi: 10.1085/jgp.111.2.313.

Vu, S., V. Singh, H. Wulff, V. Yarov-Yarovoy, and J. Zheng. 2020. "New capsaicin analogs as molecular rulers to define the permissive conformation of the mouse TRPV1 ligand-binding pocket." *Elife* 9. doi: 10.7554/eLife.62039.

Yang, F., X. Xiao, W. Cheng, W. Yang, P. Yu, Z. Song, V. Yarov-Yarovoy, and J. Zheng. 2015a. "Structural mechanism underlying capsaicin binding and activation of the TRPV1 ion channel." *Nat Chem Biol* 11 (7):518-524. doi: 10.1038/nchembio.1835.

Yang, Fan, Xian Xiao, Wei Cheng, Wei Yang, Peilin Yu, Zhenzhen Song, Vladimir Yarov-Yarovoy, and Jie Zheng. 2015b. "Structural mechanism underlying capsaicin binding and activation of the TRPV1 ion channel." *Nature chemical biology* 11 (7):518-524.

Yang, Fan, Xian Xiao, Bo Hyun Lee, Simon Vu, Wei Yang, Vladimir Yarov-Yarovoy, and Jie Zheng. 2018. "The conformational wave in capsaicin activation of transient receptor potential vanilloid 1 ion channel." *Nature communications* 9 (1):1-9.

Yin, Yue, Yawen Dong, Simon Vu, Fan Yang, Vladimir Yarov‐Yarovoy, Yuhua Tian, and Jie Zheng. 2019. "Structural mechanisms underlying activation of TRPV1 channels by pungent compounds in gingers." *British Journal of Pharmacology* 176 (17):3364-3377.

Zagotta, W. N., T. Hoshi, and R. W. Aldrich. 1994. "Shaker potassium channel gating. III: Evaluation of kinetic models for activation." *J Gen Physiol* 103 (2):321-62. doi: 10.1085/jgp.103.2.321.

Zhang, Kaihua, David Julius, and Yifan Cheng. 2021. "Structural snapshots of TRPV1 reveal mechanism of polymodal functionality." *Cell* 184 (20):5138-5150. e12.

Zheng, Jie, and Matthew C Trudeau. 2023. *Textbook of Ion Channels: Three Volume Set*: CRC Press.

Acknowledgements

I would like to express my deep appreciation to my mentor Dr. Jie Zheng, from whom I have received the best scientific training and support I could get, which have made my 5-year PhD smooth and enjoyable. I would also like to thank current and former Zheng lab members (Dr. Jade Tian, Abdullah Al Tekreeti, Dr. Simon Vu …) as well as professors (Dr. Vladimir Yarov-Yarovoy, Dr, Qizhi Gong…) and colleagues (Dr. Phuong Tran Nguyen, Sitong Zhu…) for their guidance, help and support.

Besides the academic support, I am grateful to the mental companion from my parents, families, friends (Ruili Fang, Qianjin Jiang, Sida Li, Zhangyu Wang, Yi Pan, NS…).